

Bridging Native and Intrinsic Structures of Microhydrated Biomolecules by Cold Ion Spectroscopy

Présentée le 22 septembre 2023

Faculté des sciences de base
Laboratoire de chimie physique moléculaire
Programme doctoral en chimie et génie chimique

pour l'obtention du grade de Docteur ès Sciences

par

Andrei ZVIAGIN

Acceptée sur proposition du jury

Dr A.-S. Chauvin, présidente du jury
Prof. O. Boyarkine, directeur de thèse
Prof. A. Rijs, rapporteuse
Prof. J. Fernández, rapporteur
Dr S. Takahama, rapporteur

Abstract

Life is built from myriads of molecules, the vast majority of which are bio- ones. The functionality of biomolecules in living organisms greatly depends on the three-dimensional (3D) structure they adopt *in vivo*, where they are surrounded by a dynamic shell of water molecules. The hydration shell morphs this structure and maintains the stability of biomolecules through a network of intermolecular non-covalent interactions. Knowledge of the native structures which biomolecules adopt in solutions enables modeling and prediction of specific roles, interactions, and mechanisms of action of biomolecules, which is crucial in many fields of life science, ranging from disease diagnosis and treatment to accelerating drug development through the aid of artificial intelligence. Understanding how the structure relates to function is crucial for deciphering the molecular basis of biological processes and designing targeted interventions.

Solving native structures of such large molecules, like biomolecules, is often challenging, particularly due to the potentially infinite number of non-covalent interactions with water. In this thesis, we report the use of cold ion gas-phase action spectroscopy of microhydrated biomolecules to develop an approach for revealing the native-like structures of biomolecules. Unlike spectroscopy in solution, gas-phase IR and UV cold-ion spectroscopy may provide vibrationally resolved spectra that can be used for stringent validation of 3D structures calculated *in silico*, while microhydration of biomolecules allows bridging the gap between the gas-phase and the native structures, of which only the latter remains truly biologically relevant.

The first part of this thesis describes an ion source that was developed and used for stable generation of large quantities of protonated microhydrated complexes. This source allows generating microsolvated complexes by two different methods: incomplete desolvation of water droplets with the embedded biomolecule during electrospray ionization and cryogenic condensation of solvent molecules onto the electrosprayed bare ions.

In the second part, we study two microhydrated amino acids – protonated arginine and tryptophan. Microhydrated ArgH^+ is an example of the complexes with kinetically trapped structures. The native-like structure of ArgH^+ complexed with water molecules appears to be kinetically trapped due to evaporative cooling that significantly lowers the temperature of the complexes and slows down the conformational rearrangements. Microhydrated TrpH^+ , on the other hand, is an example of a system that, under our experimental conditions, undergoes the solution to the gas phase transition adiabatically, without kinetic trapping. All the studied

complex sizes of $\text{TrpH}^+(\text{H}_2\text{O})_n$ ($n = 0-6$) reside in their lowest energy structures, which is experimentally verified by the fact that the spectra of these complexes with retained and condensed water molecules are identical. We also performed theoretical calculations to find the structure of both of these complexes. While the standard approach of searching for the lowest energy structures provides a good match with experimental spectra for the water complexes of TrpH^+ , it does not work well with the complexes of ArgH^+ . For this case, we proposed another computational workflow, which closely mimics the conditions of generation of the complexes and finally led to a better consistency with the experiment.

The last part of this thesis demonstrates the application of cold ion spectroscopy for large biomolecules, such as proteins. We showed that both IR and UV spectroscopy can provide valuable information about the protein ubiquitin. IR spectroscopy allows tracing the global conformational rearrangements of the protein, such as unfolding, while UV spectroscopy provides information about noncovalent interactions and local molecular structures around chromophores. We also showed that evaporative cooling plays a crucial role in retaining the folded native-like structure of the protein. Even a few water molecules retained on the protein ensure its low temperature and protect the native-like structure during the electrospray ionization. However, if the water molecules are condensed on the already unfolded protein, its structure does not refold into the native one.

Keywords: microhydration, cold ions spectroscopy, non-covalent interactions, kinetic trapping, conformers, native mass spectrometry, infrared spectroscopy, ultraviolet spectroscopy, double resonance spectroscopy.

Zusammenfassung

Das Leben besteht aus unzähligen Molekülen, von denen die überwiegende Mehrheit Biomoleküle sind. Die Funktionalität von Biomolekülen in lebenden Organismen hängt stark von ihrer dreidimensionalen (3D) Struktur ab, die sie *in vivo* annehmen, umgeben von einer dynamischen Schale aus Wassermolekülen. Diese Hydratationshülle verändert die Struktur und gewährleistet die Stabilität der Biomoleküle durch ein Netzwerk von zwischenmolekularen, nicht-kovalenten Wechselwirkungen. Das Wissen über diese nativen Strukturen ermöglicht die Modellierung und Vorhersage spezifischer Funktionen, Interaktionen und Wirkmechanismen von Biomolekülen, was in vielen Bereichen der Lebenswissenschaften entscheidend ist - von der Krankheitsdiagnose und -behandlung bis zur Beschleunigung der Arzneimittelentwicklung durch den Einsatz künstlicher Intelligenz. Das Verständnis der Struktur-Funktions-Beziehung ist entscheidend für die Entschlüsselung der molekularen Grundlage biologischer Prozesse und die Entwicklung gezielter Interventionen.

Die Lösung nativer Strukturen solch großer Moleküle wie Biomoleküle ist häufig eine Herausforderung, insbesondere aufgrund der potenziell unendlichen Anzahl von nicht-kovalenten Wechselwirkungen mit Wasser. In dieser Arbeit berichten wir über den Einsatz von Kälteionen-Gasphasen-Aktionsspektroskopie mikrohydratisierter Biomoleküle, um einen Ansatz zur Aufdeckung nativähnlicher Strukturen von Biomolekülen zu entwickeln. Im Gegensatz zur Spektroskopie in Lösung können Gasphasen-IR- und UV-Kälteionenspektroskopie vibroresolvierte Spektren liefern, die zur strengen Validierung von *in silico* berechneten 3D-Strukturen verwendet werden können. Die Mikrohydratisierung von Biomolekülen ermöglicht dabei eine Brücke zwischen der Gasphase und den nativen Strukturen, wobei letztere biologisch relevanter sind.

Im ersten Teil dieser Arbeit beschreiben wir eine Ionenquelle, die entwickelt wurde und zur stabilen Erzeugung großer Mengen protonierter mikrohydratisierter Komplexe verwendet wurde. Diese Quelle ermöglicht die Erzeugung mikrosolvatisierter Komplexe durch zwei verschiedene Methoden. Eine davon beruht auf einer unvollständigen Desolvatisierung von Wassertropfen mit dem eingebetteten Biomolekül während der Elektrospray-Ionisierung. Ein alternativer Ansatz beruht auf der kryogenen Kondensation von Lösungsmittelmolekülen auf die elektroprühetrockneten bloßen Ionen.

Im zweiten Teil untersuchen wir zwei mikrohydratisierte Aminosäuren - protoniertes Arginin und Tryptophan. Mikrohydratisiertes ArgH⁺ ist ein Beispiel für Komplexe mit

kinetisch gefangenen Strukturen. Die nativähnliche Struktur des ArgH⁺-Komplexes mit Wassermolekülen scheint kinetisch gefangen zu sein, aufgrund einer Verdampfungskühlung, die die Temperatur der Komplexe erheblich senkt und die konformationellen Umlagerungen verlangsamt. Mikrohydratisiertes TrpH⁺ hingegen ist ein Beispiel für ein System, das unter unseren experimentellen Bedingungen adiabatisch vom Lösungsmittel in die Gasphase übergeht, ohne kinetisch gefangen zu sein. Alle untersuchten Komplexgrößen von TrpH⁺(H₂O)_n ($n = 0-6$) befinden sich in ihren energetisch niedrigsten Strukturen, was experimentell durch die Tatsache bestätigt wird, dass die Spektren dieser Komplexe mit erhaltenen und kondensierten Wassermolekülen identisch sind. Wir haben auch theoretische Berechnungen durchgeführt, um die Struktur beider Komplexe zu finden. Während der Standardansatz zur Suche nach den energetisch niedrigsten Strukturen eine gute Übereinstimmung mit den experimentellen Spektren für die Wasserkomplexe von TrpH⁺ liefert, funktioniert er nicht gut für die Komplexe von ArgH⁺. In diesem Fall haben wir einen anderen Berechnungsworkflow vorgeschlagen, der die Bedingungen der Komplexerzeugung eng simuliert und schließlich zu einer besseren Übereinstimmung mit dem Experiment geführt hat.

Der letzte Teil dieser Arbeit zeigt die Anwendung der Kälteionenspektroskopie für große Biomoleküle wie Proteine. Wir haben gezeigt, dass sowohl IR- als auch UV-Spektroskopie wertvolle Informationen über das Protein Ubiquitin liefern können. Die IR-Spektroskopie ermöglicht die Verfolgung globaler konformationeller Umlagerungen des Proteins, wie zum Beispiel die Entfaltung, während die UV-Spektroskopie strukturelle Informationen in der Nähe der Chromophore liefert. Wir haben auch gezeigt, dass die Verdampfungskühlung eine entscheidende Rolle bei der Erhaltung der gefalteten nativähnlichen Struktur des Proteins spielt. Selbst wenige Wassermoleküle, die am Protein haften bleiben, gewährleisten eine niedrige Temperatur und schützen die nativähnliche Struktur während der Elektrospray-Ionisierung. Wenn jedoch die Wassermoleküle auf das bereits entfaltete Protein kondensieren, faltet sich die Struktur nicht wieder in die natürliche Form zurück.

Schlüsselwörter: Mikrohydratisierung, Kaltionenspektroskopie, nicht-kovalente Wechselwirkungen, kinetische Einschließung, Konformer, native Massenspektrometrie, Infrarotspektroskopie, Ultraviolett-Spektroskopie, Doppelresonanzspektroskopie.

Table of Contents

Abstract.....	i
Zusammenfassung.....	iii
Table of Contents.....	v
List of Abbreviations	vii
Chapter 1. Introduction.....	9
References	16
Chapter 2. Experimental setup.....	21
2.1. Tandem mass spectrometer	21
2.1.1. Design and cooling of the cold ion trap and cold pre-trap.	23
2.1.2. Differential pumping of the Tandem Mass Spectrometer	24
2.1.1. Timing of events.....	26
2.2. Optical setup.....	27
References	28
Chapter 3. Gentle nano-electrospray ion source for reliable and efficient generation of microsolvated ions.....	29
3.1. Abstract	29
3.2. Introduction	29
3.3. Instrumentation.....	31
3.4. Results and discussion.....	33
3.5. Conclusion.....	38
Appendix	39
References	40
Chapter 4. Salt bridge structure of microhydrated arginine kinetically trapped in the gas phase by evaporative cooling	42
4.1. Abstract	42
4.2. Introduction	43
4.3. Methods.....	44
4.4. Results and discussion.....	45
4.5. Conclusion.....	52
Appendix	53
References	68

Chapter 5. Revealing the Native-like Structure of Tryptophan by Cold Ion Spectroscopy of Microhydrated Complexes.....	71
5.1. Abstract	71
5.2. Introduction	72
5.3. Methods.....	73
5.4. Results and discussion.....	74
5.5. Conclusion.....	79
Appendix	80
References	85
Chapter 6. Tracking local and global structural changes in a protein by cold ion spectroscopy.....	89
6.1. Abstract	89
6.2. Introduction	90
6.3. Experimental section	92
6.4. Results and discussion.....	93
6.4.1. UV spectroscopy of bare Ubi	93
6.4.2. UV spectroscopy of hydrated Ubi.....	99
6.4.3. IR spectroscopy	102
6.5. Conclusion.....	103
Appendix	105
References	109
Chapter 7. Revealing the folded and unfolded structure of differently formed microhydrated complexes of the ubiquitin protein.....	114
7.1. Results and discussion.....	114
7.2 Conclusion.....	119
References	120
Chapter 8. Summary and Outlook	121
Acknowledgments.....	125
Curriculum Vitae	126

List of Abbreviations

Abbreviation	Definition
3D	Three-Dimensional
B3LYP	Becke-3-Lee-Yang-Parr hybrid functional
BBO	Beta Barium Borate
DFT	Density Functional Theory
ESI	Electrospray Ionization
nESI	Nano-Electrospray Ionization
IM-MS	Ion Mobility Mass Spectrometry
IR	Infrared
IRMPD	Infrared Multiple Photon Dissociation
Tyr	Tyrosine
Glu	Glutamic Acid
MALDI	Matrix-Assisted Laser Desorption/Ionization
NMR	Nuclear Magnetic Resonance
CIS	Cold Ion Spectroscopy
Arg	Arginine
Ubi	Ubiquitin
SS	Stainless Steel
CIT	Cold Ion Trap
PC	Personal Computer
PEEK	Polyether Ether Ketone
RF	Radio Frequency
OPO	Optical Parametric Oscillator
Nd:YAG	Neodymium-Doped Yttrium Aluminum Garnet
H-bond	Hydrogen Bond
MS	Mass Spectrometry
IM	Ion Mobility
DIF	Double Ion-Funnel
UVPD	Ultraviolet Photodissociation
LC-MS	Liquid Chromatography Mass Spectrometry

Phe	Phenylalanine
S/N	Signal to Noise
MD	Molecular Dynamics
His	Histidine
Gly	Glycine
Trp	Tryptophan
AI	Artificial Intelligence
Cryo-EM	Cryogenic Electron Microscopy
OPA	Optical Parametric Amplifier
IVR	Intramolecular Vibrational energy Redistribution

Chapter 1. Introduction

The functions and properties of biological molecules crucially depend on their 3D structure. Knowledge of these structures allows for better understanding of how biomolecules function, assist in development of new drugs and substances with desired properties. A variety of experimental methods have been developed to determine the 3D structure of biomolecules. These methods can be divided into two categories: condensed phase and gas phase techniques.

NMR spectroscopy, X-ray crystallography, and recently developed cryo-EM are powerful and widely used techniques for determining 3D structure of biomolecules in condensed phase. None of these methods is however comprehensive, they all own certain drawbacks and limitations. NMR is, so far, a golden standard for solving native structures of molecules. On the negative side, the method has low sensitivity and can only detect the nuclei with a non-zero magnetic moment. The NMR analysis therefore requires large amounts of ultrapure sample, and very often isotopic enrichment is necessary to determine the positions of C, N, and O nuclei. Moreover, spectral congestion limits application of the method to large molecules; NMR has low power to resolve conformers and lacks mass resolution. X-ray crystallography, as implied by the name, requires crystallization of the molecules for analysis. Crystallization of some molecules can be extremely difficult and sometimes simply impossible. Furthermore, crystallization disturbs the native molecular structure, which also limits the application of this method. Cryo-EM has developed tremendously over the last years. Recent technological and software advances allowed for pushing the resolution of cryo-EM from 10 Å to as high as 1.2 Å, at which even the individual hydrogen atoms can be resolved.¹ This truly atomic resolution makes cryo-EM the most promising method for elucidating the 3D structure of biomolecules in the condensed phase. However, this method still has many challenges to overcome, including but not limited to sample preparation, data collection, and computational analysis of the images.

Gas-phase methods provide the possibility to distinguish intrinsic molecular properties and the properties resulting from solvent environment. Gas-phase methods are highly sensitive, can be relatively fast, and do not require special sample preparation. Among different gas phase methods, mass spectrometry (MS) plays a key role, as it can be extremely mass-selective and sensitive. When combined with activation techniques, it provides a powerful tool for structural elucidation and, for instance, sequencing of DNA and proteins. Combination of gas-phase action spectroscopy of cold ions with MS detection of charged photofragments benefits from

high specificity of the former and high sensitivity and mass resolution of the latter. In conjunction with high-level quantum-chemical calculations, this combination makes it possible to determine the accurate 3D structure of small to midsize biomolecules.

Gas-phase spectroscopy of biological molecules has a long and rich history.² The first experiments date back to mid-1980s and were dedicated to the electronic spectra of (non-charged) amino acid tryptophan cooled in a supersonic molecular beam.³⁻⁶ These experiments identified a number of stable conformers of tryptophan in the gas phase. One of the challenges at that time was transferring biomolecules into the gas phase without their thermal decomposition. Sample heating was used to transfer biomolecules into the gas phase by that time. This simple technique limited its use to amino acids and their derivatives only.³⁻⁹ The advent of laser desorption techniques allowed for volatilization of larger biomolecules without their decomposition. This ignited intensive studies of cooled in the supersonic jet neutral peptides with up to 15 residues.¹⁰⁻¹⁸ The advent of MALDI^{19,20} and ESI^{21,22} techniques enabled the revolutionary introduction of very large, up to protein complexes and even viruses, biomolecular systems into the gas phase as multiply charged molecular ions. The ability to produce large ionized molecules that can be easily manipulated by electric and magnetic fields has opened up new avenues in exploring biomolecules by mass spectrometric methods. This also enabled optical spectroscopy of ionized biomolecules in the gas phase. The increased spectral complexity, caused by the increased number of molecular vibrations, for long time hindered the development of IR and UV gas phase spectroscopy. Cooling molecular ions to cryogenic temperatures was required to suppress inhomogeneous spectral broadening and make the spectra suitable for stringent validation of theory.

The first step toward cold ion spectroscopy was taken in the study of protonated tryptophan stored in a liquid nitrogen-cooled Paul trap.²³ Shortly thereafter, the first spectroscopic measurements of biomolecular ions in the cold, linear, 22-pole ion trap at 6 K were performed.²⁴ Cooling molecules to cryogenic temperature significantly reduces the population of excited vibrational states, which in turn suppresses thermal congestion arising mainly from the presence of vibrational hot bands. Resolved transitions in IR and UV spectra have been used for conformer selective multiple-resonance IR-UV,²⁵⁻²⁷ UV-UV,²⁸⁻³⁰ IR-IR,³¹⁻³³ and even IR-IR-UV³⁴⁻³⁶ spectroscopy. Thus, CIS allows for a significant reduction or even complete elimination of inhomogeneous spectral broadening. Moreover, at cryogenic temperatures, non-covalent complexes with H₂, D₂, or even He can be formed.³⁷⁻⁴⁰ These so-called tags have little/almost no effect on the structure of biomolecular ions and can be used for single-photon IR predissociation spectroscopy. This kind of spectroscopy is particularly convenient, when a

molecule of interest does not have a UV chromophore or its UV spectrum is vibrationally unresolved. Highly resolved conformer-selective IR spectra provided by CIS can be used for stringent validation of the 3D structure of individual conformers in the gas phase.

Unlike ion mobility, where a 3D structure of molecules is calculated based on their average collision cross-section,⁴¹ spectroscopy measures the energy and intensity of optical transitions between quantum states of molecules, which are extremely sensitive to the spatial arrangement of atoms, and therefore reflect the molecular structure.⁴² Advances in computational chemistry and the exponential growth of computational power have made it possible to calculate the structures and vibrational spectra of relatively large molecules using high-level quantum chemistry methods. Comparing the experimental vibrational spectrum with the calculated ones may provide rigorous and unambiguous validation of the molecular structure. To date, the largest biomolecule with a validated structure in the gas phase remains decapeptide gramicidin s and its doubly hydrated non-covalent complex.^{43,44} Further increasing the molecular size brings some challenges from both experimental and theoretical perspectives, although it still remains feasible to determine the main structural motives of such biomolecules.

The structures of biomolecules isolated from noncovalent interactions in the gas phase are conventionally called intrinsic structures, while the geometries that biomolecules adopt in aqueous solutions prior electrospraying, are often termed in the field of mass spectrometry as native structures.⁴⁵ Despite the success of CIS in solving intrinsic structures of small to midsize biomolecules, there is an ongoing debate about the relevance of these structures to the native ones. The vast majority of biochemical processes occur in water and its solutes, where the 3D structure, properties, and functionality of biomolecules greatly depend on the intermolecular non-covalent interactions. While the main structural motifs of large biomolecules, such as proteins, can be preserved during the transition into the gas phase, the gas-phase structure of small biomolecules can differ significantly from their geometries in aqueous solutions. A notable example is amino acids, which adopt a zwitterion structure with a protonated N-terminus and deprotonated C-terminus at physiological conditions, whereas in the gas phase they adopt canonical structure.⁴⁶ However, the practical value of these gas-phase structures for life science applications is fairly limited.

To bridge the gap between the native structures of biomolecules and their gas phase or intrinsic structures, one can study microhydrated biomolecules in the gas phase. By retaining a limited number of water molecules on the biomolecular ion, the main native structural features, potentially, can be preserved. Furthermore, precisely controlled level of hydration provides an opportunity to investigate in the gas phase the effect of individual water molecules on the

structure and properties of biomolecular ions at fundamental level. Cryogenic IM-MS, developed by D. Russel and colleagues, is an elegant technique that enables rapid evaluation of the number of water molecules required for structural rearrangements in a hydrated biomolecular ion.^{47,48} CIS in combination with quantum-chemical calculations provides a mean of stringent structural assignment. This approach, however, has its limitations, which are worth mentioning. As the size of the complex increases, the IR spectra become more congested, making structural assignment more challenging. Additionally, structural calculations become more complex for microhydrated molecules due to the labile nature of non-covalent complexes and the need to sample a larger conformational space. There is no exact number of the retained water molecules required to protect the native structure of a biomolecule or, at least, to preserve its main structural features. If these numbers are sufficiently small, the experimental spectra may conserve certain level of vibrational resolution and calculations remain feasible to solve the “native-like” structure of the biomolecule. Additional experimental and computational techniques, such as isotope labeling, chemical substitutions, targeting conformational search, etc. help in this to some extent.

The first practical task in studying microhydrated biomolecules is how to prepare them. In fact, this is not a simple and straightforward process, and it required some prior investigation and design of a special electrospray ionization (ESI) source, as described in this thesis below.

Microsolvated ions in the gas phase can be generated by two fundamentally different methods. The first method involves a gentle transfer of microsolvated ions directly from the solution using ESI. Conventional ESI implies the formation of charged droplets that undergo a series of solvent evaporation and Coulomb fission events until bare ions are formed. During ESI the ions with retained solvent molecules can be preserved and transferred into the gas phase. While this method may appear simple, it requires a careful control of ESI conditions and fine-tuned, low-activation ion optics. Currently, there are no commercially available ion sources designed specifically for generating microsolvated ions, and only a few independent scientific groups have developed home-build ion sources capable of retaining microsolvated ions after ESI.⁴⁹⁻⁵¹ The lack of detailed design and characterization of these ion sources limits their wider adoption, dissemination, and further improvements.

Another method for producing microsolvated ions involves condensation of solvent molecules onto bare ions in the gas phase.⁵²⁻⁵⁴ In this approach, any ionization technique can be used to produce fully desolvated bare ions. Once the bare ions are produced, they need to be stored in a trap and cooled down to cryogenic temperatures to enable solvent condensation. The ions are cooled in collisions with He or N₂ buffer gas in the temperature-controlled ion

trap. A small stream of the buffer gas mixed with solvent vapor is introduced into the trap to facilitate cooling and condensation.

These two methods of producing microsolvated ions with retained and condensed solvent molecules can, potentially, lead to complexes with different 3D structures. Microhydrated ions produced directly from an ESI source initially retain their native structure from the solution. The transition to the gas phase at room temperature involves water evaporation, which automatically leads to evaporative cooling of the microhydrated ions. This cooling can be quite significant. For instance, protonated water clusters stored in a room temperature ion trap are cooled to temperatures of 130-170 K under the typical experimental conditions.⁵⁵⁻⁵⁷ At such low temperature, conformational rearrangements may slow down, which leads to kinetic trapping of the ions in solution structures. For microhydrated ions produced by condensation, the situation is somewhat reversed. During and right after the ESI process the hydrated biomolecular ions are collisionally heated, typically to above room temperature, to fully boil off the surrounding water envelope. Under such harsh conditions a bare ion may have a high chance to overcome some structural barriers to stabilize in a gas-phase conformational state. Depending on the particular conditions (pressure, temperature, and time) of the subsequent transfer of the ions but before their cooling, these conformers may appear in the global energy minimum as intrinsic structures, but also become kinetically trapped in local energy minima. A rapid non-adiabatic cooling to cryogenic temperature can eventually “freeze” the ions in these structures, such that the subsequent condensation of water molecules may not restore the native geometry of the ions. Although these kinetically trapped structures are typically not the primary focus of interest, they provide valuable insights into the behavior of biomolecules in the gas phase.

Both, retention and condensation approaches have been employed for producing microhydrated biomolecules since a long time, although rarely the same molecular system were addressed by the two methods. One example is a recent spectroscopic study of microhydrated glycine produced by condensation in the group of Garand and by retention in our laboratory.⁵⁸⁻⁶⁰ Certain differences in spectroscopy of the same microhydrated GlyH⁺, produced by the two methods were detected. The spectral differences could be explained by a difference in conformational distribution of the embedded ions, but also by different spectroscopic techniques and conditions in “spectroscopic” cryogenic ion traps. To resolve this ambiguity, both types of complexes are to be probed on the same instrument. To the best of our knowledge, so far nobody could do such measurements due to the lack of the required two source of hydrated biomolecular ions interfaced to the same cold ion spectroscopy instrument. Therefore,

validating the hypothesis of structural differences in complexes produced by different methods under nearly identical conditions requires an ion source capable of producing microhydrated ions with both retained and condensed water molecules. Design, construction, testing, and use of such ion source interfaced with our cold ion spectroscopy instrument was one of the objectives of my PhD project described in this thesis.

Chapter 2 provides an overview of the experimental setup used throughout this work. It includes a description of the latest version of the ion source, which enables the generation of ions with retained or condensed solvent molecules, the main features of the tandem mass spectrometer, the optical layout, and how everything works together during a typical experiment.

Chapter 3 gives a detailed description and characterization of our “gentle” nano-electrospray ion source, which is based on a triple molecular skimmer scheme. This ion source is thoroughly described and characterized, showcasing its efficiency and reliability in generating microsolvated ions with retained solvent molecules. Additionally, the ion source can be easily re-optimized to produce bare ions, with performance and short-term stability comparable, for instance, to our commercial ion funnel-based source.

Chapter 4 is dedicated to the study of microhydrated amino acid arginine, $\text{ArgH}^+(\text{H}_2\text{O})_n$ ($n = 1-5$). Experimental spectra of microhydrated arginine produced by retaining water molecules, together with quantum chemistry calculations (performed by our partners), are employed to explain the previously revealed discrepancy between the predicted and experimentally observed number of water molecules required to stabilize the salt bridge structure of arginine in the gas phase.

Chapter 5 describes how comparison of the spectra measured for the complexes generated by retention and by condensation assist in the conformational search of the truly present in the experiment structures among many computed low-energy conformers of tryptophan hydrated by up to 6 water molecules. The pairs of IR and/or UV spectra measured for $\text{TrpH}^+(\text{H}_2\text{O})_n$ ($n = 1-6$) complexes that were generated by the two methods of microhydration appeared to be almost identical. This observation implies lack of kinetically-trapped structures in the experiment, such that the observed conformers could be search among the lowest energy structures only.

Chapter 6 documents our efforts in pushing the limits of cold ion spectroscopy toward the molecules as large as proteins. A small protein ubiquitin and its microhydrated complexes were spectroscopically studied across various charge states and under different ionization conditions. Cold ion UV and IR spectroscopy allows us to distinguish the folded and unfolded

conformations of ubiquitin. We put forward a hypothesis that even a few water molecules remaining on the protein at the moment of spectroscopic interrogation indicate that, after ESI ubiquitin was always hydrated and therefore experienced an evaporative cooling. This “auto” cooling allows conserving the folded, native-like configuration of the protein before its complete freezing at 10 K in the cryogenic trap.

Chapter 7 reports our very latest spectroscopic study of ubiquitin. Here we employ water retention and water condensation to verify whether the native-like folded structure of the molecule can be restored by condensing water molecules onto the unfolded structure. The results indicate that the condensation of water molecules does not fold the protein back into its native-like conformation.

Chapter 8 concludes this thesis by summarizing the main findings and contributions of conducted research. It also provides an outlook for the future development and application of cold ion spectroscopy of non-covalent complexes and cold ion spectroscopy in general, highlighting potential areas for further investigation and advancement.

References

1. Nakane, T. *et al.* Single-particle cryo-EM at atomic resolution. *Nature* **587**, 152–156 (2020).
2. Rizzo, T. R., Stearns, J. A. & Boyarkin, O. V. Spectroscopic studies of cold, gas-phase biomolecular ions. *Int. Rev. Phys. Chem.* **28**, 481–515 (2009).
3. Rizzo, T. R., Park, Y. D. & Levy, D. H. A molecular beam of tryptophan. *J. Am. Chem. Soc.* **107**, 277–278 (1985).
4. Rizzo, T. R., Park, Y. D., Peteanu, L. & Levy, D. H. Electronic spectrum of the amino acid tryptophan cooled in a supersonic molecular beam. *J. Chem. Phys.* **83**, 4819–4820 (1985).
5. Rizzo, T. R., Park, Y. D., Peteanu, L. A. & Levy, D. H. The electronic spectrum of the amino acid tryptophan in the gas phase. *J. Chem. Phys.* **84**, 2534–2541 (1985).
6. Rizzo, T. R., Park, Y. D. & Levy, D. H. Dispersed fluorescence of jet-cooled tryptophan: Excited state conformers and intramolecular exciplex formation. *J. Chem. Phys.* **85**, 6945–6951 (1986).
7. Philips, L. A. & Levy, D. H. Rotationally resolved electronic spectroscopy of tryptamine conformers in a supersonic jet. *J. Chem. Phys.* **89**, 85–90 (1988).
8. Park, Y. D., Rizzo, T. R., Peteanu, L. A. & Levy, D. H. Electronic spectroscopy of tryptophan analogs in supersonic jets: 3-Indole acetic acid, 3-indole propionic acid, tryptamine, and N-acetyl tryptophan ethyl ester. *J. Chem. Phys.* **84**, 6539–6549 (1986).
9. Peteanu, L. A. & Levy, D. H. Spectroscopy of complexes of tryptamine and 3-indolepropionic acid with various solvents. *J. Phys. Chem.* **92**, 6554–6561 (1988).
10. Cable, J. R., Tubergen, M. J. & Levy, D. H. The electronic spectra of small peptides in the gas phase. *Faraday Discuss. Chem. Soc.* **86**, 143 (1988).
11. Cable, J. R., Tubergen, M. J. & Levy, D. H. Laser Desorption Molecular Beam Spectroscopy: The Electronic Spectra of Tryptophan Peptides in the Gas Phase. *J. Am. Chem. Soc.* **109**, 6198–6199 (1987).
12. Cable, J. R., Tubergen, M. J. & Levy, D. H. Electronic Spectroscopy of Small Tryptophan Peptides in Supersonic Molecular Beams. *J. Am. Chem. Soc.* **110**, 7349–7355 (1988).
13. Cable, J. R., Tubergen, M. J. & Levy, D. H. Fluorescence Spectroscopy of Jet-Cooled Tryptophan Peptides. *J. Am. Chem. Soc.* **111**, 9032–9039 (1989).
14. Chin, W. *et al.* Spectroscopic evidence for gas-phase formation of successive β -turns in

- a three-residue peptide chain. *J. Am. Chem. Soc.* **127**, 1388–1389 (2005).
15. Chin, W. *et al.* Intrinsic folding of small peptide chains: Spectroscopic evidence for the formation of β -turns in the gas phase. *J. Am. Chem. Soc.* **127**, 707–712 (2005).
 16. Abo-Riziq, A., Crews, B. O., Callahan, M. P., Grace, L. & De Vries, M. S. Spectroscopy of isolated gramicidin peptides. *Angew. Chem. Int. Ed.* **45**, 5166–5169 (2006).
 17. De Vries, M. S. & Hobza, P. Gas-phase spectroscopy of biomolecular building blocks. *Annu. Rev. Phys. Chem.* **58**, 585–612 (2007).
 18. Unterberg, C., Gerlach, A., Schrader, T. & Gerhards, M. Structure of the protected dipeptide Ac-Val-Phe-OMe in the gas phase: Towards a β -sheet model system. *J. Chem. Phys.* **118**, 8296–8300 (2003).
 19. Karas, M., Bachmann, D., Bahr, U. & Hillenkamp, F. Matrix-assisted ultraviolet laser desorption of non-volatile compounds. *Int. J. Mass Spectrom. Ion Process.* **78**, 53–68 (1987).
 20. Karas, M. & Hillenkamp, F. Laser Desorption Ionization of Proteins with Molecular Masses Exceeding 10 000 Daltons. *Anal. Chem.* **60**, 2299–2301 (1988).
 21. Fenn, J. B., Mann, M., Meng, C. K., Wong, S. F. & Whitehouse, C. M. Electrospray ionization—principles and practice. *Mass Spectrom. Rev.* **9**, 37–70 (1990).
 22. Fenn, J. B., Mann, M., Meng, C. K., Wong, S. F. & Whitehouse, C. M. Electrospray ionization for mass spectrometry of large biomolecules. *Science.* **246**, 64–71 (1989).
 23. Nolting, D., Marian, C. & Weinkauff, R. Protonation effect on the electronic spectrum of tryptophan in the gas phase. *Phys. Chem. Chem. Phys.* **6**, 2633–2640 (2004).
 24. Boyarkin, O. V., Mercier, S. R., Kamariotis, A. & Rizzo, T. R. Electronic spectroscopy of cold, protonated tryptophan and tyrosine. *J. Am. Chem. Soc.* **128**, 2816–2817 (2006).
 25. Chin, W. *et al.* Gas phase formation of a 3_{10} -helix in a three-residue peptide chain: Role of side chain-backbone interactions as evidenced by IR-UV double resonance experiments. *J. Am. Chem. Soc.* **127**, 11900–11901 (2005).
 26. Nagornova, N. S., Rizzo, T. R. & Boyarkin, O. V. Exploring the Mechanism of IR-UV Double-Resonance for Quantitative Spectroscopy of Protonated Polypeptides and Proteins. *Angew. Chemie* **125**, 6118–6121 (2013).
 27. Burke, N. L., Redwine, J. G., Dean, J. C., Mcluckey, S. A. & Zwier, T. S. UV and IR spectroscopy of cold protonated leucine enkephalin. *Int. J. Mass Spectrom.* **378**, 196–205 (2015).
 28. Hünig, I., Seefeld, K. A. & Kleinerhanns, K. REMPI and UV-UV double resonance spectroscopy of tryptophan ethylester and the dipeptides tryptophan-serine, glycine-

- tryptophan and proline-tryptophan. *Chem. Phys. Lett.* **369**, 173–179 (2003).
29. Wako, H. *et al.* A conformational study of protonated noradrenaline by UV–UV and IR dip double resonance laser spectroscopy combined with an electrospray and a cold ion trap method. *Phys. Chem. Chem. Phys.* **19**, 10777–10785 (2017).
 30. Ishiuchi, S. ichi, Wako, H., Kato, D. & Fujii, M. High-cooling-efficiency cryogenic quadrupole ion trap and UV-UV hole burning spectroscopy of protonated tyrosine. *J. Mol. Spectrosc.* **332**, 45–51 (2017).
 31. Leavitt, C. M. *et al.* Isomer-specific IR-IR double resonance spectroscopy of D 2-tagged protonated dipeptides prepared in a cryogenic ion trap. *J. Phys. Chem. Lett.* **3**, 1099–1105 (2012).
 32. Warnke, S., Ben Faleh, A., Pellegrinelli, R. P., Yalovenko, N. & Rizzo, T. R. Combining ultra-high resolution ion mobility spectrometry with cryogenic IR spectroscopy for the study of biomolecular ions. *Faraday Discuss.* **217**, 114–125 (2019).
 33. Yang, N., Duong, C. H., Kelleher, P. J., Johnson, M. A. & McCoy, A. B. Isolation of site-specific anharmonicities of individual water molecules in the I⁺·(H₂O)₂ complex using tag-free, isotopomer selective IR-IR double resonance. *Chem. Phys. Lett.* **690**, 159–171 (2017).
 34. Shubert, V. A. & Zwier, T. S. IR-IR-UV hole-burning: Conformation specific IR spectra in the face of UV spectral overlap. *J. Phys. Chem. A* **111**, 13283–13286 (2007).
 35. Pereverzev, A. Y. *et al.* Vibrational Signatures of Conformer-Specific Intramolecular Interactions in Protonated Tryptophan. *J. Phys. Chem. A* **120**, 5598–5608 (2016).
 36. Pereverzev, A. Y., Kopysov, V. N. & Boyarkin, O. V. Peptide Bond Ultraviolet Absorption Enables Vibrational Cold-Ion Spectroscopy of Nonaromatic Peptides. *J. Phys. Chem. Lett.* **9**, 5262–5266 (2018).
 37. DePalma, J. W., Kelleher, P. J., Tavares, L. C. & Johnson, M. A. Coordination-Dependent Spectroscopic Signatures of Divalent Metal Ion Binding to Carboxylate Head Groups: H₂- and He-Tagged Vibrational Spectra of M²⁺·RCO₂⁻ (M = Mg and Ca, R = -CD₃, -CD₂CD₃) Complexes. *J. Phys. Chem. Lett.* **8**, 484–488 (2017).
 38. Johnson, C. J. *et al.* Communication: He-tagged vibrational spectra of the SarGlyH⁺ and H⁺(H₂O)_{2,3} ions: Quantifying tag effects in cryogenic ion vibrational predissociation (CIVP) spectroscopy. *J. Chem. Phys.* **140**, 221101 (2014).
 39. Kamrath, M. Z. *et al.* Vibrational characterization of simple peptides using cryogenic infrared photodissociation of H₂-tagged, mass-selected ions. *J. Am. Chem. Soc.* **133**, 6440–6448 (2011).

40. Garand, E. *et al.* Determination of noncovalent docking by infrared spectroscopy of cold gas-phase complexes. *Science*. **335**, 694–698 (2012).
41. Laphorn, C., Pullen, F. & Chowdhry, B. Z. Ion mobility spectrometry-mass spectrometry (IMS-MS) of small molecules: Separating and assigning structures to ions. *Mass Spectrom. Rev.* **32**, 43–71 (2013).
42. Boyarkin, O. V. Cold ion spectroscopy for structural identifications of biomolecules. *Int. Rev. Phys. Chem.* **37**, 559–606 (2018).
43. Roy, T. K. *et al.* Conformational structures of a decapeptide validated by first principles calculations and cold ion spectroscopy. *ChemPhysChem* **16**, 1374–1378 (2015).
44. Roy, T. K., Nagornova, N. S., Boyarkin, O. V. & Gerber, R. B. A Decapeptide Hydrated by Two Waters: Conformers Determined by Theory and Validated by Cold Ion Spectroscopy. *J. Phys. Chem. A* **121**, 9401–9408 (2017).
45. Leney, A. C. & Heck, A. J. R. Native Mass Spectrometry: What is in the Name? *J. Am. Soc. Mass Spectrom.* **28**, 5–13 (2017).
46. Wytttenbach, T., Witt, M. & Bowers, M. T. On the stability of amino acid zwitterions in the gas phase: The influence of derivatization, proton affinity, and alkali ion addition. *J. Am. Chem. Soc.* **122**, 3458–3464 (2000).
47. Servage, K. A., Silveira, J. A., Fort, K. L. & Russell, D. H. Cryogenic Ion Mobility-Mass Spectrometry: Tracking Ion Structure from Solution to the Gas Phase. *Acc. Chem. Res.* **49**, 1421–1428 (2016).
48. Hebert, M. J. & Russell, D. H. Tracking the Structural Evolution of 4-Aminobenzoic Acid in the Transition from Solution to the Gas Phase. *J. Phys. Chem. B* **124**, 2081–2087 (2020).
49. Stachl, C. N. & Williams, E. R. Effects of Temperature on Cs+(H₂O)₂₀Clathrate Structure. *J. Phys. Chem. Lett.* **11**, 6127–6132 (2020).
50. Silveira, J. A., Servage, K. A., Gamage, C. M. & Russell, D. H. Cryogenic ion mobility-mass spectrometry captures hydrated ions produced during electrospray ionization. *J. Phys. Chem. A* **117**, 953–961 (2013).
51. Yang, N., Duong, C. H., Kelleher, P. J., McCoy, A. B. & Johnson, M. A. Deconstructing water’s diffuse OH stretching vibrational spectrum with cold clusters. *Science (80-.)*. **364**, 275–278 (2019).
52. Wytttenbach, T. & Bowers, M. T. Hydration of biomolecules. *Chem. Phys. Lett.* **480**, 1–16 (2009).
53. Marsh, B. M., Voss, J. M. & Garand, E. A dual cryogenic ion trap spectrometer for the

- formation and characterization of solvated ionic clusters. *J. Chem. Phys.* **143**, 204201 (2015).
54. Hirata, K., Haddad, F., Dopfer, O., Ishiuchi, S. I. & Fujii, M. Collision-assisted stripping for determination of microsolvation-dependent protonation sites in hydrated clusters by cryogenic ion trap infrared spectroscopy: the case of benzocaineH + (H₂O)_n. *Phys. Chem. Chem. Phys.* **24**, 5774–5779 (2022).
 55. Schmidt, M. & Von Issendorff, B. Gas-phase calorimetry of protonated water clusters. *J. Chem. Phys.* **136**, 164307 (2012).
 56. Lee, S. W., Freivogel, P., Schindler, T. & Beauchamp, J. L. Freeze-dried biomolecules: FT-ICR studies of the specific solvation of functional groups and clathrate formation observed by the slow evaporation of water from hydrated peptides and model compounds in the gas phase. *J. Am. Chem. Soc.* **120**, 11758–11765 (1998).
 57. Schindler, T., Berg, C., Niedner-Schatteburg, G. & Bondybey, V. E. Solvation of hydrochloric acid in protonated water clusters. *Chem. Phys. Lett.* **229**, 57–64 (1994).
 58. Fischer, K. C., Voss, J. M., Zhou, J. & Garand, E. Probing Solvation-Induced Structural Changes in Conformationally Flexible Peptides: IR Spectroscopy of Gly 3 H + ·(H₂O). *J. Phys. Chem. A* **122**, 8213–8221 (2018).
 59. Saparbaev, E., Aladinskaia, V., Zviagin, A. & Boyarkin, O. V. Microhydration of Biomolecules: Revealing the Native Structures by Cold Ion IR Spectroscopy. *J. Phys. Chem. Lett.* **12**, 907–911 (2021).
 60. Sherman, S. L., Nickson, K. A. & Garand, E. Comment on “Microhydration of Biomolecules: Revealing the Native Structures by Cold Ion IR Spectroscopy”. *J. Phys. Chem. Lett.* **13**, 2046–2050 (2022).

Chapter 2. Experimental setup

This chapter describes the experimental setup used in this work. The first part of this chapter provides a general description of the last version of the tandem mass spectrometer and its application for CIS of biomolecules in the gas phase. The second part gives an overview of the optical setup for generating the wavelength tunable IR and UV laser beams required for CIS.

2.1. Tandem mass spectrometer

Since its construction about 15 years ago, our tandem mass spectrometer has undergone many changes. Its previous versions have been described elsewhere.¹⁻⁵ During the last four years, we implemented two significant modifications of the ion source part of the instrument. These modifications were aimed at producing microsolvated complexes of biomolecular ions. The first version of our gentle ion source which allows efficient retaining of microsolvated ions during nESI is described and characterized in Chapter 3. The last version of the instrument includes the ion source that is capable of producing microsolvated ions with either retained or condensed solvent molecules. This version is schematically shown in figure 2.1.

Protonated ions are produced directly from solution by n-ESI that uses metal-coated borosilicate emitters at a typical applied voltage of 800-1500 V. The ions are transferred to the first vacuum section through a temperature-controlled stainless steel (SS) capillary (10 cm long, 0.5 mm I.D.). The rapid pressure drop is provided by three closely spaced, consecutive molecular skimmers (S1-3) with an orifice diameter of 1, 2, and 3 mm for the first, second, and third skimmer, respectively. After skimmers, the ions are transferred into the first temperature-controlled, linear octupole ion trap (pre-trap) through an octupole ion guide (O1).

This pre-trap operates at a constant pressure, which is controlled by two independent gas dosing valves. One valve supplies pure nitrogen, while the other supplies pure solvent vapors or any other chemicals which sublime in vacuum at room temperature. The pre-trap is cooled by a pulse tube cryocooler (TC4189, Lihan). The cryocoolers of this type are light and compact compared to traditional closed cycle He cryocoolers. At the same time, they are powerful enough and can cool down to 35-40 K without a thermal load, what is a significant advantage over the nitrogen cryostats with the lowest temperature of 77 K. Temperature controlled pre-trap has multiple functions which depend on the type of experiment and required ions. At room temperature, it is used for the accumulation of bare ions. At cryogenic temperatures, it can be

used either for an accumulation of microsolvated ions produced in the “gentle” mode of operation of our n-ESI source or for condensation of the solvent molecules onto the bare ions, which were generated in the “harsh” mode of the source.

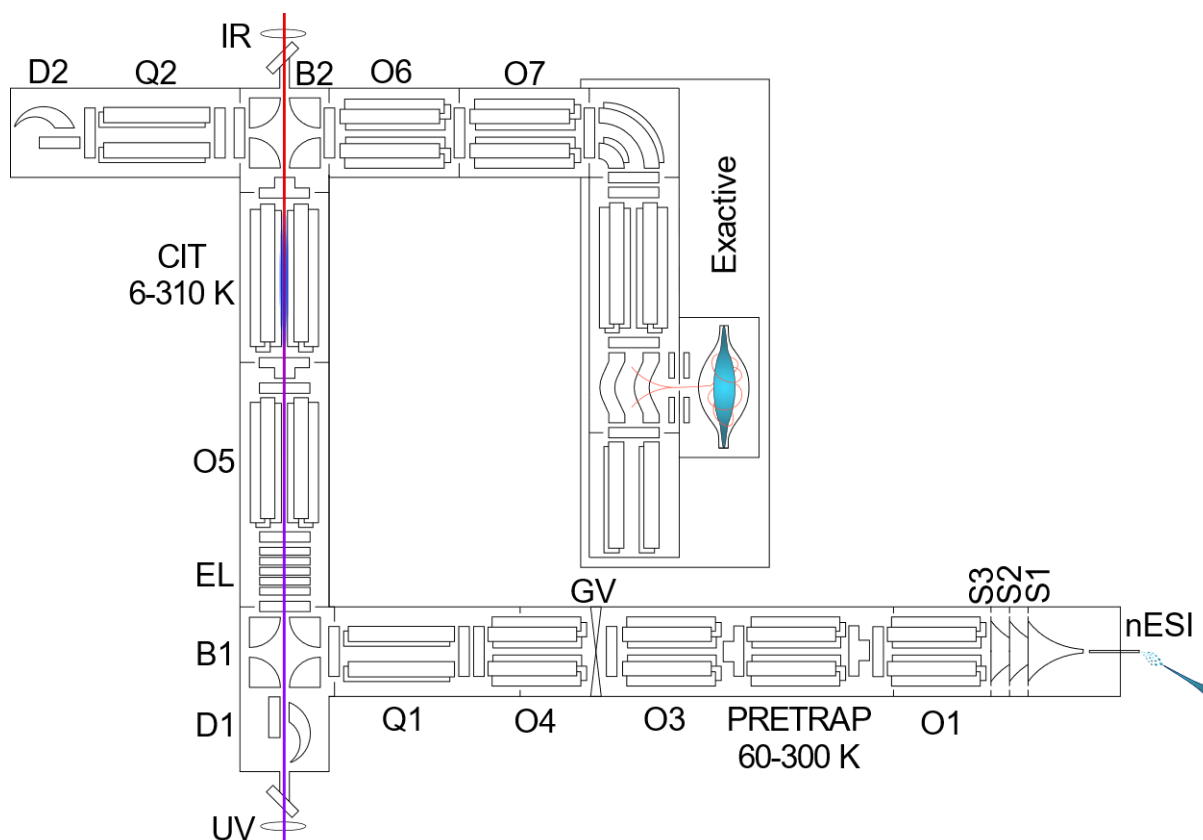


Figure 2.1. Schematic view of the tandem mass spectrometer for spectroscopy of cryogenically cooled ions.

Once the ions are released from the pre-trap, they are mass-selected by a quadrupole mass filter (Q1) (Extrel), 90° steered by an electrostatic quadrupole bender (B1), decelerated and focused by a stack of five electrostatic lenses (EL), and guided into a linear cold octupole ion trap (CIT). This trap is cooled by a two-stage closed-cycle cryocooler (RDK-408, Sumitomo) to a temperature of 6 K. The ions are trapped and cooled by collisions with He buffer gas, which is seeded by a pulse solenoid valve. The cooling happens during the hundreds of microseconds to the vibrational temperature of ≈ 10 K.^{6,7} The cold ions are interrogated by IR, UV, or IR-UV laser pulses which counter-propagate along the axis of CIT. Absorption of the photons induces photofragmentation of the ions. The resulting parent and fragment ions are guided to the second quadrupole mass filter (Q2) (Extrel) equipped with a channeltron detector (D2). The signal from the channeltron is counted by a photon counter (SR400, SRS Inc) and transmitted to a PC with a data acquisition program written in LabView software. Alternatively, the ions can be detected by a high-resolution Orbitrap-based mass spectrometer (Exactive,

Thermo Fisher Scientific). However, under the conditions of this mass spectrometer, the solvent molecules evaporate before the mass analysis, which hinders its application in this work.

Operation of any complex instrument requires regular maintenance, and mass spectrometers are not an exception. Intensive work on the mass spectrometer leads to contamination of its ion optics, which leads to a decrease in ion transmission efficiency and an increase in signal fluctuations. This degradation requires occasional cleaning of the ion optics. To ease the access to the ion source section of the mass spectrometer which is most prone to contaminations, a gate valve (GV) was placed between the third and fourth octupole ion guides (O3 and O4). This allows us to maintain and modify the ion source section while keeping a high vacuum in the rest of the mass spectrometer.

2.1.1. Design and cooling of the cold ion trap and cold pre-trap.

Both CIT and pre-trap are linear octupole ion traps and their design is nearly identical (fig. 2.2a and 2.2b). At each of the ends, the SS electrodes are mounted to the copper collars, which, in turn, mounted onto sapphire plates. The sapphire plates are in contact with copper housing and provide electrical insulation as well as good thermal conductivity between the housing, collars, and SS endcap electrodes. The difference between these two traps is, mainly, in their length and in the way they are mounted inside the respective vacuum chambers. The length of the rods of CIT is 60 mm, while the length of the rods in the pre-trap is 100 mm. The latter is made in order to trap ions at a lower background pressure of $\sim 4 \cdot 10^{-4}$ mbar in the pre-trap, but also with the purpose of storing larger number of mass-unfiltered ions. CIT is mounted directly to the cold head of a two-stage closed-cycle 10 K cryocooler, while the pre-trap and its cryocooler are spatially separated. The pre-trap is mounted to the internal construction element of the mass spectrometer through the PEEK spacers. The cryocooler is thermally connected with the pre-trap by a 15 cm long braided copper cable. Although this connection is not ideal, it allows the cryocooler to be placed away from the pre-trap, which was necessary to minimize changes in the rest of the ion source. Figure 2.2c shows the temperature of the cold head and the pre-trap during cooling. About 3 hours is required to cool pre-trap to the ultimate temperature of 60 K in this configuration. The final difference between the temperature of the pre-trap and cold head is 15 K, and it is explained by different heating sources (heating through the PEEK spacers, background gas, black-body radiation), which increase the temperature of the pre-trap. CIT cools down to 6 K during about 50 minutes (fig. 2.2d), which is the lowest temperature of our two-stage closed-cycle cryocooler.

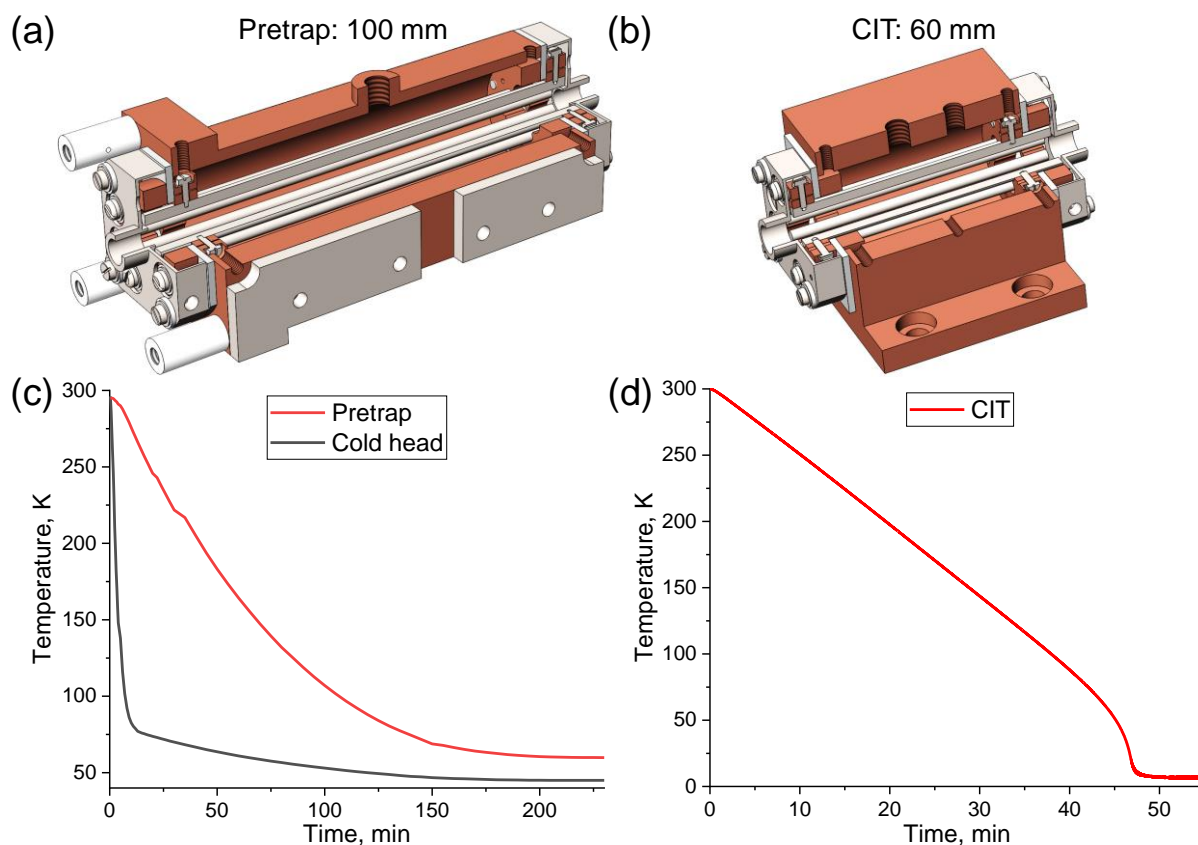


Figure 2.2. Schematic 3D view of (a) pre-trap and (b) CIT with a 90° cut and the graphs which represent the cooling time of (c) pre-trap and (d) CIT starting from room temperature.

2.1.2. Differential pumping of the Tandem Mass Spectrometer

Figure 2.3 shows a schematic view of differentially pumped vacuum stages of the tandem mass spectrometer. Table 2.1 contains information about the vacuum pumps used for different vacuum section as well as the typical pressures at idle and operating mode of the instrument. The idle pressures are the ultimate pressures when the inlet capillary and the gas valves are closed. Operating pressures are the typical pressures when the inlet capillary is open and the gas valves supply the required amount of a gas into the pre-trap and CIT to trap and cool the ions.

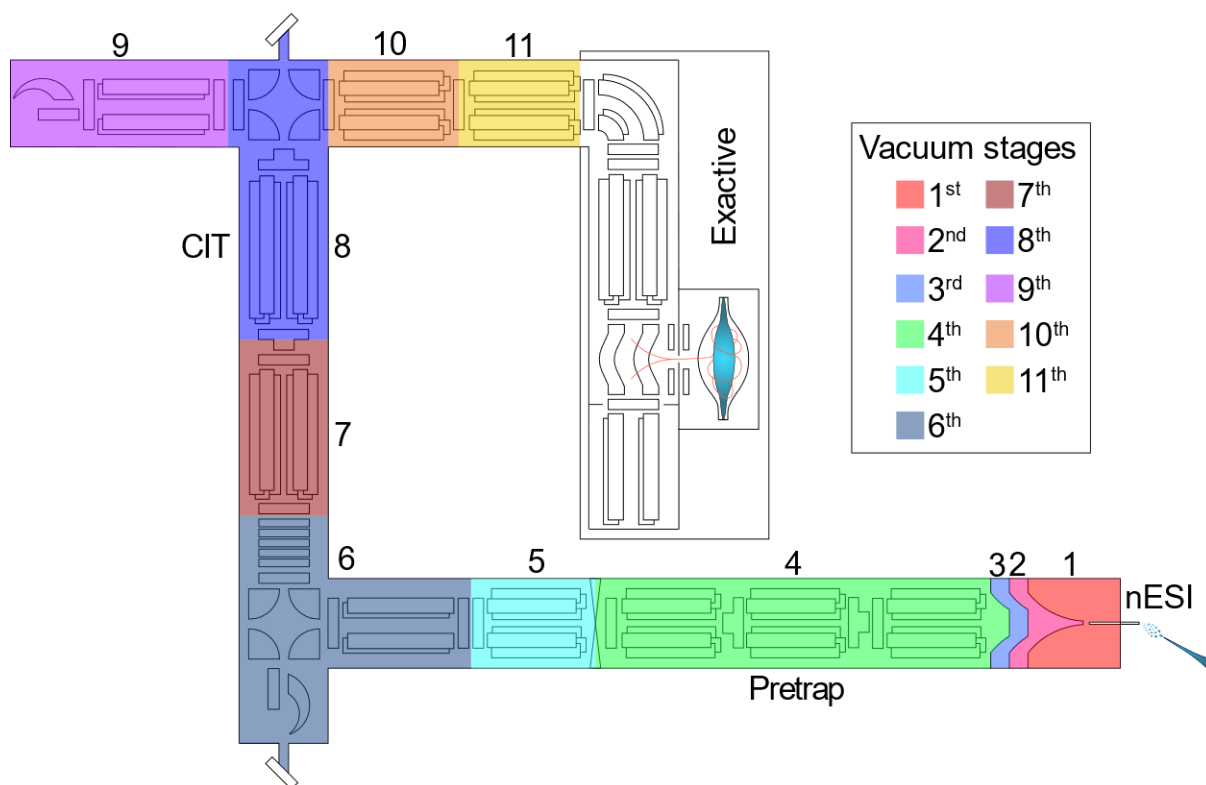


Figure 2.3. Schematic view of the differential pumping stages of the tandem mass spectrometer.

Table 2.1. Idle and operating pressures of different stages of the tandem mass spectrometer. Letters in brackets indicate the type of the pump: O – oil pump; D – dry pump; M – membrane pump; T – turbomolecular pump.

Stage	Idle pressure, mbar	Operating pressure, mbar	Vacuum pump	Fore vacuum pump
1	$6.7 \cdot 10^{-2}$	2.3	–	[O] CIT Alcatel Annecy 2033
2	$1.3 \cdot 10^{-2}$	$2.0 \cdot 10^{-1}$	–	[D] XDS 35 (Edwards)
3	$1.8 \cdot 10^{-3}$	$3.8 \cdot 10^{-3}$	[T] HiPace 300 (Pfeiffer)	[O] Duo 35 (Pfeiffer)
4	$\sim 10^{-5}$	$\sim 4 \cdot 10^{-4}$	[T] HiPace 80 (Pfeiffer)	
5	$7.3 \cdot 10^{-7}$	$4.9 \cdot 10^{-5}$	[T] TMU 521 (Pfeiffer)	[M] MVP 055-3 (Pfeiffer)
6	$9.5 \cdot 10^{-9}$	$6.7 \cdot 10^{-6}$	[T] TMU 521 Y P (Pfeiffer)	[D] nXDS 10i (Edwards)
7	$< 2 \cdot 10^{-9}$	$5.5 \cdot 10^{-6}$	[T] TMU 071 P (Pfeiffer)	
8	$< 2 \cdot 10^{-9}$	$7.1 \cdot 10^{-6}$	[T] TMU 521 (Pfeiffer)	
9	$< 2 \cdot 10^{-9}$	$1.6 \cdot 10^{-6}$	[T] HiPace 300 (Pfeiffer)	
10	$1.1 \cdot 10^{-8}$	$2.5 \cdot 10^{-6}$	[T] TMU 071 P (Pfeiffer)	
11	$6.1 \cdot 10^{-8}$	$2.7 \cdot 10^{-7}$	[T] HiPace 300 (Pfeiffer)	

2.1.1. Timing of events

Our lasers typically operate at a repetition rate of 10 Hz, while the mass spectrometer operates at 20 Hz. This allows alternating measurements of the fragment ions when the laser is on and the parent ions when the laser is off. The signal of parent ions is used for normalization of the spectrum, what excludes the influence of signal fluctuations on the spectrum. Figure 2.2. shows the timings of different events during the experimental cycle, which are controlled by multichannel pulse generators (BNC 575, Berkeley Nucleonics Corporation).

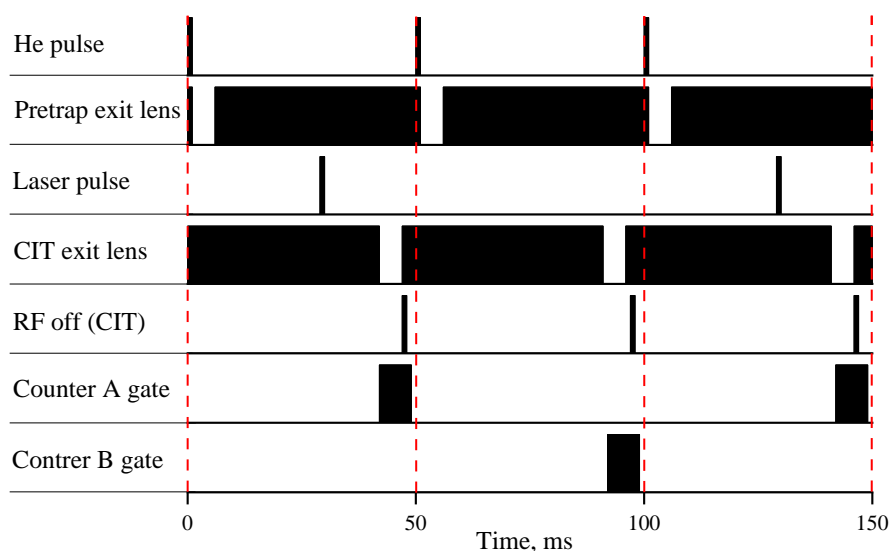


Figure 2.2. Typical time diagram of the instrument at the repetition rate of 20 Hz.

Each cycle starts with a pulse of He into CIT. He quickly thermalizes in collisions with cold walls of the trap. Shortly after, the pre-trap opens by reducing the potential at the exit lens for 5 ms. About 200 μ s later, the ions arrive into CIT, lose their energy and cool down via collisions with He buffer gas. Once the ions are cold, they are interrogated by a laser pulse or by a couple of laser pulses in the case of double resonance experiments. The exact time delay between the He gas and the laser pulses is not very important and is usually kept at 25-30 ms as a compromise between collisional deactivation of the photoactivated ions and the time allowed for photo fragmentation in the 50 ms cycle. Typically, 43 ms after the He gas pulse the CIT opens by reducing the potential at the exit lens below the trap pole bias for 5 ms. The ions are guided into Q2, which filters the fragment ions, and, subsequently, they are detected by the channeltron ion detector, equipped with conversion dinode. The signal from the channeltron is counted within gate A of the photon counter. Once the CIT is again closed, we switch off the RF waveforms applied to the rods of the CIT for 1 ms to ensure that CIT will be emptied. The subsequent cycle is laser free. During this cycle Q2 is switched to transmit the parent ions only, which are then detected by the same channeltron and counted within gate B

of the photon counter. To increase the signal-to-noise ratio, we usually average 10 measurements for each data point.

2.2. Optical setup

IR light is produced by a tunable OPO/A system (Laser Vision), pumped at repetition rate of 10 Hz by 7 ns pulses of Nd:YAG laser (Surelite III-Ex, Continuum). The energy of the pulses is ranging from 0.5-1.5 mJ at 10-6 μm range and up to 20-25 mJ in the 3 μm range. The spectral resolution of IR OPO is about 1 and 2 cm^{-1} in the spectral region of 3 and 6 μm , respectively. The beam is focused by a BaF₂ lens with a focus point located at the center of the CIT. The beam enters the mass spectrometer through a BaF₂ window (Fig. 2.1) placed at Brewster's angle (BW). A wavelength meter (WS5, HighFinesse) measures the visible wavelength of the signal wave, generated in the IR OPO with $\pm 0.2 \text{ cm}^{-1}$ accuracy. The idler wave of the OPO is used for generating tunable pulses of $\sim 3 \mu\text{m}$ wavelength through the difference mixing of this idler ($\sim 1.5 \mu\text{m}$) with the output of Nd:YAG (1064.21 nm) in the subsequent 4-crystal OPA stage. IR light in the 10-6 μm range is generated by mixing the signal ($\sim 1.5 \mu\text{m}$) and the idler ($\sim 3.5 \mu\text{m}$) of the OPA in an additional nonlinear crystal outside of the OPO/A main frame.

UV light can be produced by two different instruments: a UV OPO and a dye laser. Depending on the experiment, one instrument is preferable to the other. UV OPO (NT 340C, EKSPLA) is a widely wavelength tunable instrument, which covers 192-2600 nm spectral range, operates at 10 Hz and generates pulses of 4-11 mJ in the UV spectral region. Its spectral resolution is, however, only $\sim 5 \text{ cm}^{-1}$. In the experiments, where higher spectral resolution is required, we use a narrow linewidth (0.1 cm^{-1}) dye laser. In this case, the UV light with the energy of 1.5-2.5 mJ is produced by frequency doubling the visible output of a dye laser (HD-500, Lumonics) in a BBO (beta barium borate) crystal, using an Autotracker III (InRad) device. The dye laser is pumped by $\sim 150 \text{ mJ}$ of the third harmonic (355 nm) of a Nd:YAG laser (GCR-250, Spectra-Physics) at the repetition rate of 10 Hz. The same wavelength meter (WS5, HighFinesse) measures the visible output of the dye laser. The beam is focused by a fused silica lens 2-3 cm in front of the CIT entrance and enters the mass spectrometer through another BaF₂ window, placed at Brewster's angle.

For both IR and UV beams, the back reflections from the lenses are used to monitor the relative average power of the respective light sources by pyroelectric detectors (PEM12E, Scitec Instruments Ltd). The data from the wavelength meter and from the two pyroelectric detectors are gathered in the LabView program and used in processing the spectra.

References

1. Kamariotis, A. *et al.* Infrared spectroscopy of hydrated amino acids in the gas phase: Protonated and lithiated valine. *J. Am. Chem. Soc.* **128**, 905–916 (2006).
2. V. Boyarkin, O., R. Mercier, S., Kamariotis, A. & R. Rizzo, T. Electronic Spectroscopy of Cold, Protonated Tryptophan and Tyrosine. *J. Am. Chem. Soc.* **128**, 2816–2817 (2006).
3. Kopysov, V., Makarov, A. & V. Boyarkin, O. Colors for Molecular Masses: Fusion of Spectroscopy and Mass Spectrometry for Identification of Biomolecules. *Anal. Chem.* **87**, 4607–4611 (2015).
4. Pereverzev, A. Y. *et al.* Vibrational Signatures of Conformer-Specific Intramolecular Interactions in Protonated Tryptophan. *J. Phys. Chem. A* **120**, 5598–5608 (2016).
5. Saparbaev, E. *et al.* Identification and Quantification of Any Isoforms of Carbohydrates by 2D UV-MS Fingerprinting of Cold Ions. *Anal. Chem.* **92**, 14624–14632 (2020).
6. Boyarkin, O. V. & Kopysov, V. Cryogenically cooled octupole ion trap for spectroscopy of biomolecular ions. *Rev. Sci. Instrum.* **85**, 033105 (2014).
7. Pereverzev, A. Multilaser Conformer-Selective Spectroscopy of Cold Biomolecular Ions in the Gas Phase. (EPFL, 2017). doi:10.5075/EPFL-THESIS-8012

Chapter 3. Gentle nano-electrospray ion source for reliable and efficient generation of microsolvated ions

Disclaimer: This chapter is adapted from a published article with permission of the publisher and all co-authors.

Zviagin, A., Kopysov, V., & Boyarkin, O. V. (2022). Gentle nano-electrospray ion source for reliable and efficient generation of microsolvated ions. *Review of Scientific Instruments*, 93(11), 114104, DOI: <https://doi.org/10.1063/5.0119580>.

Personal contribution: Conceptualization, methodology, formal analysis, visualization, original draft preparation.

3.1. Abstract

We present herein the design of a nano-electrospray ion source capable of reliable generation of large quantities of microsolvated ions. The source is based on a triple molecular skimmer scheme and can be quickly tuned to generate bare ions or their ionic complexes with up to more than 100 solvent molecules retained from solution. The performance of this source is illustrated by recording the mass spectra of distributions of ionic complexes of protonated water, amino acids, and a small protein ubiquitin. Protonated water complexes with more than 110 molecules and amino acids with more than 45 water molecules could be generated. Although the commercial ion source based on the double ion funnel design with orthogonal injection, which we used in our laboratory, is more efficient in generating ions than our triple skimmer ion source, they both exhibit comparable short-term stability in generating bare ions. In return, only the new source is capable of generating microsolvated ions.

3.2. Introduction

Non-covalent ionic complexes of biomolecules with solvent molecules are of great interest in a variety of structural and analytical studies that employ mass spectrometry (MS). The structural study of microhydrated biomolecular ions allows building a bridge between their gas-phase and solution phase geometries and properties,¹⁻⁸ the complexes of biomolecules and solution tags (e.g., molecules of solvent, soluble aromatics) can be used for spectroscopic identifications of isomers,⁹⁻¹¹ the study of protonated clusters of water molecules sheds light on the structure of liquid water,^{12,13} etc. Despite many decades of research, reliable generation of large quantities of microsolvated biomolecular ions still remains a technically difficult

task.^{14,15} There are two common approaches for the production of weakly bound charged molecular complexes. In one of them, charged biomolecules are, first, produced by electrospray ionization (ESI) in the gas phase as fully desolvated species. These bare ions are then trapped and collisionally cooled in a cryogenic ion trap to which a desired solvent in the form of vapor is injected through a gas valve. The vapor condenses onto the cold ions, producing charged microsolvated biomolecules with different numbers of non-covalently bound solvent molecules.^{7,14,16,17} While technically relatively simple, the method of cryogenic condensation cannot ensure that rehydration of a fully desolvated biomolecule will reshape it back from intrinsic to native structure unless the structure is “kinetically” trapped.¹⁴ On the technical side, the injected vapor not only unavoidably condenses onto the ions but also freezes onto the electrodes of cryotrap. The formed non-conductive patches may charge and distort the performance of the trap, ultimately leading to interruption of measurements and heating the trap to evaporate the solvent.

A more “natural” approach for producing non-covalent ionic complexes is to transfer them directly from the solution phase using a sufficiently “gentle” ESI process.^{2,13,15,18} Retaining a few water molecules on a biomolecule should allow for the preservation of, at least, the main features of its native structures. Despite a few decades of study on the microsolvated biomolecules and protonated water clusters, the construction of a robust and efficient ESI source capable of reliable generation of large quantities of such non-covalent complexes directly from a solution still remains problematic. There is a subtle balance to be found and maintained between full desolvation and lack of ionization for the reliable generation of large quantities of microsolvated ions. In most common gentle ESI sources, ions enter a vacuum chamber from the atmosphere through a few cm long heated metal capillary of less than 1 mm internal diameter and subsequently pass through one or two closely spaced consecutive molecular skimmers, which work as conductance limits for differentially pumped sections of the chamber. This arrangement enables a sharp drop in pressure over the short pathway of ions to minimize energy and the number of collisions during the transportation of ions from the exit of the capillary to the high vacuum part of the chamber. We previously employed such a source, which was based on a long glass capillary and single skimmer.^{2,19} The source could produce microhydrated complexes of, for instance, a doubly protonated decapeptide with as many as 50 water molecules.³ Despite a series of successful experiments, our experience with such a source revealed its low stability and productivity, as well as high dependence of these characteristics on humidity in the laboratory. For still not fully understandable reasons, a good

distribution of clusters could be generated on rainy days only, while the use of various humidifiers did not help.

Here, we report the design of a nano-ESI source that exhibits a high stability and good efficiency in generating small to large microhydrated clusters of different charged biomolecules directly from a solution by retaining water molecules. The performance of the source is illustrated by the mass spectra of the generated distributions of microhydrated complexes. We compare some key characteristics of this gentle source with those of a commercial one based on electrodynamic ion funnels.

3.3. Instrumentation

Figure 3.1 shows the cross section of the vacuum chamber that accommodates the gentle ion source. The main feature of the chamber is the use of three differentially pumped sections separated by three inline closely spaced molecular skimmers. This arrangement allows the efficient transportation of ions in the gas flow from the atmospheric pressure ionization region to an RF octupole ion trap, which operates at a pressure of $\sim 10^{-4}$ mbar, over the distance as short as ~ 125 mm. The ions are generated from a solution by a nano-ESI (Proxeon) that uses metal coated borosilicate emitters (Thermo Fisher; emitters with “long” tip). Depending on the cut of the tip, the typical flow of the solution through these emitters is 50 to 150 nL/min with $5 \cdot 10^{-5}$ M concentration of biomolecules. The ions are transferred from the atmosphere to the first section of the source vacuum chamber through a 10 cm long stainless steel (SS) capillary of 0.5 mm I.D. All sections of the chamber are made of aluminum and vacuum-sealed together with Viton® O-rings. The capillary is mounted in a SS block, which also contains a 50 W heater cartridge and a thermocouple to control the temperature of the block within 20-170 °C. A 35 m³/h oil mechanical pump allows for maintaining the pressure of 2.5 mbar in this section. The exit of the capillary is axially aligned with the orifice of the first molecular skimmer, which separates the 1st and the 2nd sections of the source. The skimmer is a thin SS cone with an opening angle of 90° and an orifice of 1 mm diameter. The second section is pumped to 0.25 mbar pressure by a 35 m³/h dry scroll pump. Downstream, this section is limited by the 2nd molecular skimmer, glued at the base to the supporting aluminum cylinder; the glue (vacuum epoxy) also serves the purpose of insulating the skimmer electrically. The 2nd skimmer (Beam Dynamics) has a 2 mm diameter orifice and is placed 8 mm downstream from the orifice of the 1st skimmer. The 3rd vacuum section is limited by the 3rd skimmer (3 mm diameter orifice, Beam Dynamics), which is glued on top of an aluminium cone. The distance between the openings of the 2nd and 3rd skimmers is set to 15 mm, but varying it within ± 2 mm appears not

to be critical for the overall performance of the source. This section is pumped to the pressure of $5 \cdot 10^{-3}$ mbar by a 260 L/s turbomolecular pump backed by a 30 m³/h mechanical pump. The ions that pass through the orifice of the 3rd skimmer enter a 26 cm long octupole ion guide, where they can be, optionally, accumulated to increase their total number. This final octupole section of the source is equipped with a 67 L/s turbopump mounted on a tube that crosses through the 3rd section of the source. To accumulate ions, the potential of the octupole exit endcap is raised by 10-15 V above the pole bias of the ion guide for the period of accumulation. The trap opens by lowering the potential of the endcap to 1-2 V below the pole bias. The released ions are guided to a quadrupole mass filter, and, finally, the m/z-selected ions are detected by a Channeltron and counted by a gated photon counter.

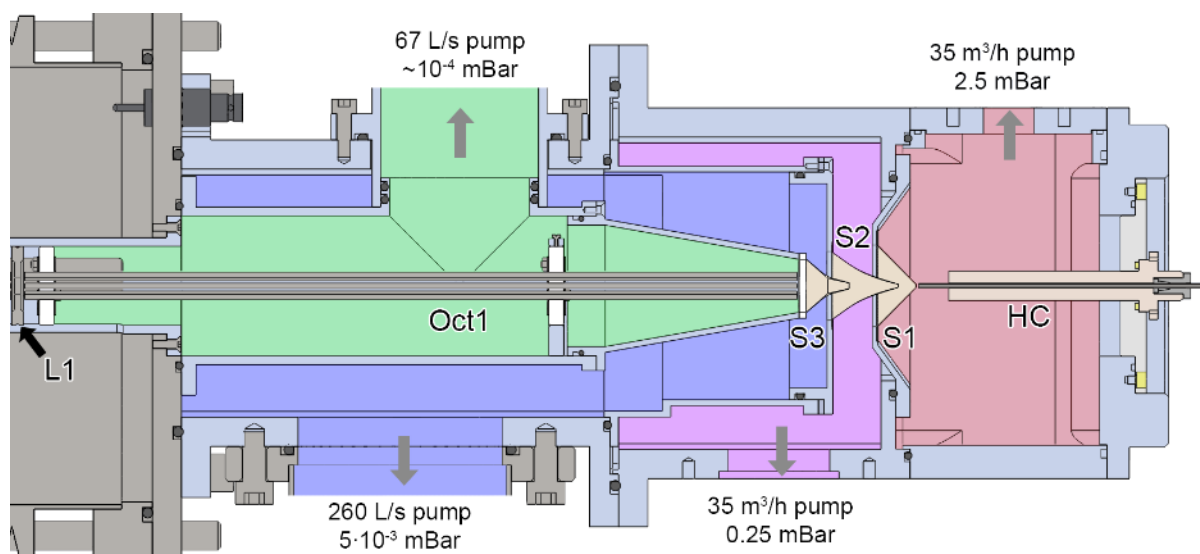


Figure 3.1. Cross section of the “gentle” ion source. The four differentially pumped sections of the source vacuum chamber are differently colored. HC – heated capillary; S1, S2, and S3 – molecular skimmers with the orifice diameters of 1, 2, and 3 mm, respectively; Oct1 – octupole ion guide/trap; and L1 – endcap electrode.

A distance of 2-3 mm between the capillary and the first skimmer appears to be optimal to balance the maximum size of microhydrated complexes and the total ion current. Shortening this distance sharply induces desolvation of ions, while increasing this spacing leads to a rapid drop in the ion current. The distribution of microsolvated ions is largely controlled by the temperature of the capillary and by its electric potential relative to the 1st skimmer. Raising this voltage slightly increases the total ion current but shifts the distribution of complexes to smaller sizes. This operation mode of the source can be used whenever retaining solvent molecules on ions is undesired. Although the ion current (or the number of trapped ions, when the pre-trap is engaged) is stable even under the dry atmosphere of our air-conditioned laboratory (relative

humidity <20 %), an elevated local air humidity in the volume between the emitter and the entrance capillary yet improves the stability of microhydrated ions. It is interesting that only the commercial humidifiers that are based on room-temperature “drying” of wet paper filters work well; neither ultrasonic-based nor heat-assisted evaporative humidifiers improve the generation of microhydrated ions.

3.4. Results and discussion

Figure 3.2 shows the mass spectra of the protonated water complexes that are produced by the new gentle ESI source from LC-MS grade water with 0.2% of acetic acid in the continuous mode of operation (no pre-trapping in the octupole ion guide). In these four measurements, all settings of the source were kept the same, except the capillary voltage and temperature. These two parameters appeared to be the important parameters for controlling the “gentleness” of the process. Fig. 3.2a shows the distribution of the protonated water complexes at the capillary temperature and voltage of $T = 150\text{ }^{\circ}\text{C}$ and $V = 60\text{ V}$, respectively. With these values, the source becomes relatively harsh such that only small complexes with the number of water molecules $n = 4\text{--}21$ are generated. Lowering the capillary temperature to $T = 50\text{ }^{\circ}\text{C}$ widens the distribution of the clusters (Fig. 3.2b), which spans now from $n \approx 11$ to $n \approx 100$ with the characteristic “magic” number $n = 21$.²⁰ The increase in the temperature of the capillary to $T = 80\text{ }^{\circ}\text{C}$ and the decrease in the potential to $V = 40\text{ V}$ narrow the distribution, but shift its maximum toward larger sizes of the clusters (Fig. 3.2c). At the softest conditions that allow stable generation of large quantities of protonated water clusters ($T = 50\text{ }^{\circ}\text{C}$, $V = 40\text{ V}$), the distribution further shifts toward very large complexes (Fig. 3.2d). The largest observed clusters contain $n \sim 110$ water molecules ($m/z = 1980\text{ Th}$); larger clusters, apparently, are generated, too, but cannot be detected due to the upper m/z limit of 2000 Th for the transmittance of our quadrupole mass filter. Overall, the average size of the clusters can be controlled by both parameters, although the width of the distribution is more sensitive to the temperature of the capillary. Other parameters such as skimmer voltages and the amplitude of RF waveforms applied to the ion guide have a minor influence on the harshness of the ion source. It is worth mentioning that the total number of the generated ions remained, roughly, almost the same for all the settings in Figure 3.2 with a slight increase for higher voltages on the capillary. Maximizing the ion signal for one particular size of the clusters with a low number of water molecules requires an increase in the capillary temperature and potential. We attribute this to the consecutive dissociation of the larger clusters, which feed the population of the smaller ones.

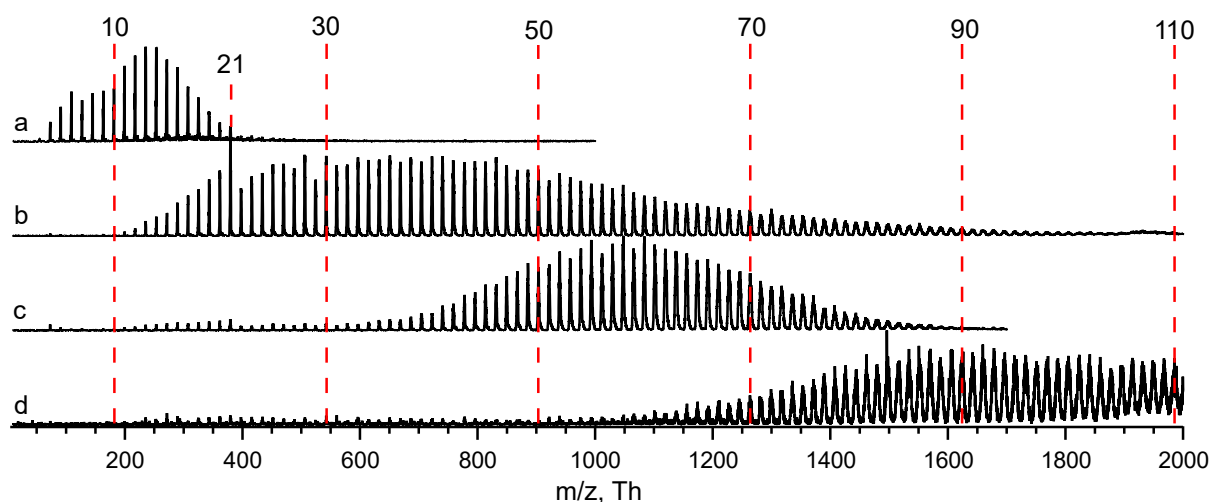


Figure 3.2. Mass spectra of protonated water complexes $(\text{H}_2\text{O})_n\text{H}^+$ generated by the nano-ESI source at the capillary temperature and the voltage of (a) 150 °C and 60 V, (b) 50 °C and 150 V, (c) 80 °C and 40 V, and (d) 50 °C and 40 V. The numbers on top indicate the number n of water molecules in the mass peaks aligned with respective vertical dashed red lines. Ions were not trapped in the octupole ion guide.

As an example, Figure 3.3 shows the distributions of microhydrated HisH^+ complexes generated by our nano-ESI source at the temperature of 130 °C and different capillary voltages. Lowering the capillary voltage gradually changes the most intense peak in the distribution from the bare ion, HisH^+ (Figure 3.3a), to the $\text{HisH}^+(\text{H}_2\text{O})_{25}$ complex (Figure 3.3e). The minor distributions in the spectra correspond to the protonated and sodiated water complexes, which are typically present in the mass spectra of microsolvated biomolecules. The mass spectra also contain low intensity peaks corresponding to dimers, trimers, and tetramers of singly protonated histidine.

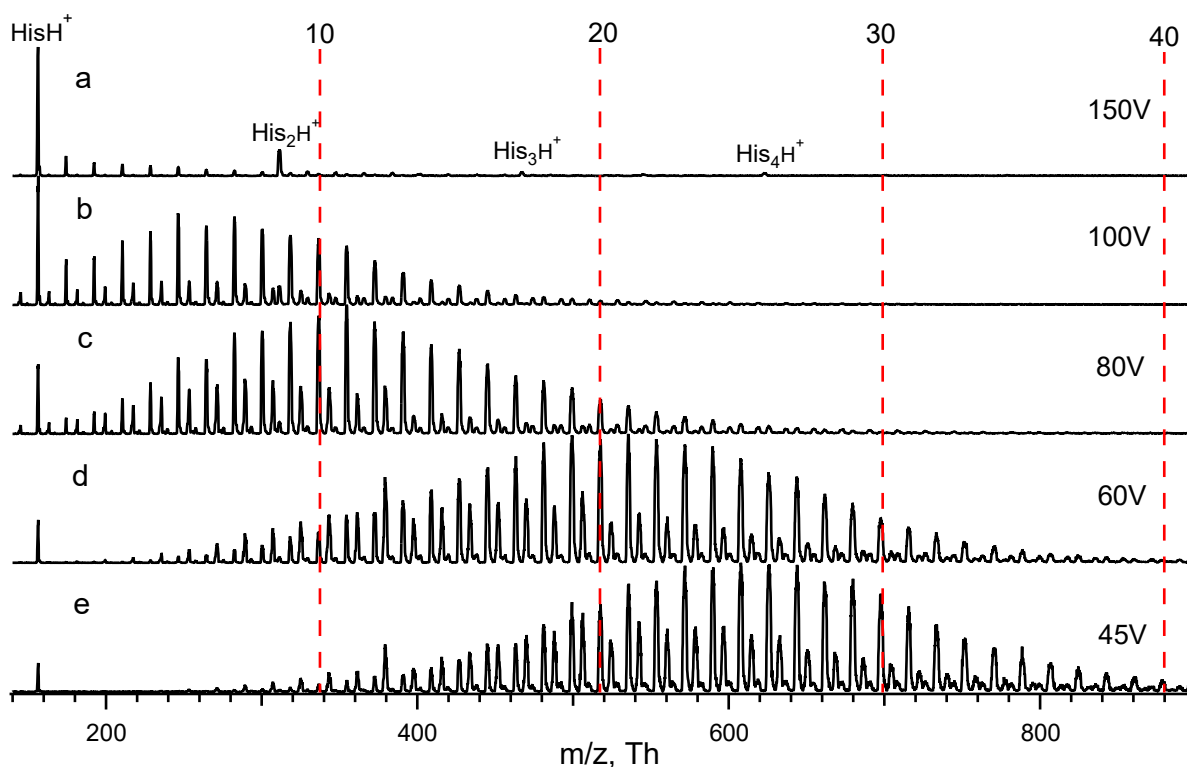


Figure 3.3. Mass spectra of microhydrated protonated amino acid $\text{HisH}^+(\text{H}_2\text{O})_n$ that are generated by the triple-skimmer nano-ESI source with different potentials of the metal capillary (labeled on the right). The numbers on top indicate the number n of water molecules in the mass peaks that are aligned with the respective vertical dashed red lines. Ions were not trapped in the octupole ion guide/trap.

Large quantities of complexes with single to several retained water molecules have been generated with the new source for larger ions such as protonated tripeptide $\text{Gly}_3\text{H}^{+5}$ and pentapeptide enkephalin (see Fig. 3.S1) and even for the small protein ubiquitin.⁶ In addition to water, other solvent molecules such as methanol, acetonitrile, and 2-butanol could be retained on carbohydrates (the former three solvents) and on lipids (the latter solvent) using the gentle mode of operation of the source.¹¹ Ultimately, by raising the capillary temperature and potential, the source can be tuned to a standard, harsh mode of operation, to generate only fully desolvated positive ions in large quantities.

In our spectroscopic experiments, we, typically, accumulate and thermalize ions by pre-trapping them at room temperature in the octupole ion guide for almost 50 ms prior to transferring the ions into a cold ion trap for performing photofragmentation. This maximum duration of pre-trapping is determined by the repetition rate of the lasers used for photofragmentation. Figure 3.4 shows a comparison of the size distributions of microhydrated complexes of amino acid ArgH^+ with and without this accumulation. The relative abundances

of the complexes were derived from the respective mass spectra. Without accumulation, the distribution of the complexes appears to be broad with the maximum at $\text{ArgH}^+(\text{H}_2\text{O})_{12}$ and with 12% abundance of the fully dehydrated amino acid. Trapping results in the evaporation of water from the complexes, which are metastable at room temperature, such that after 50 ms of accumulation, large complexes become almost fully suppressed and the whole distribution shifts toward smaller clusters. Notably, the abundance of small ($n = 1-3$) complexes increases significantly, which makes pre-trapping an advantage in studies of small complexes. In addition, the accumulation substantially reduces the fluctuations in the number of ions that can be finally trapped in the cold ion trap.

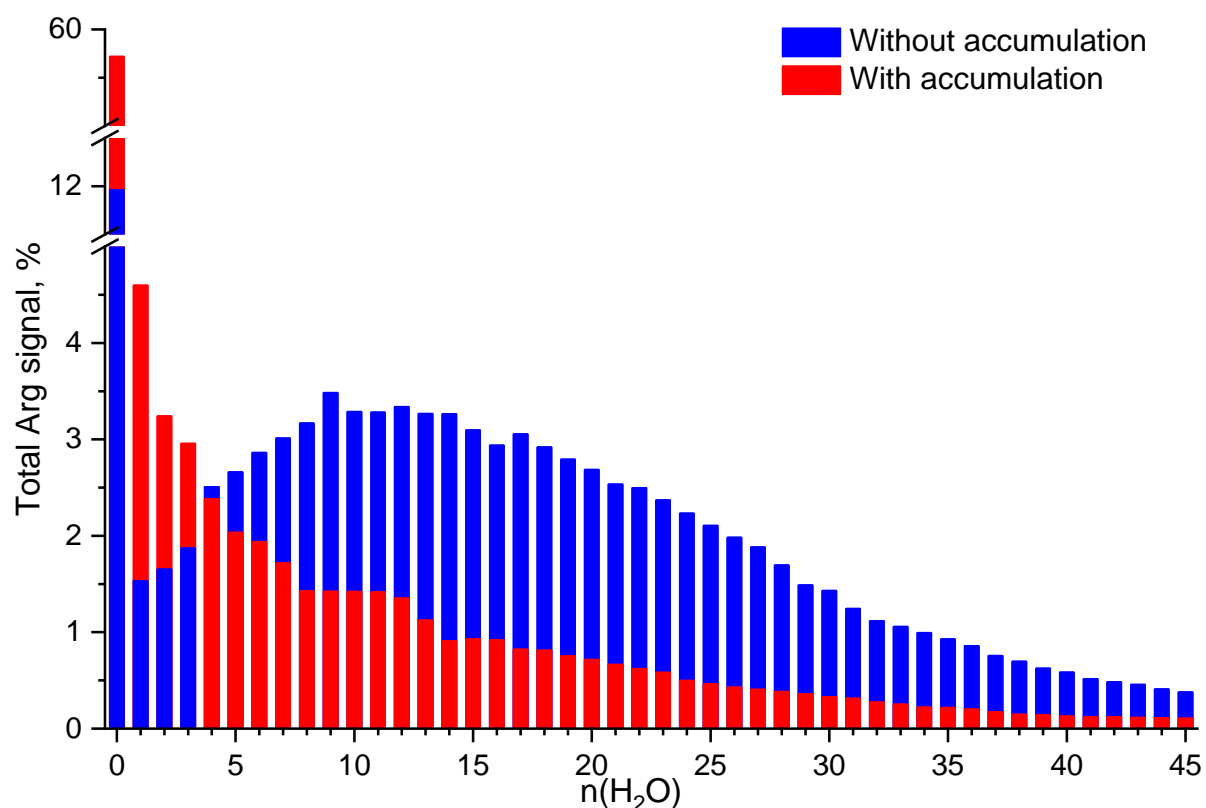


Figure 3.4. Distributions of $\text{ArgH}^+(\text{H}_2\text{O})_n$ non-covalent complexes measured with and without accumulation for almost 50 ms in the octupole ion guide.

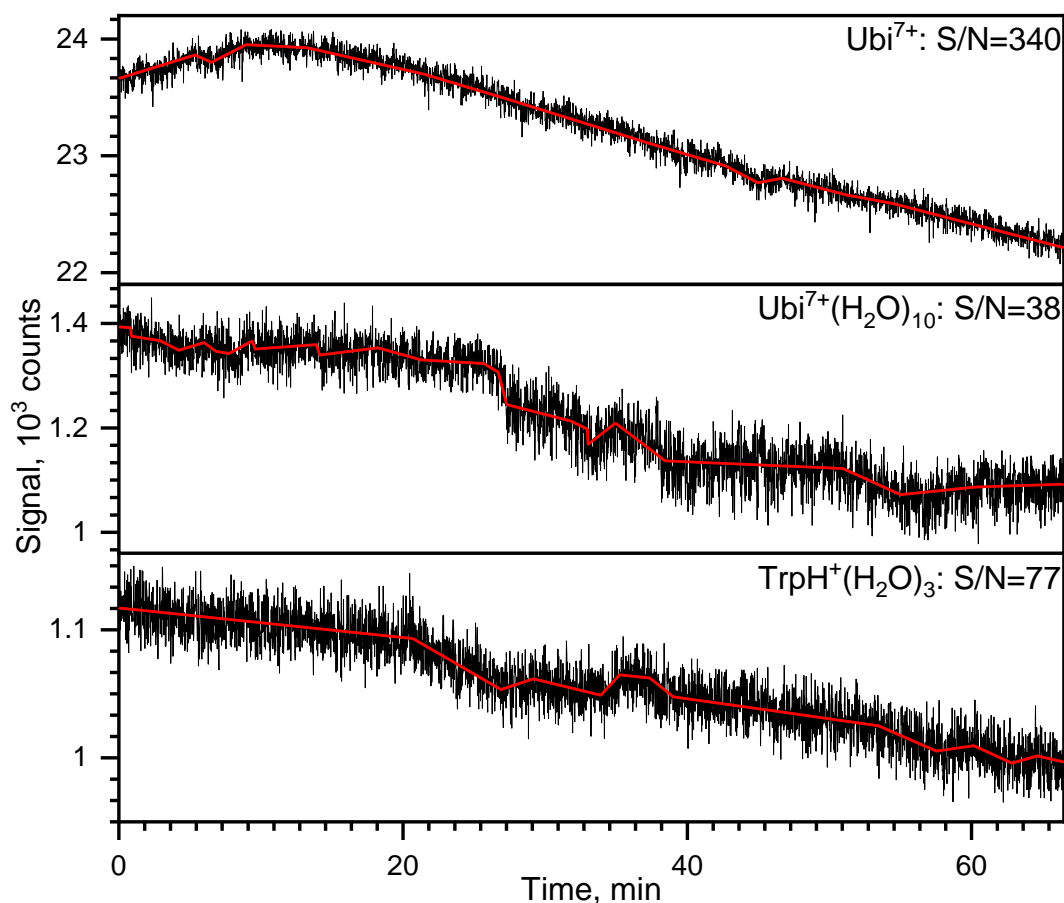


Figure 3.5. Typical time evolution of the number of parent ions generated by the new triple-skimmer nano-ESI source and counted within the 3 ms time-gate in spectroscopic experiments with (from top to bottom) with protein ubiquitin in +7 charged state (Ubi^{7+}), with $\text{Ubi}^{7+}(\text{H}_2\text{O})_{10}$ complex, and with microhydrated amino acid $\text{TrpH}^+(\text{H}_2\text{O})_3$. Each data point is an average of ten measurements; each trace (black lines) is labeled by the signal to noise ratio calculated with respect to the average (red lines).

Figure 3.5 illustrates the level and time stability of ion signals in our typical spectroscopic experiments with the triple-skimmer ion source. In all the measurements, the source settings were optimized to maximize the generation of the ions of interest. In the experiments with fully desolvated protein ubiquitin in the +7 charge-state, the ion signal appears to be only about 25% less with the new source, compared with the double ion funnel (DIF) ESI source that we previously used with the same instrument. For smaller ions (e.g., singly protonated amino acids), the efficiency of the triple skimmer ion source becomes, however, 30-60% lower than that of the DIF ESI source. The measured ion signals (Figure 3.5) drop by 15-20 times when the new source is optimized for maximum efficiency in generating $\text{Ubi}^{7+}(\text{H}_2\text{O})_{10}$ and $\text{TrpH}^+(\text{H}_2\text{O})_3$ complexes, although, as we mentioned above, the integral ion signal for each

distribution of the complexes remained nearly the same as the signals in the experiments optimized for maximum signals of the respective fully desolvated ions. It is worth mentioning that only the monomers of the bare and microhydrated protein could be formed under the conditions of our experiments.⁶ The short-term stability of the new source is quite high and comparable with our DIF ESI source in generating fully desolvated ions. It reduces, however, by 9 and 4.5 times for the microhydrated complexes of Ubi⁷⁺ and TrpH⁺, respectively (Figure 3.5). This higher instability reflects the subtle balance that is to be found every time between softness and the efficiency of the source. We attribute the mid- and long-term changes of the signals in Figure 3.5 to typical instabilities of the solution flow through the glass capillary or to those of the electric discharge in the ionization region of our nano-ESI sources. Finally, it is worth noting that all our efforts to generate any water complexes with a DIF ESI source or with a combination of one funnel and one/two skimmers have failed. Our intermediate and simpler design, which is based on two consecutive skimmers, demonstrated a moderate stability but an order of magnitude lower efficiency in generating microsolvated complexes.

3.5. Conclusion

In conclusion, we designed and tested a nano-ESI source, which is based on a triple skimmer configuration. The source can be quickly tuned to a “gentle” mode of operation for generation of a large number of microhydrated ions with, for instance, more than 100 retained water molecules but also to a standard “harsh” mode of operation to generate fully desolvated ions. In comparison with our previous double ion funnel nano-ESI source, which could not produce any ion-solvent complexes, the new source is less efficient in generating fully desolvated ions but demonstrates a good short-term stability in generating both bare protonated biomolecules and their microhydrated complexes. Such a gentle ion source can be used not only for spectroscopy of microhydrated biomolecules but, potentially, also in native mass spectrometry of proteins and protein complexes. We earlier spectroscopically shown for protonated ubiquitin in the charge states +7 to +9 that even a few water molecules retained on the electrosprayed proteins preserve their unfolded native-like structures.⁶ Continuous evaporation of weakly bound water molecules protects the ions from excessive heating during and after ESI, which may lead to unfolding of the protein. A biomolecule that is electrosprayed from the solution to the gas phase with a few water molecules has a good chance to retain its native structure on the timescale that is sufficient for MS interrogations.

Appendix

(YAGFL)H⁺

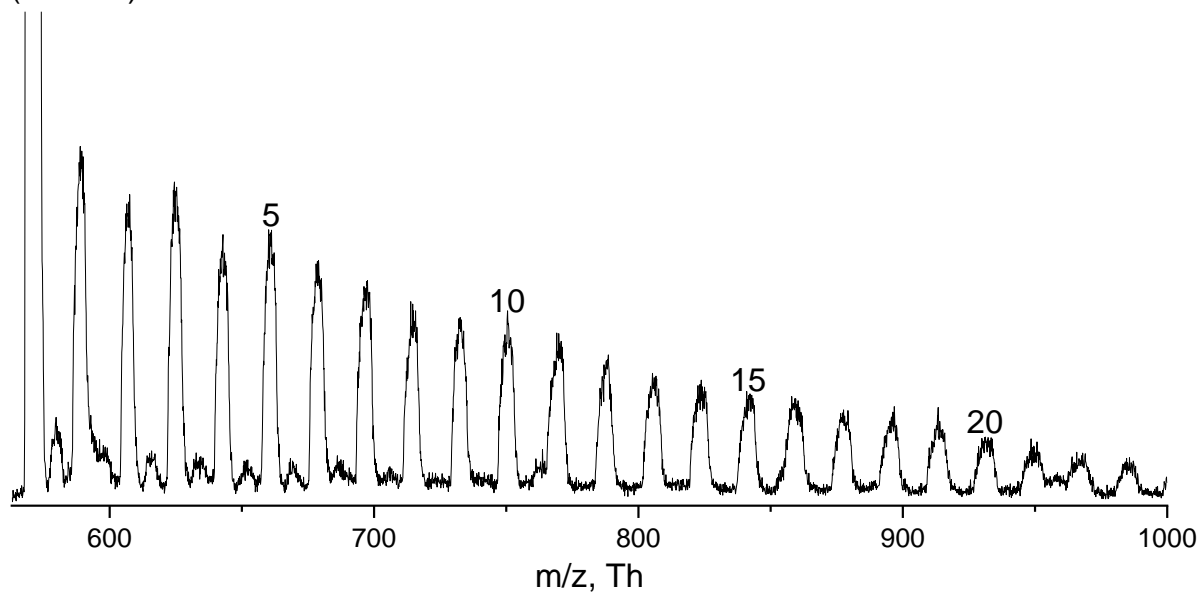


Figure 3.S1. Mass spectrum of microhydrated protonated pentapeptide DL-Enkephalin (YAGFL)H⁺(H₂O)_n that is generated by the triple-skimmer nano-ESI source. The numbers on top indicate the number *n* of water molecules in the mass peaks. Ions were not trapped in the octupole ion guide/trap.

References

1. Rodriguez-Cruz, S. E., Klassen, J. S. & Williams, E. R. Hydration of gas-phase gramicidin S ($M + 2H$) $2+$ ions formed by electrospray: The transition from solution to gas-phase structure. *J. Am. Soc. Mass Spectrom.* **8**, 565–568 (1997).
2. Mercier, S. R. *et al.* Microsolvation Effects on the Excited-State Dynamics of Protonated Tryptophan. *J. Am. Chem. Soc.* **128**, 16938–16943 (2006).
3. Nagornova, N. S., Rizzo, T. R. & Boyarkin, O. V. Interplay of Intra- and Intermolecular H-Bonding in a Progressively Solvated Macrocyclic Peptide. *Science*. **336**, 320–323 (2012).
4. Silveira, J. A. *et al.* From Solution to the Gas Phase: Stepwise Dehydration and Kinetic Trapping of Substance P Reveals the Origin of Peptide Conformations. *J. Am. Chem. Soc.* **135**, 19147–19153 (2013).
5. Saparbaev, E., Aladinskaia, V., Zviagin, A. & Boyarkin, O. V. Microhydration of Biomolecules: Revealing the Native Structures by Cold Ion IR Spectroscopy. *J. Phys. Chem. Lett.* **12**, 907–911 (2021).
6. Zviagin, A., Kopysov, V., Nagornova, N. S. & Boyarkin, O. V. Tracking local and global structural changes in a protein by cold ion spectroscopy. *Phys. Chem. Chem. Phys.* **24**, 8158–8165 (2022).
7. Wyttenbach, T. & Bowers, M. T. Hydration of biomolecules. *Chem. Phys. Lett.* **480**, 1–16 (2009).
8. Boyarkin, O. V. Cold ion spectroscopy for structural identifications of biomolecules. *Int. Rev. Phys. Chem.* **37**, 559–606 (2018).
9. Saparbaev, E. *et al.* Identification and Quantification of Any Isoforms of Carbohydrates by 2D UV-MS Fingerprinting of Cold Ions. *Anal. Chem.* **92**, 14624–14632 (2020).
10. Saparbaev, E., Yamaletdinov, R. & Boyarkin, O. V. Identification of Isomeric Lipids by UV Spectroscopy of Noncovalent Complexes with Aromatic Molecules. *Anal. Chem.* **93**, 12822–12826 (2021).
11. Saparbaev, E., Zviagin, A. & Boyarkin, O. V. Identification of Isomeric Biomolecules by Infrared Spectroscopy of Solvent-Tagged Ions. *Anal. Chem.* **94**, 9514–9518 (2022).
12. Schmidt, M. & von Issendorff, B. Gas-phase calorimetry of protonated water clusters. *J. Chem. Phys.* **136**, 164307 (2012).
13. Yang, N., Duong, C. H., Kelleher, P. J., McCoy, A. B. & Johnson, M. A. Deconstructing water's diffuse OH stretching vibrational spectrum with cold clusters. *Science* (80-.).

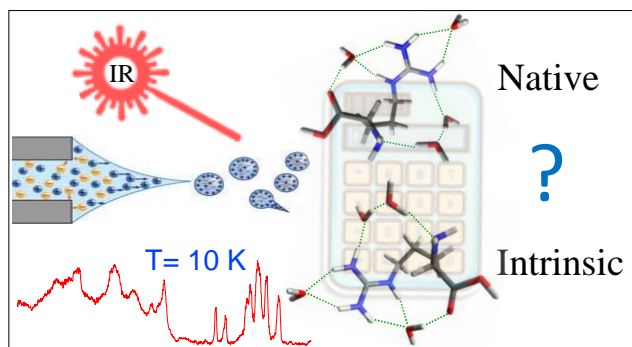
- 364**, 275–278 (2019).
14. Marsh, B. M., Voss, J. M. & Garand, E. A dual cryogenic ion trap spectrometer for the formation and characterization of solvated ionic clusters. *J. Chem. Phys.* **143**, 204201 (2015).
 15. Silveira, J. A., Servage, K. A., Gamage, C. M. & Russell, D. H. Cryogenic Ion Mobility-Mass Spectrometry Captures Hydrated Ions Produced During Electrospray Ionization. *J. Phys. Chem. A* **117**, 953–961 (2013).
 16. Hirata, K., Haddad, F., Dopfer, O., Ishiuchi, S. & Fujii, M. Collision-assisted stripping for determination of microsolvation-dependent protonation sites in hydrated clusters by cryogenic ion trap infrared spectroscopy: the case of benzocaineH + (H₂O)_n. *Phys. Chem. Chem. Phys.* **24**, 5774–5779 (2022).
 17. Wang, X.-B. & Wang, L.-S. Development of a low-temperature photoelectron spectroscopy instrument using an electrospray ion source and a cryogenically controlled ion trap. *Rev. Sci. Instrum.* **79**, 073108 (2008).
 18. Stachl, C. N. & Williams, E. R. Effects of Temperature on Cs + (H₂O)₂₀ Clathrate Structure. *J. Phys. Chem. Lett.* **11**, 6127–6132 (2020).
 19. Kamariotis, A. *et al.* Infrared Spectroscopy of Hydrated Amino Acids in the Gas Phase: Protonated and Lithiated Valine. *J. Am. Chem. Soc.* **128**, 905–916 (2006).
 20. Liu, J. *et al.* Towards complete assignment of the infrared spectrum of the protonated water cluster H⁺(H₂O)₂₁. *Nat. Commun.* **12**, 6141 (2021).

Chapter 4. Salt bridge structure of microhydrated arginine kinetically trapped in the gas phase by evaporative cooling

Disclaimer: This chapter is adapted from a published article with permission of the publisher and all co-authors.

Zviagin, A., Cimas, A., Gaigeot, MP., & Boyarkin, O. V. (2023). Salt Bridge Structure of Microhydrated Arginine Kinetically Trapped in the Gas Phase by Evaporative Cooling. *The Journal of Physical Chemistry A*, 127(22), 4832-4837, DOI: <https://doi.org/10.1021/acs.jpca.3c02023>.

Personal contribution: Conceptualization, methodology, formal analysis, visualization, original draft preparation.



4.1. Abstract

Amino acids and peptides generally exhibit zwitterionic form with salt bridge (SB) structures in solution but charge-solvated (CS) motifs in the gas phase. Here, we report a study of non-covalent complexes of the protonated amino acid arginine, $\text{ArgH}^+(\text{H}_2\text{O})_n$ ($n = 1-5$), produced in the gas phase from an aqueous solution with a controlled number of retained water molecules. These complexes were probed by cold ion spectroscopy and treated by quantum chemistry. The spectroscopic changes induced upon gradual dehydration of arginine were assigned by structural calculations to the transition from SB to CS geometries. SB conformers appear to be present for the complexes with as few as 3 retained water molecules, although energetically CS structures should become prevailing already for ArgH^+ with 7-8 water molecules. We attribute the revealed kinetic trapping of arginine in native-like zwitterionic forms to evaporative cooling of the hydrated complexes to as low as below 200 K.

4.2. Introduction

Water is one of the few molecules that are vital to our life. The myriads of water functions range from such large-scale ones as stabilizing the globe's temperature by oceans to the molecular scale of biology, where water serves as the universal solvent, supports cellular structure, etc. The amazing ability of H₂O to form intermolecular H-bonds makes it an essential part of many types of biomolecules and thus regulates their structure and, at the end, biological functionality. Understanding the structure-function relations remains essential in many fields of life science, but the complexity of the, eventually, endless H-bond network of waters often makes the determination of accurate structures of biomolecules in bulk aqueous solutions challenging even with time-proven methods like NMR. Although spectroscopy in conjunction with quantum chemistry computations may provide accurate geometries of small to midsize biomolecules isolated in the gas phase,¹⁻⁵ these intrinsic structures can substantially differ from the native solution ones, which are truly biologically relevant.

A clear example of how drastically water may conform biomolecules is a comparison of structures of amino acids and peptides in aqueous solution and in the gas phase. In aqueous solutions with neutral or slightly lower pH, these biomolecules adopt a zwitterionic form with a salt bridge (SB) bond between the protonated N- and deprotonated C-termini. In the gas phase, the C-terminus appears neutral due to the water-mediated N- to C-terminus proton transfer, which happens when the remaining waters cannot anymore stabilize the SB structure. Detection of this critical level of hydration can be performed with charged microhydrated biomolecules in the gas phase, where one can benefit from the finite size of such molecular complexes. Extensive work has been done to investigate the effect of metal cations for stabilization of SB structures of bare amino acids,⁶⁻¹⁰ as well as of amino acids solvated by a single water molecule.¹¹⁻¹³ Stabilization of SB structures by microhydration of natively protonated amino acids has been studied on a few occasions theoretically¹⁴⁻¹⁸ but only little experimentally.^{19,20} It was shown that the zwitterionic form of the studied amino acids can be stabilized in the gas phase by complexation with metal cations and/or water molecules. Arginine is one of the amino acids that exhibits protonation of its side chain under native conditions in aqueous solution and in the gas phase. This enables mass spectrometry-based tools for studying SB to charge-solvated (CS) transition in microhydrated ArgH⁺. Theoretical studies suggest that CS structures of protonated arginine solvated by up to 7 water molecules remain energetically more favorable than the SB configurations; further hydration gradually makes SB structures more favorable.¹⁴ Recent cryogenic ion mobility (IM) studies, however,

challenge this suggestion.²¹ The experiment detected an essential structural difference for ArgH⁺ in its complexes with three and with four (and more) water molecules. The difference was tentatively attributed to the transition from CS to SB structures.

Herein, we report a joint experimental and theoretical study that addresses this discrepancy and determines the minimum number of water molecules that retain the hydrated arginine in its native-like zwitterionic form. Non-covalent complexes of ArgH⁺(H₂O)_n with a controlled number of water molecules $n = 0-5$ were interrogated by cold ion IR spectroscopy and computationally treated with quantum chemistry. The spectroscopic changes induced by the gradual decrease of the level of hydration were attributed to the evolution of arginine from its native-like SB to the intrinsic CS structure. We discuss the role of evaporative cooling in the kinetic trapping of hydrated biomolecules in their native-like structures.

4.3. Methods

Our experimental approach has been described in detail elsewhere.^{1,22} The hydrated ions are generated directly from solution using a “gentle” mode of a nano-electrospray ion (n-ESI) source²³ and transferred through a metal capillary and three consecutive inline molecular skimmers to a room-temperature octupole ion trap (pre-trap) for accumulation and thermalization. Thermalized ionic complexes are mass-selected by a quadrupole mass-filter and guided into a cold octupole ion trap,²⁴ which is kept at 6 K. The trapped complexes are cooled down to ~10 K by collisions with He buffer gas, which is pulsed into the trap (gas pulse duration is ~1 ms; maximum number density of He in the trap is $\sim 2 \cdot 10^{15} \text{ cm}^{-3}$). The cold ions are then irradiated by a pulse of IR light ($6 \pm 2 \text{ mJ/pulse}$ within the 2800-3800 cm^{-1} range and $1.5 \pm 0.5 \text{ mJ/pulse}$ within the 1500-1800 cm^{-1} range; 1 to 3 cm^{-1} spectral bandwidth), produced by an optical parametric oscillator (OPO, Laser Vision). The absorption of the IR light results in the evaporation of a few water molecules. The remaining parent and the reduced fragment complexes are released from the trap and detected by a quadrupole mass spectrometer, which is tuned to transmit alternatively either one of the fragments (e.g., a loss of single water molecule) or the parent complexes. We average 10 measurements at each IR wavelength at the repetition rate of 10 Hz. Each spectrum was recorded, at least, 2 times to ensure its reproducibility; the low number of deuterated complexes (reduced due to the presence of a significant fraction of the mixed complexes with H and D atoms) forced us to measure each spectrum 5 to 7 times to ensure an acceptable quality of the data. A wavelength meter WS-5 (High-Finesse) measured the wavelength of the (visible) signal wave of the IR OPO and (only

once) of the Nd:YAG pumping laser, thus providing the wavenumber of the wave generated by the difference frequency mixing IR light with $\pm 0.2 \text{ cm}^{-1}$ accuracy.

L-Arginine from Fluka BioChemika ($\geq 99.5\%$), L-Arginine methyl ester dihydrochloride ($\geq 98\%$) from Sigma-Aldrich, and L-Arginine ($\alpha\text{-}^{15}\text{N}$) hydrochloride ($\geq 98\%$) from Cambridge Isotope Laboratories were used without further purifications. Methanol and ethanol of analytical reagent grade are from Fisher Chemical, water of HPLC Plus grade, deuterated water ($\geq 99.9\%$) and acetic acid ($\geq 99\%$) are from Sigma-Aldrich. Arginine was dissolved either in the water/methanol/ethanol (5/3/2) mixture or in the deuterated water (with no methanol) with 0.2 vol% of non-deuterated acetic acid. The arginine concentration in the prepared solutions was $50 \mu\text{M}$.

The geometries and vibrational frequencies of the complexes were calculated using the density functional theory (DFT). In particular, we have used the B3LYP exchange-correlation functional, which includes the Lee-Yang-Parr correlation functional²⁵ in conjunction with a hybrid exchange functional first proposed by Becke,²⁶ along with the basis set denoted 6-311++G**.²⁷ This basis set includes diffuse functions as well as polarization functions for both hydrogen and heavy atoms. All calculations have been carried out with the Gaussian 16 package.²⁸

Semiempirical-based Born-Oppenheimer molecular dynamics simulations have been performed with the CP2K package,²⁹ where the nuclei are treated classically and the electrons quantum mechanically within the PM6 semiempirical formalism,³⁰ the cubic cells of 3 nm side and the time-steps of 0.5 fs were used in the simulations.

4.4. Results and discussion

Figure 4.1 shows IR spectra of $\text{ArgH}^+(\text{H}_2\text{O})_n$ ($n = 0\text{-}5$) measured in the fingerprint spectral region of $3300\text{-}3800 \text{ cm}^{-1}$. The peaks above 3600 cm^{-1} are firmly assigned to the OH-stretches of water. Based on known data,¹ the peak at 3570 cm^{-1} for $n = 1$ has been assigned to the free OH stretch of the C-terminus, which, expectedly, points to the CS structure of the singly hydrated arginine. Retaining one more water ($n = 2$) significantly changes the spectrum. The increased number of the (water) OH-stretch peaks above 3600 cm^{-1} suggests that the complex resides in, at least, two conformational states. The intensity of the free OH stretch transition of the carboxyl at 3570 cm^{-1} transition weakens significantly for $n = 2$, further decreases for $n = 3$ and becomes completely unresolved for $n = 4$ and 5. This decrease implies that in some of the conformers of the $n \geq 2$ complexes either a water binds to the OH of the C-terminus, causing redshift and broadening of this transition, or the C-terminus becomes deprotonated.

Although under our experimental conditions the conformers with such structural features appear to be highly abundant, they are not present among the earlier calculated (and recalculated herein) lowest energy conformers of these complexes.¹⁴

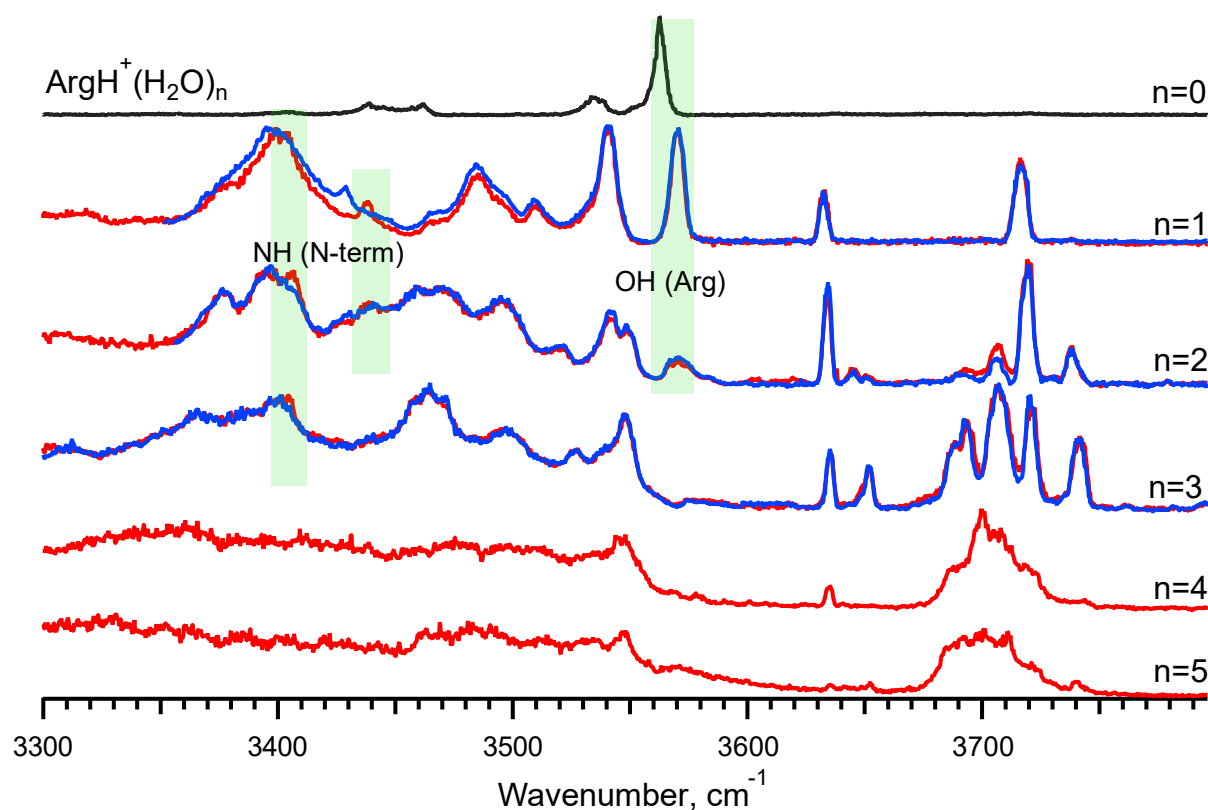


Figure 4.1. IRMPD spectrum of ArgH⁺ (black trace) measured by monitoring fragment at $m/z = 158$; IRPD spectra of ArgH⁺(H₂O)_n ($n = 0-5$; red traces) and α -¹⁵N isotopically labeled ArgH⁺(H₂O)_n ($n = 1-3$; blue traces) measured by loss of a single water molecule. Vertical green bars emphasize the assigned transitions for ArgH⁺ in the complexes.

The calculations suggest that below $n = 7$ ArgH⁺ in the complexes resides in CS states and exhibits the OH group that is free of any non-covalent interactions. In addition, the calculations suggest that for $n = 2$ and 3, the N-terminus remains free of interactions with water molecules but is involved in the intramolecular couplings with an amine of the side chain. This contradicts to the observed redshift of 32 cm⁻¹ for the NH-stretch of the N-terminus in some of the complexes with $n = 2$ and 3, relative to the ones with $n = 1$. The shift was revealed from spectroscopy of the ArgH⁺ complexes with an isotopically labeled (¹⁵N) N-terminus (Fig. 4.1, blue traces).

These observations prompt us to conclude that for $n > 1$, the complexes reside not in their global minima states, but rather appear kinetically trapped in solution-like geometries. Conformational search among the structures that reside in numerous local minima of the

potential energy (PE) surface, especially for such a flexible molecule like Arg, is very challenging. Our attempts to find among the low-energy structures those, whose spectra would reasonably match to the experiment did not succeed, although for $n = 3$, we found that the most stable both CS and SB conformers appear lower in energy than those reported earlier.¹⁴ Regarding this, our subsequent computations were focused not on solving the exact geometries of the experimental complexes but rather on revealing the characteristic spectroscopic differences between the CS and SB structures of the low PE complexes and on mapping up these differences to the experiment.

To mimic the experimental conditions, the complexes with n waters were generated based on the preceding $n + 1$ complexes. It turns out that for $n = 5$ the geometry of arginine in the lowest energy SB complex is very similar to the geometry of Arg in the most stable structure of the complex with $n = 8$, which is of SB type too.¹⁴ We therefore take the lowest energy SB $n = 5$ structure as a starting point for generating the geometries of the subsequent smaller complexes. The geometry of the $\text{ArgH}^+(\text{H}_2\text{O})_5$ complex taken from ref¹⁴ was first reoptimized at the B3LYP/6-311++G** level. Single water molecules were then removed from this structure, and the geometries of five such generated $n = 4$ SB complexes were optimized at the same level. Next, a proton was moved from the N-terminus to one of the two oxygens of the C-terminus to generate two templates of CS structures, which were then optimized too. For each pathway, the three (one SB and two CS) structures were optimized and arranged by their PE. The most stable SB structures were then used as templates to generate $n = 3$ structures, and so on, as illustrated in figure 4.2 (see Tables 4.S1-4.S3 for images of the structures). Vibrational spectra were then calculated in a harmonic approximation for all conformers of $\text{ArgH}^+(\text{H}_2\text{O})_n$ complexes ($n = 2-5$) generated through this procedure. A comparison of these results with the measured (conformation non-selective) spectra (Fig. 4.S2) does not allow for unambiguous validation of the respective structures. This roots mainly from the large size and flexibility of the studied non-covalent complexes.

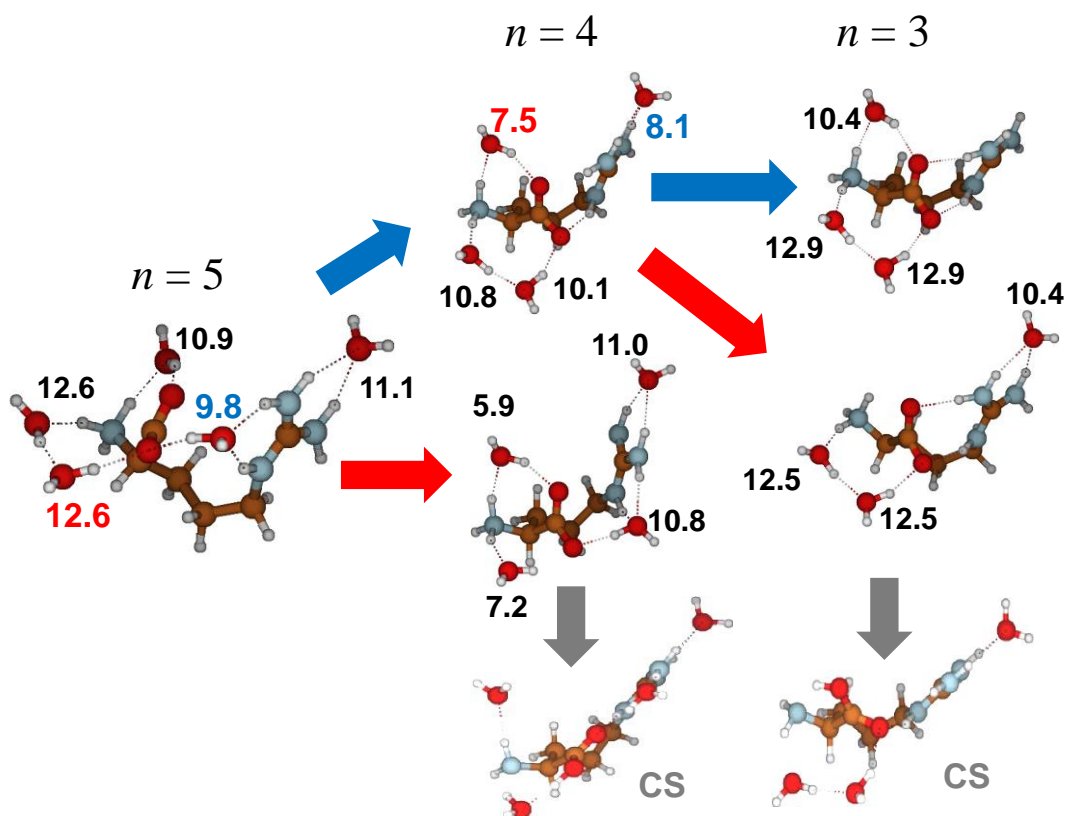


Figure 4.2. Schematic diagram illustrating the generation of SB structures of the $\text{ArgH}^+(\text{H}_2\text{O})_n$ complexes (shown partially for $n = 5$ to 3 only). The numbers near each water molecule indicate the binding energy of this water to the complex (in kcal/mol). The color of a number codes the water molecule that was removed to generate the subsequent smaller complex to which the arrow of the same color points. Vertical gray arrows for $n = 4$ and 3 indicate that the respective SB structures are less stable than the generated from them CS conformers.

In order to reduce the spectral complexity, we measured the spectra of $\text{ArgD}^+(\text{D}_2\text{O})_n$, ($n = 1-5$) complexes with all deuterated NH and OH groups. Deuteration significantly redshifts all the transitions associated with these groups, such that the few remaining peaks in the region of $1580-1650\text{ cm}^{-1}$ can be safely assigned to the redshifted C–N antisymmetric stretches of the guanidinium group.³¹ Based on the available data,¹ the remaining and only slightly redshifted (8 cm^{-1}) peaks in the $1700-1770\text{ cm}^{-1}$ region can now be assigned to a CO stretch of the H-bonded C-terminus. The detection of only one strong peak (1765 cm^{-1}) in this spectral region for the complex with $n = 1$ implies the presence of only one conformer (conformational family), which was assigned above to a CS structure. We therefore assign this peak to C=O stretch of the H-bonded C-terminus. One more redshifted ($\Delta\nu = 27\text{ cm}^{-1}$) weak peak and two more redshifted peaks ($\Delta\nu = 28$ and $\Delta\nu = 49\text{ cm}^{-1}$) of comparable intensity were detected for $n = 2$ and 3, respectively, pointing to the increase of the number of conformers upon increasing the

level of hydration. The position of the highest-frequency peak remains nearly the same for $n = 1-3$, which allows its assignment to the C=O stretch for $n = 2$ and 3 too. This assignment is further confirmed by spectroscopy of the microhydrated modified arginine that was methylated on the C-terminus (Fig. 4.S3). The methylation forbids SB structures, while a gradual ($n = 1-5$) hydration of the CS structures almost does not influence the frequency and relative intensity of the C=O stretch. In contrast, the relative intensity of this peak in the spectra of $\text{ArgH}^+(\text{H}_2\text{O})_{1-5}$ complexes (Fig. 4.3) gradually drops to zero upon hydration for $n = 4$ and 5, while the relative intensities of the two redshifted ($\Delta\nu = 12 \text{ cm}^{-1}$ and $\Delta\nu = 42 \text{ cm}^{-1}$) peaks are increasing, respectively.

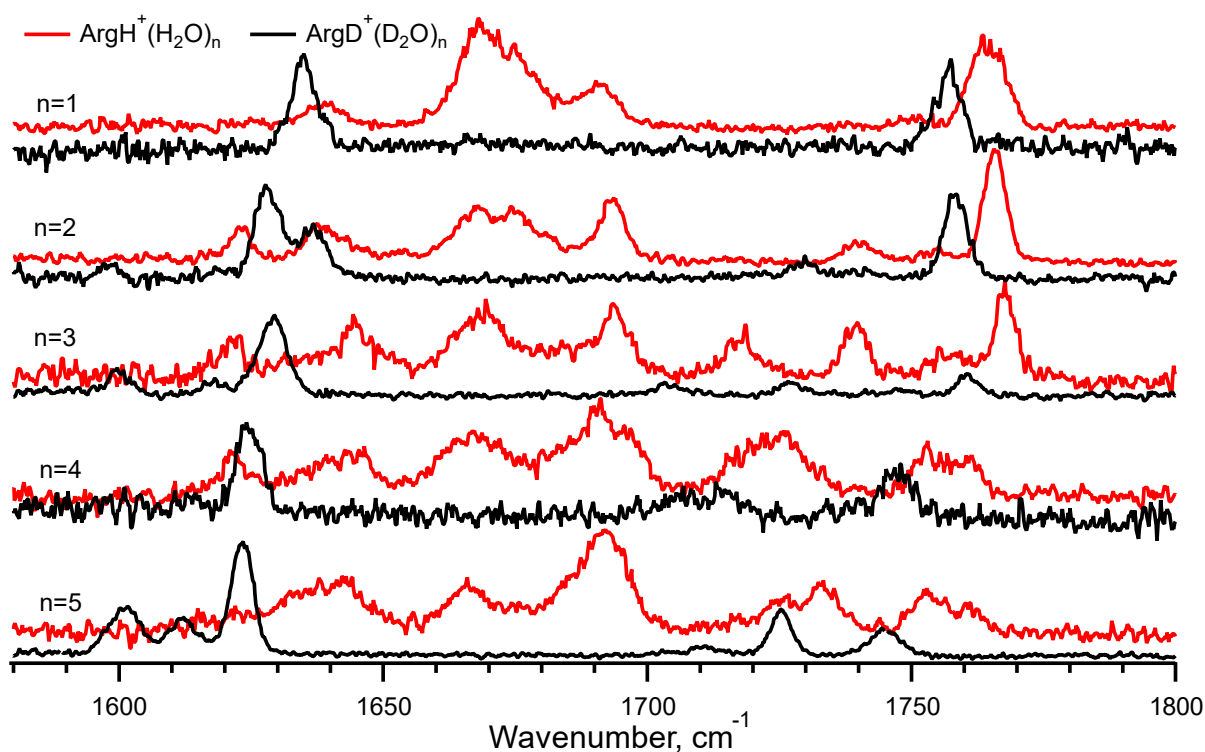


Figure 4.3. IRPD spectra of $\text{ArgH}^+(\text{H}_2\text{O})_n$ (red traces) and of its deuterated (OH and NH groups) analogue $\text{ArgD}^+(\text{D}_2\text{O})_n$ for $n = 1-5$.

Figure 4.4 compares these experimental spectra with the C=O stretch and of the $(\text{O}-\text{C}-\text{O})^-$ antisymmetric stretch vibrations of the C-terminus calculated for the locally most stable SB and CS conformers generated by water removal/proton transfer, as described above. These vibrations are unique and characteristic for each type of conformer. The complexes may remain trapped in the local minima and be observed, if the energy barriers are unfavorable for relaxation to the CS structures with lower PE. Similar to a few earlier studied cases,^{32,33} for all the computed complexes the frequencies of the $(\text{O}-\text{C}-\text{O})^-$ vibrations exhibit a clear trend to be redshifted from the C=O ones. In particular, there are no candidate CS conformers to match

the most redshifted peaks ($\sim 1710\text{ cm}^{-1}$) in the spectra of complexes with $n = 3$ and 4. In opposite, there are no SB conformers to match to the highest frequency peaks assigned to the C=O stretch in CS structures. Based on this, we may assign the most redshifted peaks in the spectra of the complexes with $n = 3$ and 4 to SB structures. This also implies the presence of kinetically trapped zwitterionic SB conformers for all larger complexes, although we have no direct evidence of this.

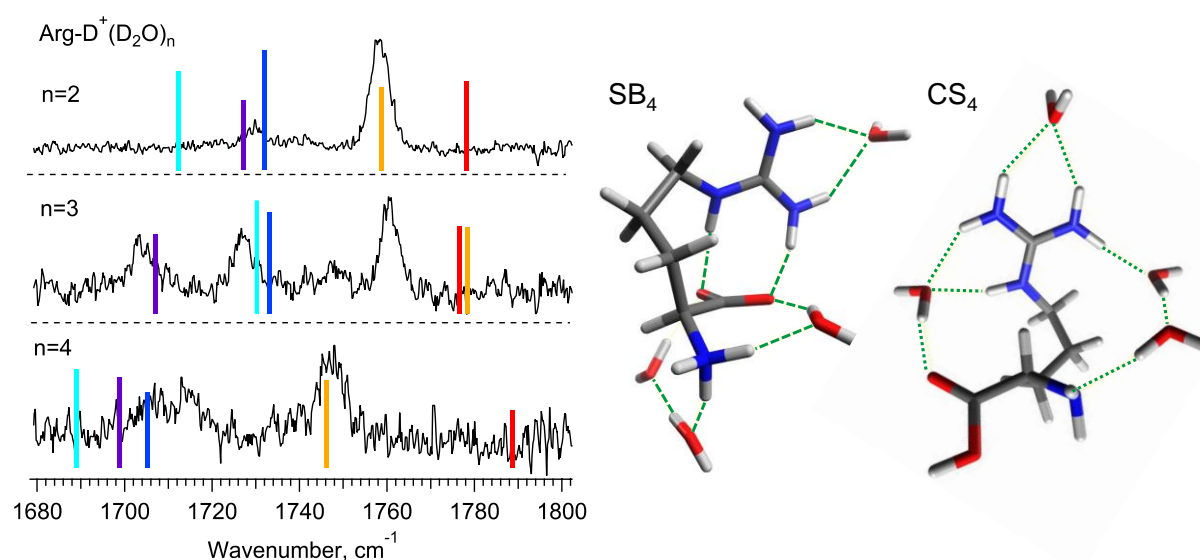


Figure 4.4. IR transitions of the (O-C-O)⁻ and C=O stretch vibrations, calculated for the locally most stable SB (blue, light blue and violet sticks) and CS (red and orange sticks) conformers of ArgD⁺(D₂O)_n complexes ($n = 2-4$), respectively. The transitions are overlapped with the respective experimentally measured spectra. The frequencies of the transitions are scaled by the factor 1.015. The globally lowest-energy structures of the $n = 4$ SB and CS complexes are shown on the right for comparison.

The fact that these zwitterionic SB conformers survive ESI and the room-temperature pre-trapping is not trivial to explain. To illustrate the dynamics of the desolvation and of the zwitterionic SB \rightarrow CS transition, we performed semi-empirical (PM6) MD simulations for the zwitterionic SB complexes with $n = 3-6$ at a few different temperatures (Fig. 4.S4). The simulations indicate that at $T = 300-450\text{ K}$, the lifetime of the complexes is on the timescale of 10-100 ps. This is by far too fast for the complexes to avoid full dehydration and zwitterionic SB to CS relaxation during the 50 ms storage in the room temperature ion pre-trap. Calculations with the ion temperature of 200 K result, however, in a complete freezing of the dynamics over the limited 500 ps timescale of the simulations. In order to estimate the lifetime of the ion complexes under our experimental conditions, we measured the abundances of all the

complexes that could be detected ($n = 0-45$) in the ion distributions for the cases of the trapped and non-trapped complexes in the ion pre-trap (Fig. 4.5).

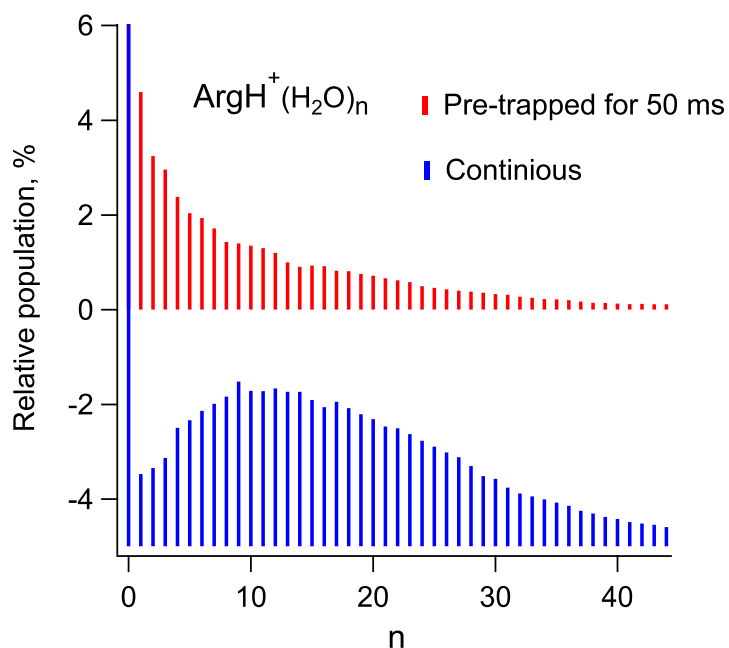


Figure 4.5. Relative population of $\text{ArgH}^+(\text{H}_2\text{O})_n$ complexes for $n \leq 45$: after 50 ms storage in the room temperature ion pre-trap (red), and continuously detected as they are generated by ESI source. (blue). The two distributions have been derived from mass spectrometric measurements and were normalized to the total number of ions (100%) in each distribution. The intensities of the fully dehydrated ions (60% for the pre-trapped ions and 12% for continuously measured ions) were truncated for graphical clarity.

This allows for calculating the fraction of water molecules that were evaporated from all the complexes during the trapping. Based on this, we roughly estimated (see Appendix for details) the rate of single water evaporation in the trap, k_1 , to 0.02 ms^{-1} , which gives ≈ 12 ms for the lifetime of, for instance, $n = 4$ complexes. This result prompts us to conclude that the evaporative cooling keeps the temperature of the ions in the pre-trap much lower than $T = 300$ K. Our MD simulations of evaporation in a microcanonical NVE ensemble (number of atoms-volume-energy being constant; see Appendix for details) suggest that the lifetime of 10 ms for the $n = 4$ complexes requires their internal temperature of $\sim 150 \pm 35$ K. This rough estimate is consistent with calorimetric studies of protonated water clusters, which indicate that balancing collisional heating by evaporative cooling stabilizes internal ion temperature at as low as ≈ 170 K.³⁴ An increase of heating accelerates the evaporation to keep the ion temperature close to this asymptotic value. We therefore conservatively propose that the evaporative cooling of the $\text{ArgH}^+(\text{H}_2\text{O})_n$ complexes may keep their internal temperature below ~ 200 K. It must be this

significant lowering of temperature that enables not only to retain water molecules for long time, but also arginine in these complexes to be kinetically trapped in zwitterionic forms, which are the most stable conformers in aqueous solutions.

A substantial evaporative cooling should be general for microhydrated ions. Regardless of the initial temperatures of the ions, boiling off waters keeps the complexes cold, provided the complexes originally own a sufficient number of water molecules to evaporate. Along with the specific intermolecular non-covalent interactions, evaporative cooling might be the key factor that protects the native-like structures of microhydrated biomolecules before a prompt cryogenic cooling. For instance, a recent spectroscopic study proposed evaporative cooling as the reason for preventing unfolding of the multiply protonated microhydrated protein ubiquitin in the gas phase.²²

4.5. Conclusion

To sum up, we suggest that a high final level of hydration of biomolecules may not be a must to reveal the main features of their native-like structures. Small water complexes always originate from the large electrosprayed ones, in which the native structural motives of the embedded biomolecules can be retained by the remaining network of H-bonds. Next, evaporative cooling to $\lesssim 200$ K hinders the transition from the native solution-like to the intrinsic gas-phase structures. Our study examples this: zwitterionic forms of Arg which are common in solution, but do not exist in the gas phase, were identified in the complexes of this protonated amino acid with as few as 3-4 water molecules. Although more extensive calculations are required to identify these structures, the relatively small level of hydration that suffice for kinetic trapping should encourage the use of microhydrated complexes in hunting for native structures of biomolecules.

Appendix

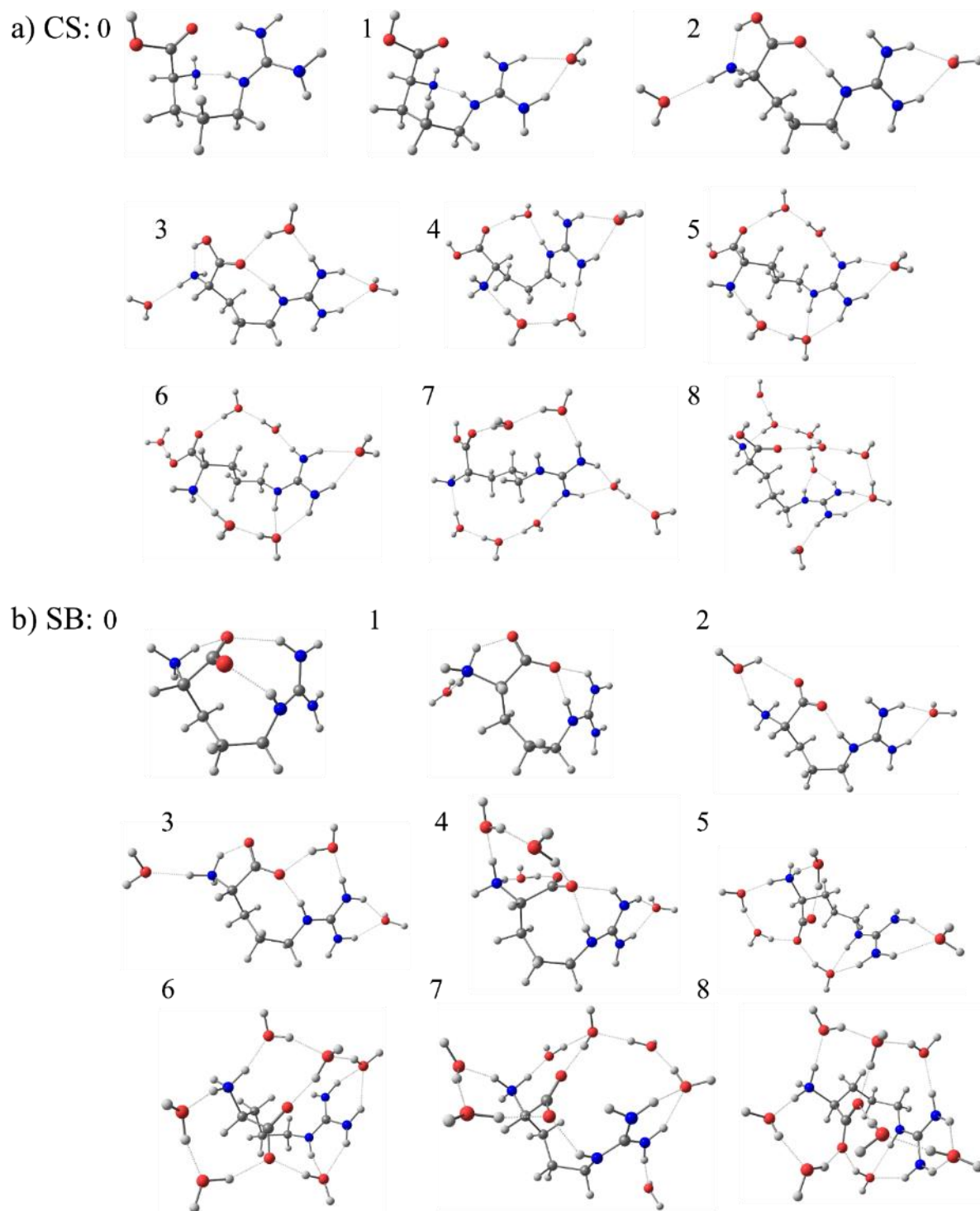
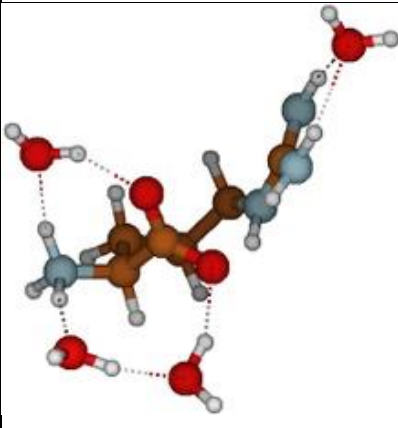
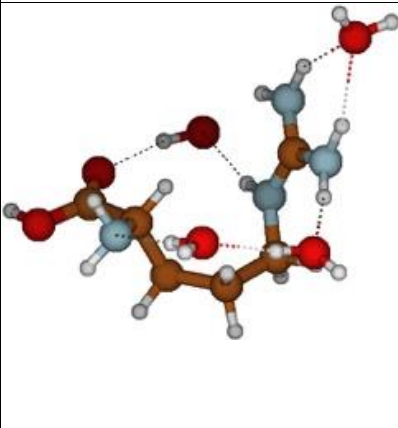
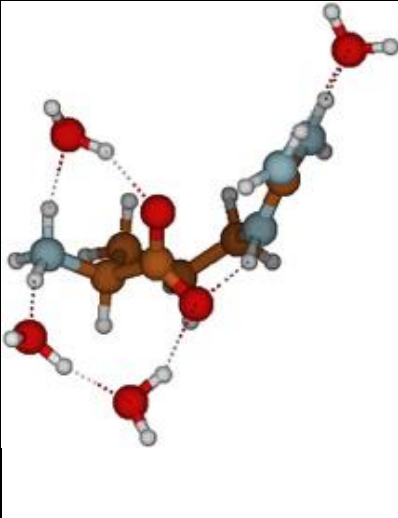
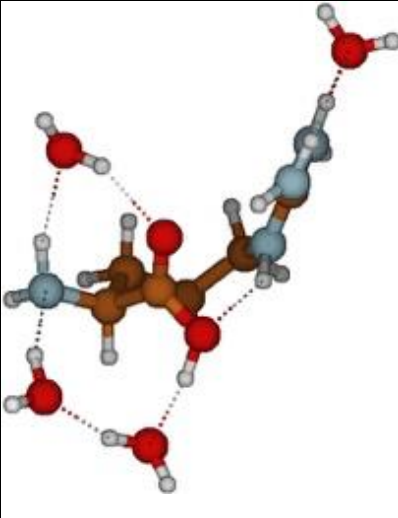
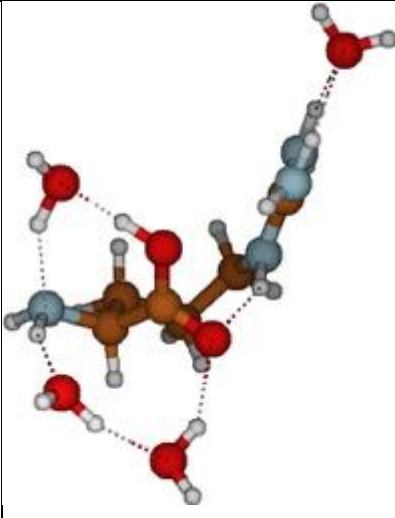


Figure 4.S1. Lowest energy optimized structures for the charge-solvated CS (a) and zwitterionic SB (b) forms of $\text{ArgH}^+(\text{H}_2\text{O})_n$, $n = 0-8$. Numbers over the structures indicate the number of water molecules in the complex.

Table 4.S1. SB and CS optimized structures at the B3LYP/6-311++G** level for ArgH⁺(H₂O)₄ complexes originated after the evaporation of one water molecule from the optimized geometry of the SB ArgH⁺(H₂O)₅ complex from Bowers et al.¹⁴ (all calculated at the same level of theory). The numbers under the structures correspond to the relative free energy in kcal/mol (free energies are calculated in the harmonic approximation at the temperature of 298 K). Identical structures are excluded from the table.

Zwitterionic SB structures	CS structures	
		
4.33	0	
		
5.12	10.76	9.61

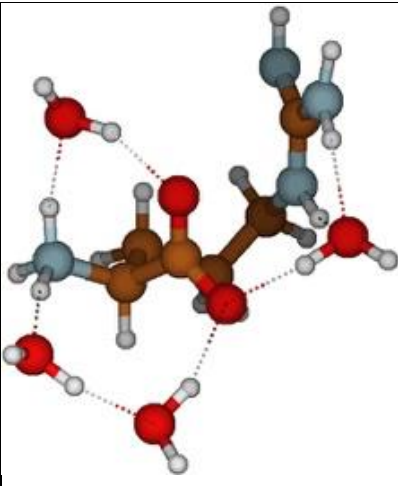
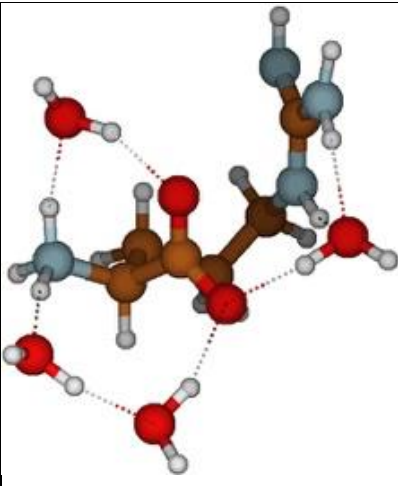
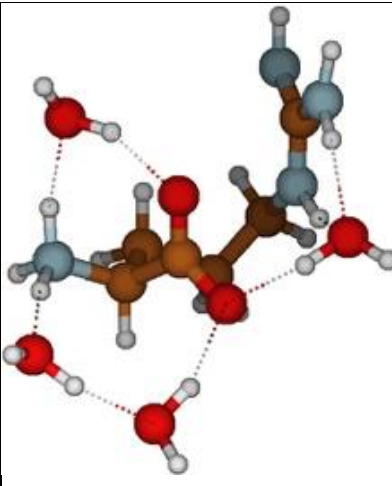
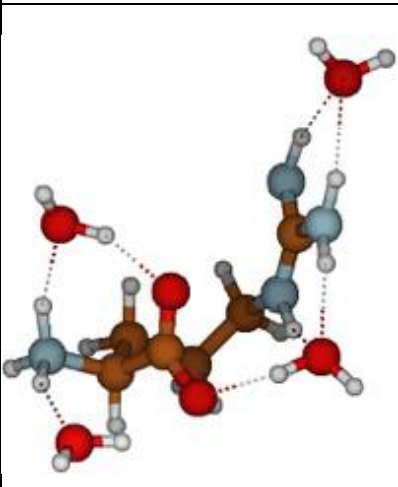
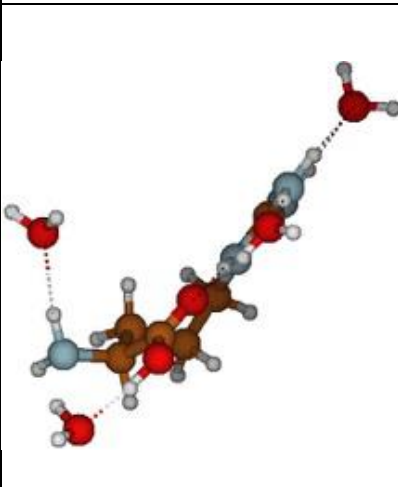
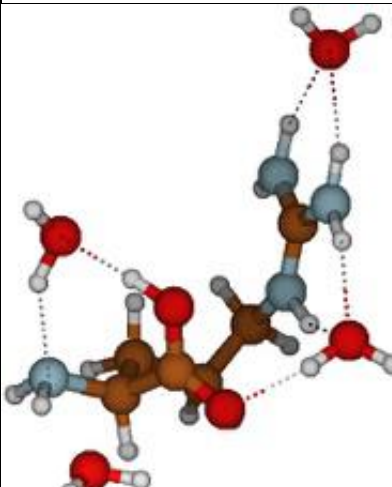
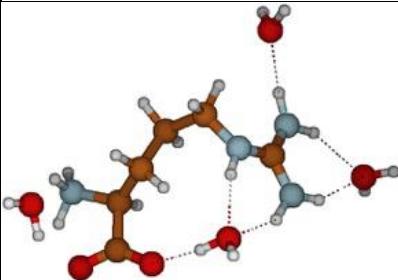
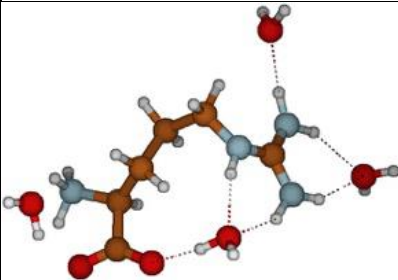
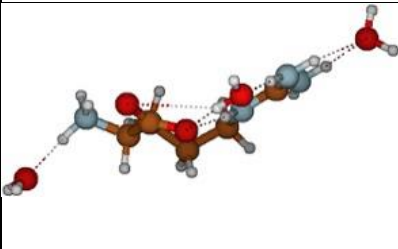
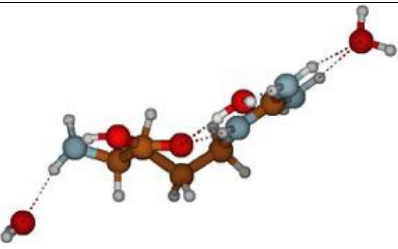
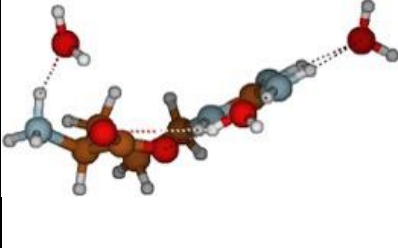
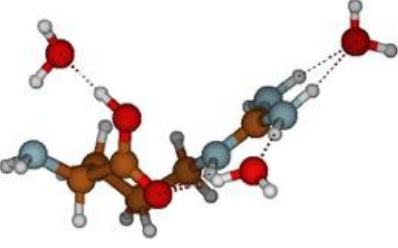
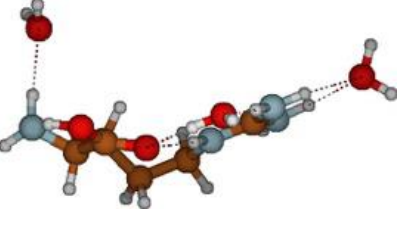
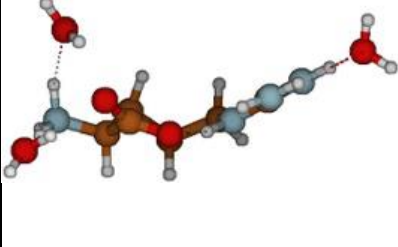
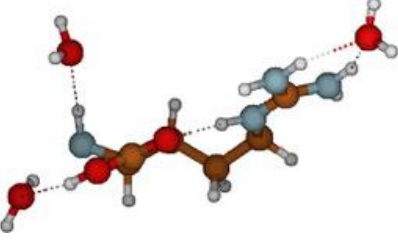
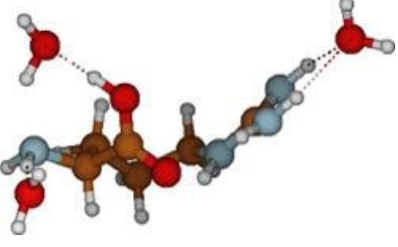
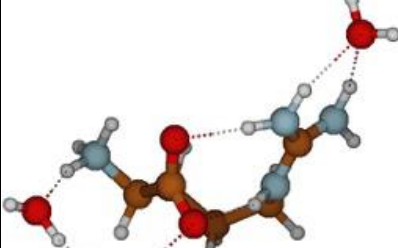
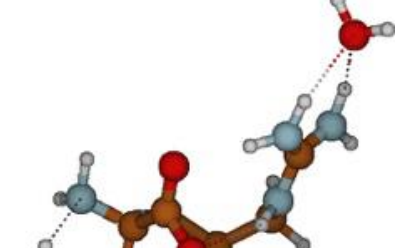
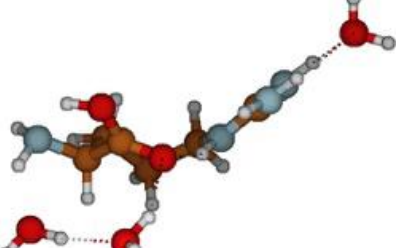
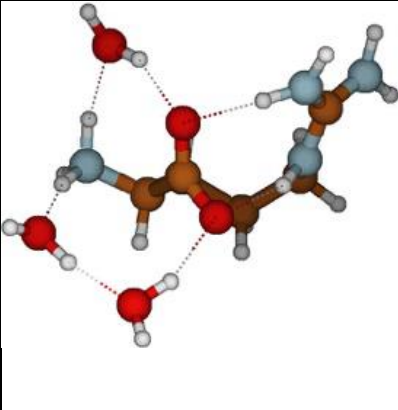
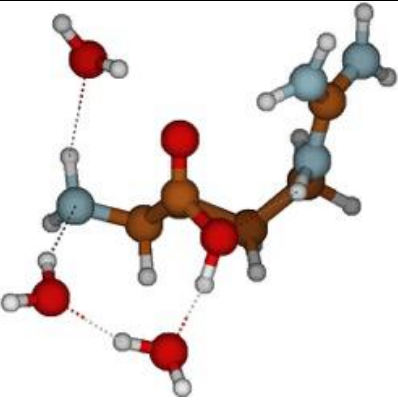
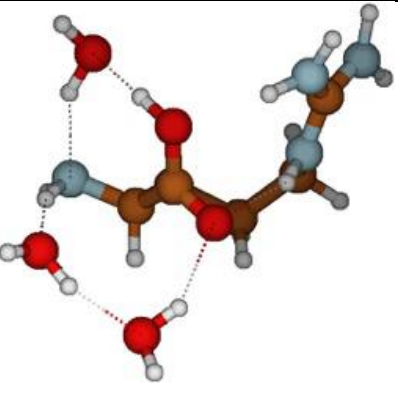
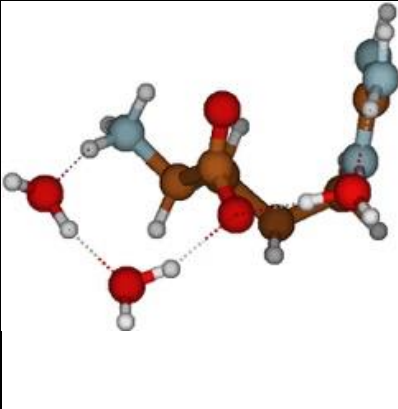
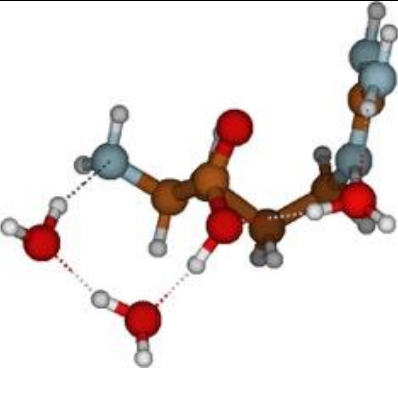
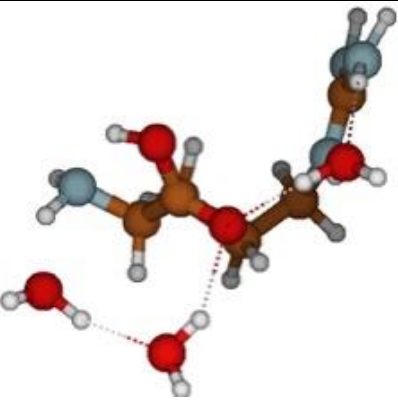
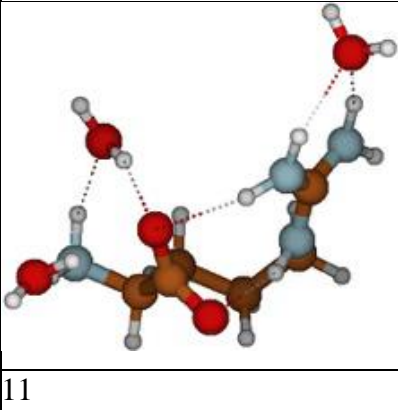
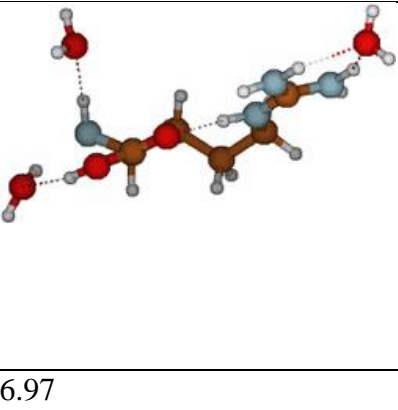
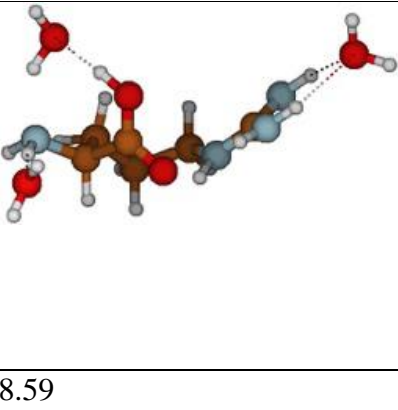
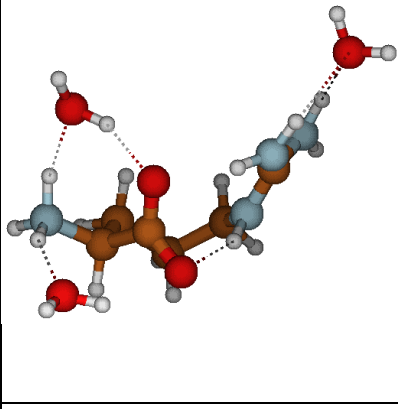
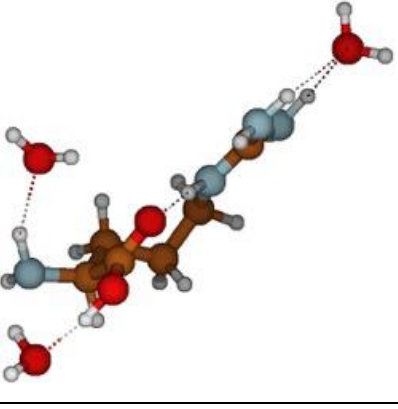
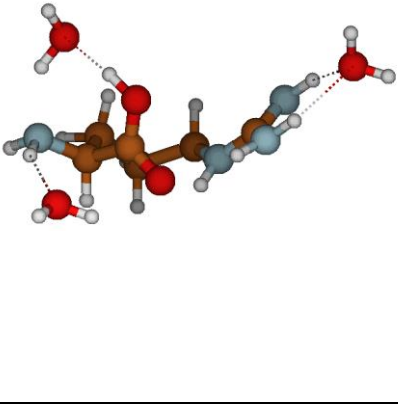
		
6.27	11.1	10.21
		
7.64	1.89	5.9
		
12.44	6.28	

Table 4.S2. SB and CS optimized structures at the B3LYP/6-311++G** level for $\text{ArgH}^+(\text{H}_2\text{O})_3$ complexes originated after the evaporation of one water molecule from the optimized geometries of $\text{ArgH}^+(\text{H}_2\text{O})_4$ complexes generated previously (see Table 4.S1) at the same level of theory. The numbers under the structures correspond to the relative free energy in kcal/mol (free energies are calculated in the harmonic approximation at the temperature of 298 K). Identical structures are excluded from the table.

Zwitterionic SB structures	CS structures	
		
4.33	0	
		
6.76	4.96	0.66
		
6.81	6.97	8.61
		
8.54	9.86	6.61

		
9.64	16.52	15.37
		
10.77	10.72	9.9
		
11	6.97	8.59
		
11.48	7.99	10.15

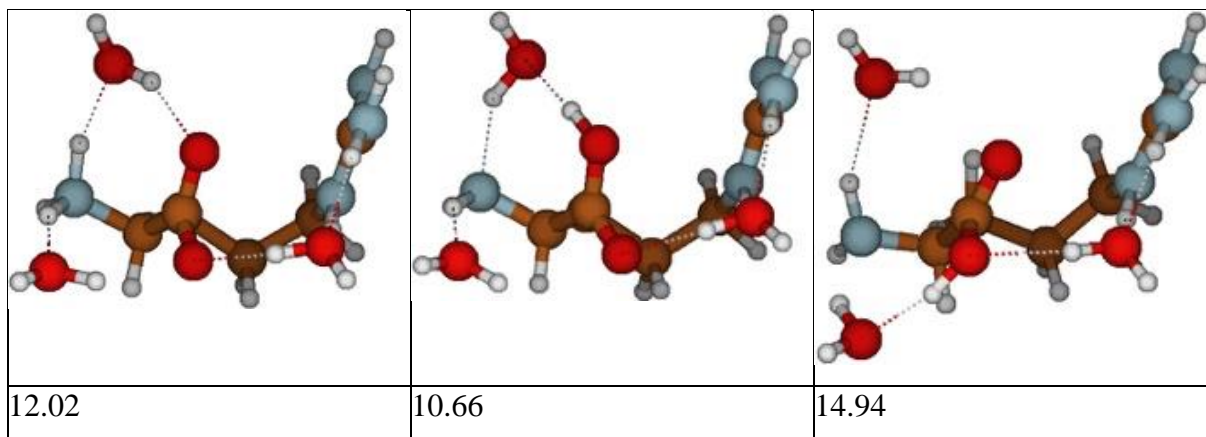
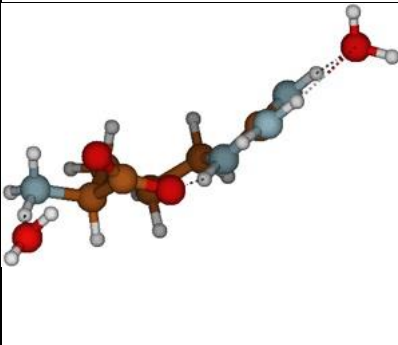
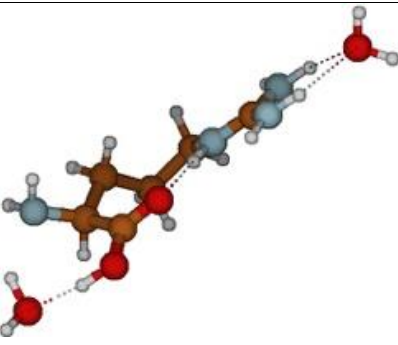
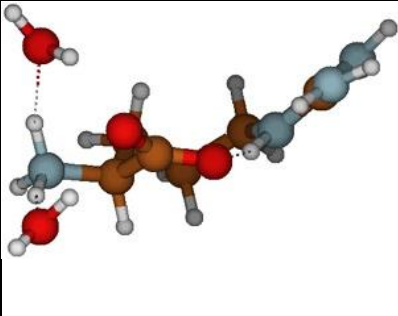
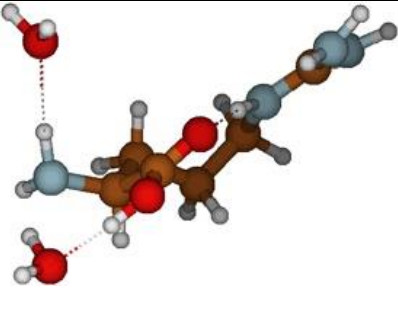
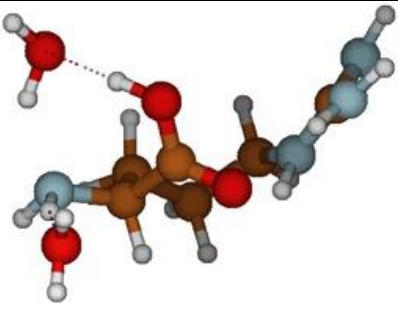
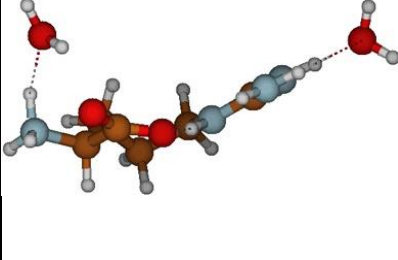
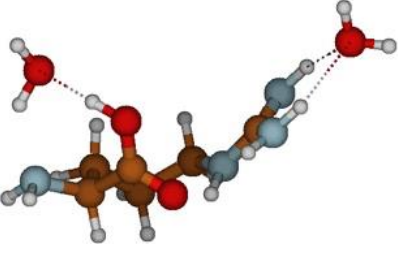
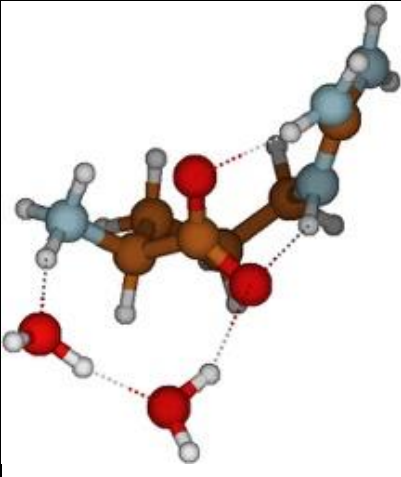
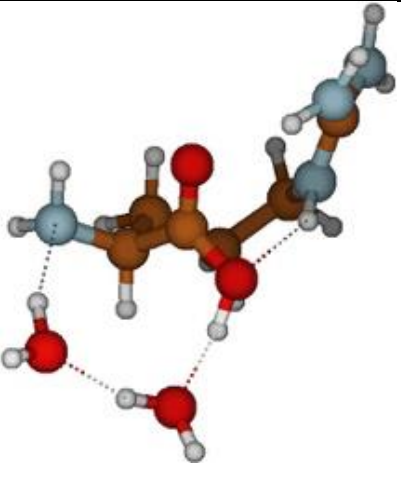
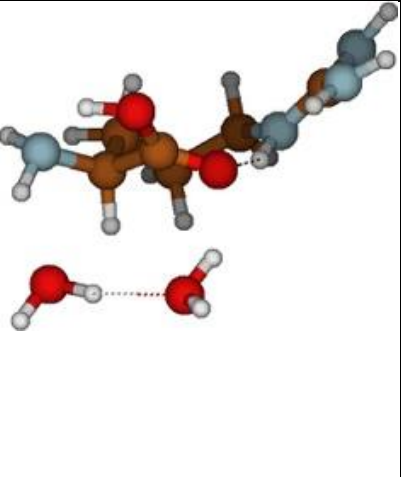
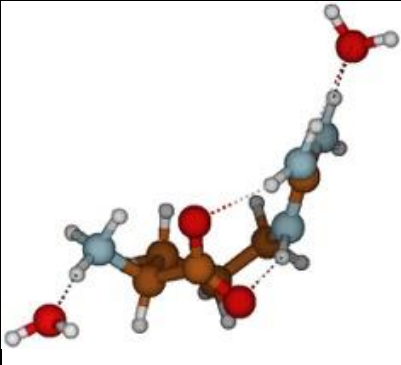
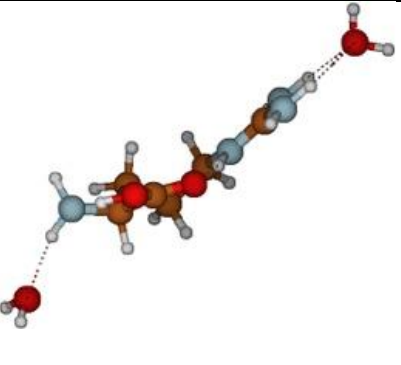
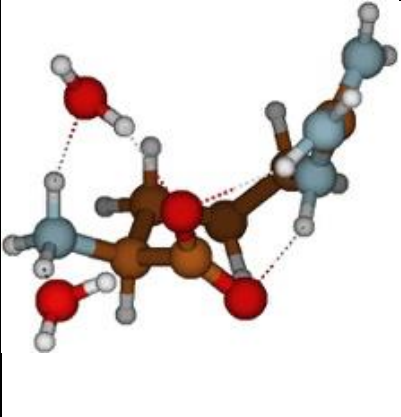
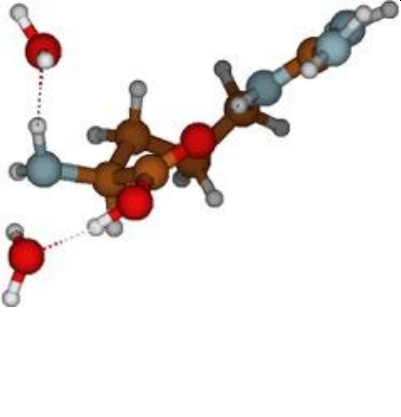
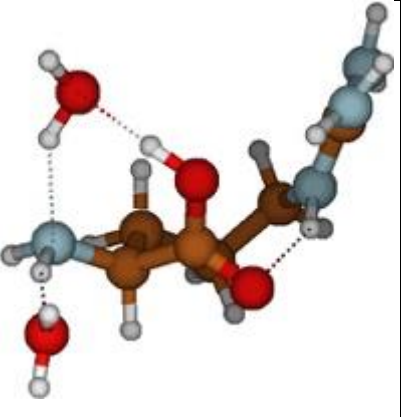


Table 4.S3. SB and CS optimized structures at the B3LYP/6-311++G** level for ArgH⁺(H₂O)₂ complexes originated after the evaporation of one water molecule from the optimized structures of ArgH⁺(H₂O)₃ complexes generated previously (see Table 4.S2) at the same level of theory. The numbers under the structures correspond to the relative free energy in kcal/mol (free energies are calculated in the harmonic approximation at the temperature of 298 K). Identical structures are excluded from the table.

Zwitterionic SB structures	CS structures	
		
6.88	2.58	
		
6.98	7.66	9.25
		
7.21	5.46	

		
8.24	10.51	7.98
		
8.27	0	
		
10.73	8.06	10.33

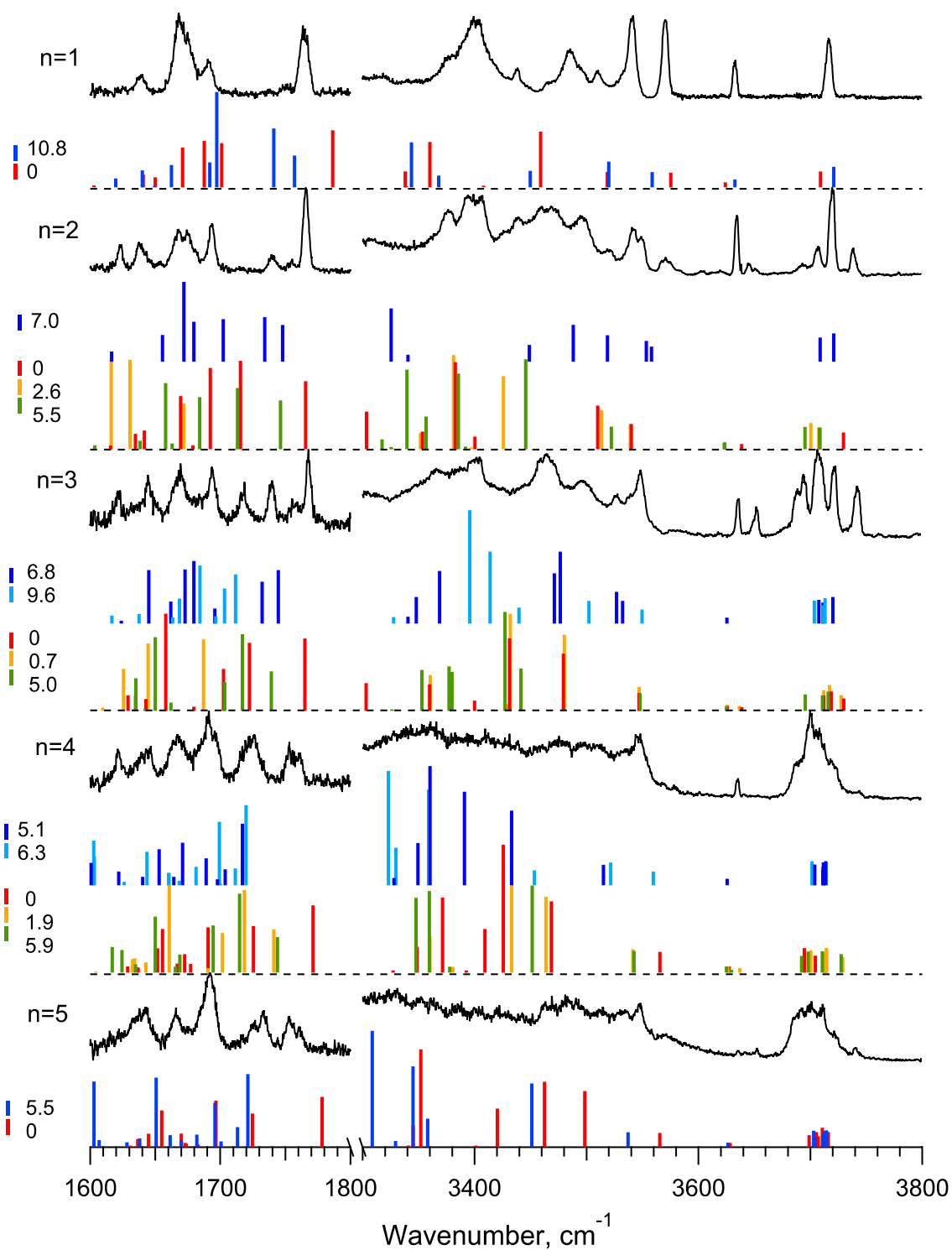


Figure 4.S2. IRPD spectra of $\text{ArgH}^+(\text{H}_2\text{O})_n$ complexes for $n = 1-5$ (black traces) and the theoretical spectra (color sticks) calculated for the optimized generated structures. Only spectra for the locally most stable structures are shown. Blue and light blue sticks designate the SB structures, and red, yellow and green sticks designate the CS structures. The relative potential energies of the structures are shown with respective color coding on the left.

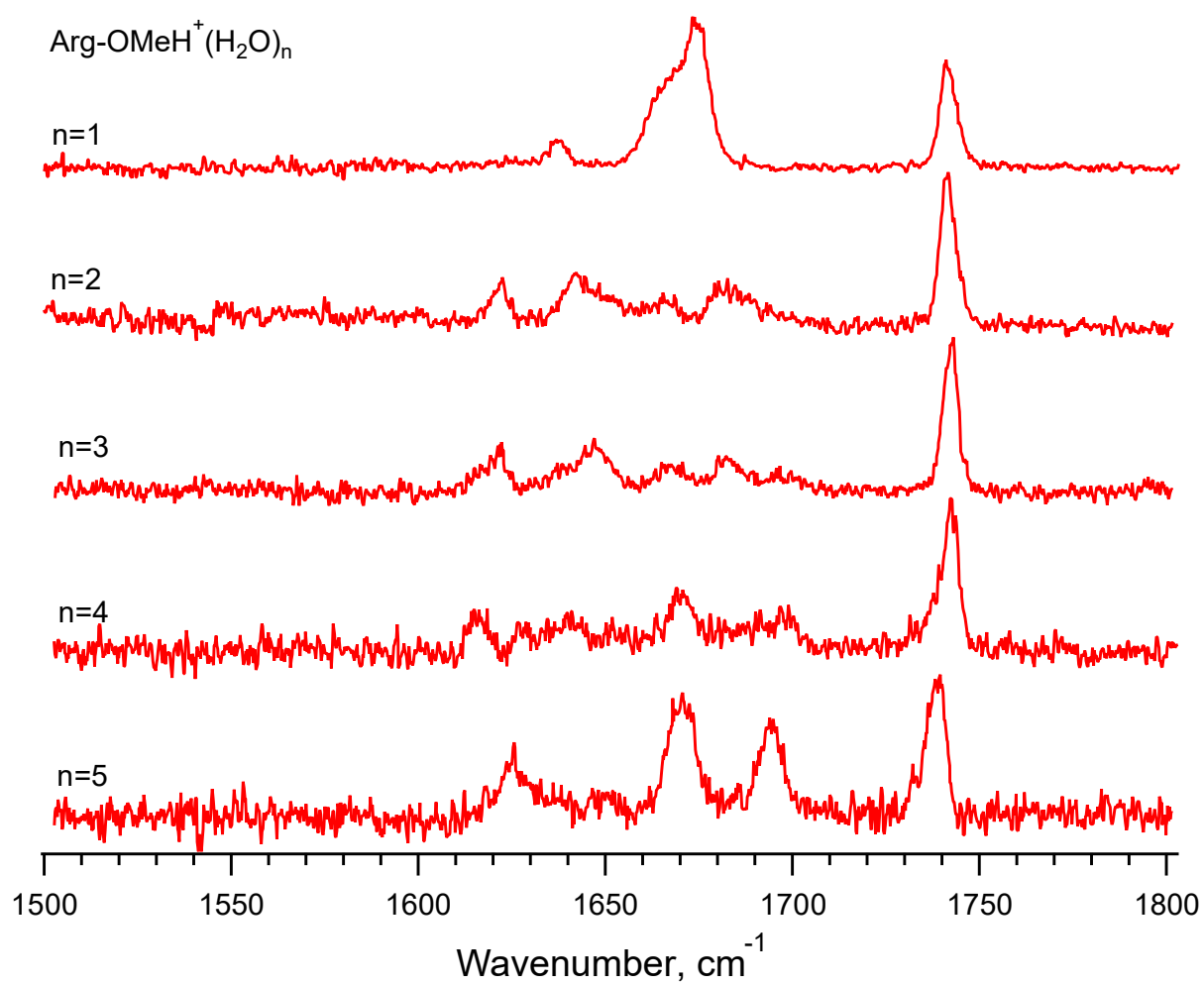


Figure 4.S3. IRPD spectra of Arg-OMeH⁺(H₂O)_n ($n = 1-5$) measured by loss of a water molecule.

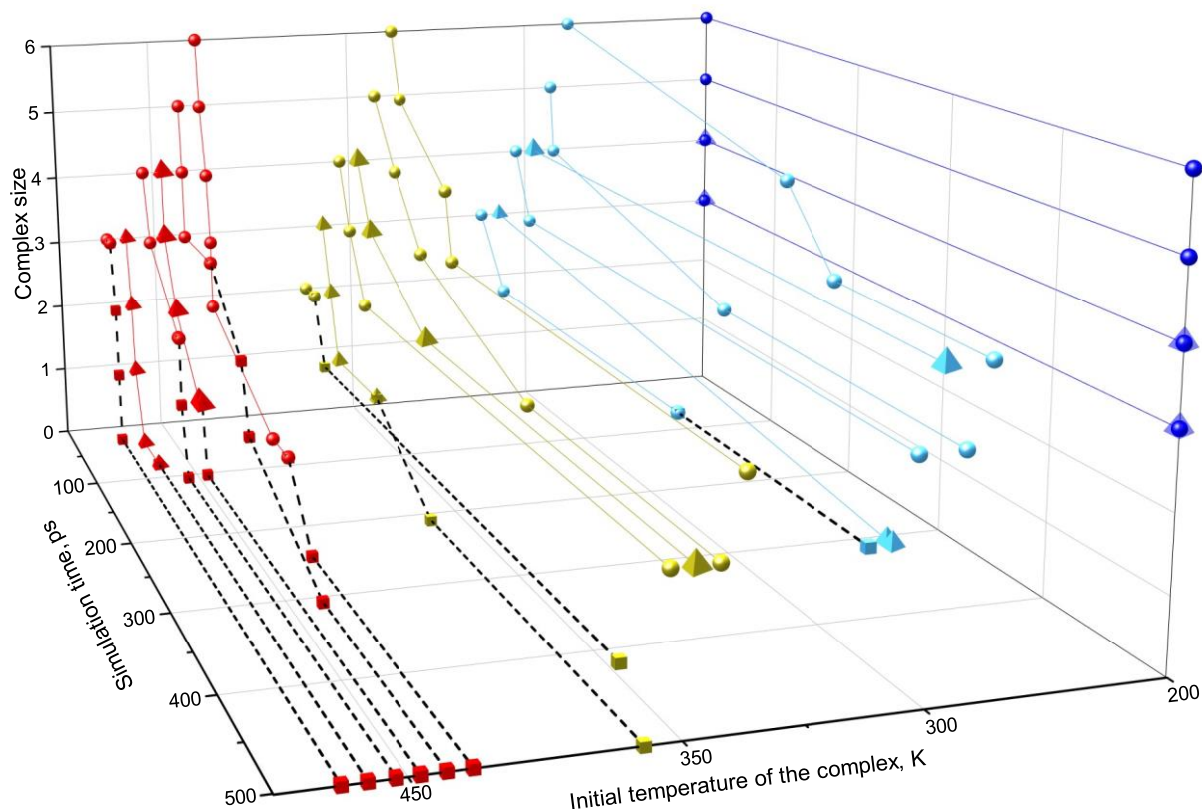


Figure 4.S4. Data from 500 ps MD simulations of the zwitterionic SB conformers of $\text{ArgH}^+(\text{H}_2\text{O})_{3-6}$ at the initial temperatures of 450 K (red), 350 K (yellow), 300 K (cyan), and 200 K (blue). Zwitterionic SB optimized structures for which the energy balance is in favor of the zwitterionic SB ones are represented by triangles, those for which the energy balance favors the CS ones are represented by circles, and CS structures are represented by squares. The relative free energies of the optimized zwitterionic SB/CS structures at $T = 298$ K of $\text{ArgH}^+(\text{H}_2\text{O})_{2-4}$ can be found in Tables 4.S1, 4.S2, and 4.S3. For $\text{ArgH}^+(\text{H}_2\text{O})_{5-6}$, the CS form is always the most stable one from the free energy point of view (6.4 kcal/mol for $n = 5$ and 5.5 kcal/mol for $n = 6$).

In order to explain why zwitterionic SB structures are still present for such small water clusters at the experimental conditions, molecular dynamics (MD) simulations are carried out (Figure 4.S4). We performed semi-empirical (PM6) molecular dynamics simulations for the $\text{ArgH}^+(\text{H}_2\text{O})_{3-6}$ clusters, at various temperatures (200 K, 300 K, 350 K, and 450 K). These temperatures are relevant for the experimental conditions where clusters are subject to a 50 ms pre-trapping in the room temperature octupole ion trap. MD simulations systematically start from a zwitterionic SB structure of the cluster as we assume that the nESI favors the existence of zwitterionic SB forms (i.e. they should dominate in the water droplet). There are always two initial conformations: one for which the energy balance is in favor of the zwitterionic SB

structure and the other for which the energy balance favors the CS one. We have accumulated 500 ps of trajectory for all the cases, of course much shorter time-scale than in the experiment but deemed enough to observe conformational dynamics and water evaporation. Starting from the 200 K dynamics, we see that all clusters are stable at this temperature (over the 500 ps time-scale), i.e. no evaporation of water, however, we observe a conformational dynamics for each cluster, with ArgH^+ changing conformation (isomerization) and also water molecules changing location within the cluster. This isomerization does not systematically lead to the formation of the lowest energy conformer of each cluster size, but rather explores different conformations. Considering that these conformers will be released into the cooling chamber, we thus expect several conformers to be cooled down and probed by spectroscopy. At higher temperatures (300 K, 350 K and 450 K), there is a systematic evaporation of water molecules along the 500 ps dynamics, whatever the size of the cluster. As expected, the timescale for the evaporation of the first water molecule depends on cluster size, temperature, and water binding energy (i.e. the smallest the binding energy, the fastest the evaporation). The evaporation takes place on the tens to hundreds of picoseconds timescale. There are also conformational dynamics/isomerizations systematically occurring before the next evaporation of the subsequent water molecule kicks in. Concerning the zwitterionic $\text{SB} \rightarrow \text{CS}$ transformations, they take place over similar timescales as the first water evaporation and we see clear dependence between the complex size and its probability to occur, i.e. the smaller the cluster size, the higher the zwitterionic $\text{SB} \rightarrow \text{CS}$ transition probability. At last, it also appears that $\text{ArgH}^+(\text{H}_2\text{O})_3$ cluster is somehow a stable system size as the end product of the successive evaporation of water from larger cluster sizes, over the time scale of the molecular dynamics.

Table 4.S4. CS-zwitterionic SB energy balance (DE_{CS-SB}) including the zero-point energy correction, in kcal/mol, for the zwitterionic SB forms of $ArgH^+(H_2O)_{n=2-6}$ complexes. $DE_{CS-SB} < 0$ means CS is more stable than zwitterionic SB.

ArgH⁺(H₂O) zwitterionic SB form	DE_{CS-SB} (kcal/mol)	
2W <i>a</i>	-5.4	
2W <i>b</i>	1.9	3.4
3W <i>a</i>	-3.5	
3W <i>b</i>	1.5	2.9
4W <i>a</i>	-4.0	
4W <i>b</i>	5.6	6.6
5W	-5.5	
6W	-1.9	

Two values mean two different CS forms related to the zwitterionic SB one.

Estimate of dissociation rate and ion temperature for hydrated ArgH⁺

The dissociation rate of the ArgH⁺(H₂O)_n ($n = 0-45$) complexes was estimated from their population distributions (Fig. 4.5) measured without pre-trapping in a room temperature ion trap ($t_0 = 0$) and measured after 50 ms of pre-trapping ($t_{50} = 50$ ms). The distributions were first normalized on their total number of ions. With this, the total number of water molecules in each normalized distribution is given as:

$$N_t = \sum_1^{45} R(n) \cdot n, \quad (1)$$

where $R(n)$ is the relative population of the cluster with n waters. The calculations yield $N_0 = 1541$ and $N_{50} = 455$. Assuming for simplicity that the rate constant for evaporating single water is independent of cluster size, one can write for the fraction of water molecules remaining in the complexes after time t_{50} :

$$\frac{N_{50}}{N_0} = e^{-k_1 \cdot t_{50}}, \quad (2)$$

where k_1 is the rate constant for loss of a single water molecule. Putting into (2) the respective numbers results in $k_1 = 0.02 \text{ ms}^{-1}$. The rate constant for evaporating four waters is, therefore, $k_4 = 0.08 \text{ ms}^{-1}$. The latter implies the average (over the ensemble of the complexes) lifetime for $n = 4$ complexes of ~ 12 ms.

To quantify the temperature of the clusters once the first water molecule evaporates, we have performed several semi-empirical (PM6) molecular dynamics simulations in the NVE ensemble at different temperatures (320-460 K) of the ArgH⁺(H₂O)₄ cluster, and considering that water molecule's evaporation time (t) follows an Arrhenius Law, fitted the latest values to the following expression:

$$\ln\left(\frac{1}{t}\right) = \ln\left(\frac{1}{t_0}\right) - \frac{\Delta G^*}{R} \cdot \frac{1}{T}$$

Figure 4.S5 shows the $\ln(1/t)$, in ps (t_{ps}), versus $1/T(\text{K}^{-1})$ curve along with the linear fitting. From this linear regression, we obtain an activation energy, ΔG^* , of 9.3 ± 1.6 kcal/mol for the process to occur and the following temperatures at time t (T_t) of the cluster if one water molecule evaporates: 160 ± 38 K for 1ms, 150 ± 35 K for 10 ms and 140 ± 33 K for 50 ms.

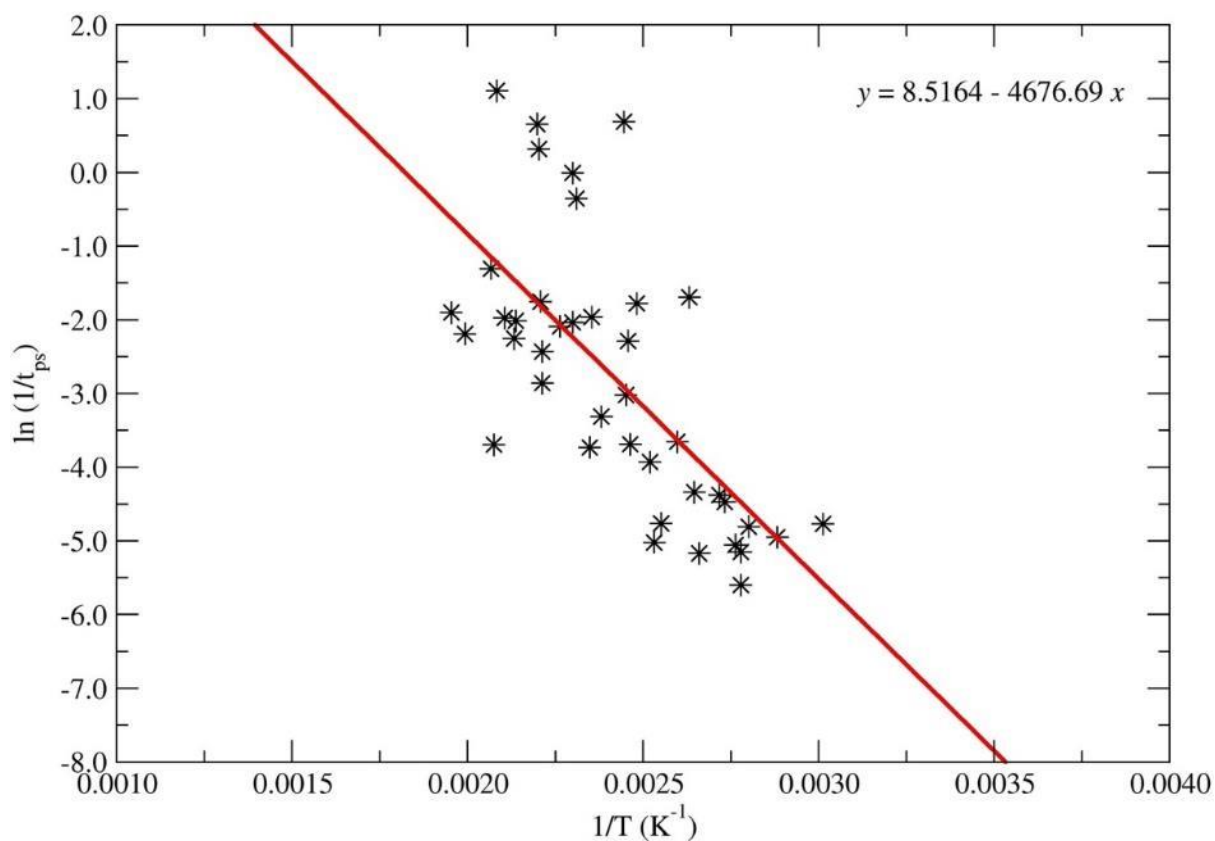


Figure 4.S5. Natural logarithm of the inverse of the 1st water molecule's evaporation time (in picoseconds, t_{ps}) versus the inverse of the temperature of $\text{ArgH}^+(\text{H}_2\text{O})_4$ cluster. The equation of the corresponding linear fitting appears as an insertion at the top-right. The data are obtained from semi-empirical PM6 molecular dynamics simulations.

References

1. Boyarkin, O. V. Cold ion spectroscopy for structural identifications of biomolecules. *Int. Rev. Phys. Chem.* **37**, 559–606 (2018).
2. Mucha, E. *et al.* Unravelling the structure of glycosyl cations via cold-ion infrared spectroscopy. *Nat. Commun.* **9**, 4174 (2018).
3. Menges, F. S. *et al.* Integration of High-Resolution Mass Spectrometry with Cryogenic Ion Vibrational Spectroscopy. *J. Am. Soc. Mass Spectrom.* **30**, 1551–1557 (2019).
4. Martens, J. *et al.* Infrared ion spectroscopy: New opportunities for small-molecule identification in mass spectrometry - A tutorial perspective. *Anal. Chim. Acta* **1093**, 1–15 (2020).
5. Greis, K., Kirschbaum, C., von Helden, G. & Pagel, K. Gas-phase infrared spectroscopy of glycans and glycoconjugates. *Curr. Opin. Struct. Biol.* **72**, 194–202 (2022).
6. Bush, M. F. *et al.* Infrared spectroscopy of cationized lysine and ϵ -N-methyllysine in the gas phase: Effects of alkali-metal ion size and proton affinity on zwitterion stability. *J. Phys. Chem. A* **111**, 7753–7760 (2007).
7. Bush, M. F., Oomens, J., Saykally, R. J. & Williams, E. R. Effects of alkaline earth metal ion complexation on amino acid zwitterion stability: Results from infrared action spectroscopy. *J. Am. Chem. Soc.* **130**, 6463–6471 (2008).
8. Bush, M. F., Oomens, J. & Williams, E. R. Proton affinity and zwitterion stability: New results from infrared spectroscopy and theory of cationized lysine and analogues in the gas phase. *J. Phys. Chem. A* **113**, 431–438 (2009).
9. Forbes, M. W. *et al.* Infrared spectroscopy of arginine cation complexes: Direct observation of gas-phase zwitterions. *J. Phys. Chem. A* **111**, 11759–11770 (2007).
10. Smith, Z. M., Steinmetz, V., Martens, J., Oomens, J. & Poutsma, J. C. Infrared multiple photon dissociation spectroscopy of cationized canavanine: Side-chain substitution influences gas-phase zwitterion formation. *Int. J. Mass Spectrom.* **429**, 158–173 (2018).
11. Bush, M. F., Prell, J. S., Saykally, R. J. & Williams, E. R. One water molecule stabilizes the cationized arginine zwitterion. *J. Am. Chem. Soc.* **129**, 13544–13553 (2007).
12. Burt, M. B. *et al.* Structures of bare and hydrated [Pb(aminoacid-H)]⁺ complexes using infrared multiple photon dissociation spectroscopy. *J. Phys. Chem. B* **115**, 11506–11518 (2011).
13. Lemoff, A. S., Bush, M. F., O'Brien, J. T. & Williams, E. R. Structures of lithiated lysine and structural analogues in the gas phase: Effects of water and proton affinity on

- zwitterionic stability. *J. Phys. Chem. A* **110**, 8433–8442 (2006).
14. Gao, B., Wytttenbach, T. & Bowers, M. T. Protonated arginine and protonated lysine: Hydration and its effect on the stability of salt-bridge structures. *J. Phys. Chem. B* **113**, 9995–10000 (2009).
 15. Gochhayat, J. K., Dey, A. & Pathak, A. K. An ab initio study on the micro-solvation of amino acids: On the number of water molecules necessary to stabilize the zwitter ion. *Chem. Phys. Lett.* **716**, 93–101 (2019).
 16. Hwang, T. K. *et al.* Microsolvation of lysine by water: Computational study of stabilized zwitterion. *J. Phys. Chem. B* **115**, 10147–10153 (2011).
 17. Kim, J. Y., Ahn, D. S., Park, S. W. & Lee, S. Gas phase hydration of amino acids and dipeptides: Effects on the relative stability of zwitterion vs. canonical conformers. *RSC Advances* vol. 4 16352–16361 at <https://doi.org/10.1039/c4ra01217h> (2014).
 18. Li, H., Hu, A., Jiang, J. & Luo, Y. Systematic Study on Hydrated Arginine: Clear Theoretical Evidence for the Canonical-to-Zwitterionic Structure Transition. *J. Phys. Chem. A* **121**, 3598–3605 (2017).
 19. Blom, M. N. *et al.* Stepwise solvation of an amino acid: The appearance of zwitterionic structures. *J. Phys. Chem. A* **111**, 7309–7316 (2007).
 20. Xu, S., Nilles, J. M. & Bowen, K. H. Zwitterion formation in hydrated amino acid, dipole bound anions: How many water molecules are required? *J. Chem. Phys.* **119**, 10696–10701 (2003).
 21. Hebert, M. J. & Russell, D. H. Hydration of Guanidinium Ions: An Experimental Search for Like-Charged Ion Pairs. *J. Phys. Chem. Lett.* **10**, 1349–1354 (2019).
 22. Zviagin, A., Kopysov, V., Nagornova, N. S. & Boyarkin, O. V. Tracking local and global structural changes in a protein by cold ion spectroscopy. *Phys. Chem. Chem. Phys.* **24**, 8158–8165 (2022).
 23. Zviagin, A., Kopysov, V. & Boyarkin, O. V. Gentle nano-electrospray ion source for reliable and efficient generation of microsolvated ions. *Rev. Sci. Instrum.* **93**, 114104 (2022).
 24. Boyarkin, O. V. & Kopysov, V. Cryogenically cooled octupole ion trap for spectroscopy of biomolecular ions. *Rev. Sci. Instrum.* **85**, 033105 (2014).
 25. Lee, C., Yang, W. & Parr, R. G. Development of the Colle-Salvetti correlation-energy formula into a functional of the electron density. *Phys. Rev. B* **37**, 785–789 (1988).
 26. Becke, A. D. Correlation energy of an inhomogeneous electron gas: A coordinate-space model. *J. Chem. Phys.* **88**, 1053 (1998).

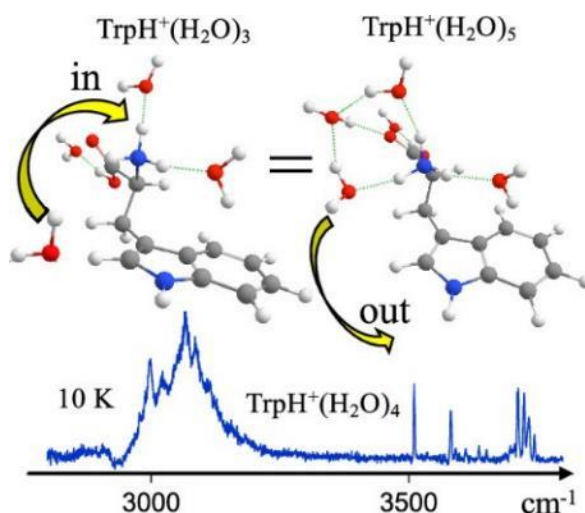
27. Krishnan, R., Binkley, J. S., Seeger, R. & Pople, J. A. Self-consistent molecular orbital methods. XX. A basis set for correlated wave functions. *J. Chem. Phys.* **72**, 650 (2008).
28. Frisch, M. J. *et al.* Gaussian 16, Revision C.01. at (2016).
29. Vandevondele, J. *et al.* Quickstep: Fast and accurate density functional calculations using a mixed Gaussian and plane waves approach. *Comput. Phys. Commun.* **167**, 103–128 (2005).
30. Stewart, J. J. P. Optimization of parameters for semiempirical methods V: Modification of NDDO approximations and application to 70 elements. *J. Mol. Model.* **13**, 1173–1213 (2007).
31. Hong, Z., Wert, J. & Asher, S. UV Resonance Raman and DFT Studies of Arginine Side Chains in Peptides: Insights into Arginine Hydration. *J. Phys. Chem. B* **117**, 7145–7156 (2013).
32. Oomens, J. & Steill, J. D. Free Carboxylate Stretching Modes. *J. Phys. Chem. A* **112**, 3281–3283 (2008).
33. Steill, J. D. & Oomens, J. Gas-Phase Deprotonation of p -Hydroxybenzoic Acid Investigated by IR Spectroscopy: Solution-Phase Structure Is Retained upon ESI. *J. Am. Chem. Soc.* **131**, 13570–13571 (2009).
34. Schmidt, M. & Von Issendorff, B. Gas-phase calorimetry of protonated water clusters. *J. Chem. Phys.* **136**, 164307 (2012).

Chapter 5. Revealing the Native-like Structure of Tryptophan by Cold Ion Spectroscopy of Microhydrated Complexes

Disclaimer: This chapter is adapted from a published article with permission of the publisher and all co-authors.

Zviagin, A., Yamaletdinov, R., Nagornova, N., Dömer, M., & Boyarkin, O. V. (2023). Revealin the structure of tryptophan in microhydrated complexes by cold ion spectroscopy. *The Journal of Physical Chemistry Letters*, 14(26), 6037-6042, DOI: <https://doi.org/10.1021/acs.jpcllett.3c01239>.

Personal contribution: Conceptualization, methodology, formal analysis, visualization, original draft preparation.



5.1. Abstract

The geometry of biomolecules isolated in the gas phase usually differs substantially from their native structures in aqueous solution, which are the only ones truly relevant to life science. To connect the high resolution of cold ion spectroscopy that can be achieved in the gas phase and the key role of intermolecular hydrogen bonds that shape biomolecules in water, we study protonated tryptophan microhydrated by 1-6 water molecules. IR/UV spectra measured with the same instrument under similar conditions appear to be identical for the complexes of the same size produced by soft dehydration and cryogenic condensation methods. This observation points to the lack of kinetic trapping in the dehydration/rehydration processes. Quantum chemistry computations allow for the unambiguous assignment of the measured IR spectra to the most stable conformers of the complexes. The calculations reveal that retaining as few as four water molecules still conserves most of the TrpH^+ native structural features.

5.2. Introduction

Knowledge of the 3D structures of biomolecules is of fundamental importance in many fields of life science. Solving the structures that these large species adopt under native conditions remains one of the biggest challenges that drives the development of new techniques for structural determinations. Cold ion spectroscopy (CIS)¹⁻⁵ in combination with quantum chemistry computations is a recent approach that can solve geometries of small to midsize (e.g., amino acids to decapeptide) biomolecules.^{4,6-11} Although the method demonstrates high accuracy and conformational resolution, it can only determine structures of biomolecules isolated in the gas phase but not in solution. The relation between these intrinsic and biologically relevant native structures often remains vague. Intermolecular noncovalent interactions of a biomolecule with water molecules may compete with the intramolecular noncovalent bonds, leading to substantial alterations of its 3D structure. As a compromise between the high accuracy of structural determinations achievable in the gas phase and the need to determine 3D structures in bulk solution, one can study in the gas phase the biomolecules that are hydrated by a few water molecules.¹²⁻²¹ This approach relies on the assumption that already a few remaining solvent molecules allow for retaining the main characteristic features of such structures in the gas phase.

Charged microhydrated biomolecules can be conveniently generated directly from solution using, for instance, “gentle” electrospray ionization sources.²² Vibrationally resolved spectra of such complexes can be used for validating computed structures. A molecule embedded into its water envelope may exhibit some sufficiently high internal energy barriers for a complex (or the bare ion) to remain kinetically trapped in its native-like geometry at some step of the desolvation.^{16,23,24} This geometry will not be the lowest-energy one, which makes a conformational search among many computed gas-phase structures extremely time-consuming. Failure of the search may point to either an insufficient pool of the tested structures or a certain deficiency of the computations.

Experiments may assist in resolving this ambiguity. Microsolvated complexes can be generated not only by an incomplete desolvation but also by condensing solvent molecules onto bare ions cooled in a cryogenic trap.^{25,26} Full desolvation of ions requires their substantial internal heating; the temperature of bare ions in ESI sources can reach 500 K.²⁷ This makes it more likely for an ion to overcome the native-to-intrinsic structural barriers than in the case of a gradual desolvation at low pressure, when the ion temperature is maintained low by evaporative cooling. The subsequent condensation of solvent molecules onto cold bare ions

will bring their structure back to that in the complexes with retained waters only, if the energy barriers for these rearrangements are smaller than the ion internal energy. The similarity of the ionic conformers in the complexes generated by the two methods can be assessed through comparison of the respective IR or UV spectra yet prior to any computations. Identical spectra for the same complexes generated by the two different techniques point to the adiabatic pathway in both directions: desolvation and condensation. The computed lowest-energy structures then should properly reflect the intrinsic structure of a bare ion but approach its native-like geometry upon increasing the level of hydration. Here we explore this approach with protonated amino acid tryptophan (TrpH^+). It is a benchmark aromatic biomolecule known for its high yield of UV fluorescence in aqueous solutions.^{28,29} Structure and photophysical properties of the gas-phase protonated bare and singly hydrated Trp have been the subject of numerous studies.^{1,12,30–36} Briefly, the most stable conformers of isolated TrpH^+ exhibit a proton– π interaction between the protonated N-terminus and the nearby indole ring. The coupling enables ultrafast barrierless transfer of the proton to the ring in the electronic excited state, which results in broadening of UV transitions.^{12,33} In one of the two conformers of singly hydrated TrpH^+ , the water molecule sticks between the two groups, blocking the proton transfer. This lengthens the lifetime of the excited state and sharpens UV transitions in the respective conformer.^{12,36} Retaining a second water on TrpH^+ increases the intensity of the sharp transitions,¹² although no full conformational analysis of this complex has been done so far.

Here we perform this structural analysis and extend it to protonated tryptophan microhydrated by either retaining or condensing up to six water molecules. For each method of generation and size of the complexes, their IR and/or UV cold ion spectra were measured with the same instrument under identical experimental conditions. The partially assigned experimental IR spectra were used for validating the low-energy structures calculated by quantum chemistry methods. Finally, we analyze the validated structures of the complexes and outline their relation to the native structure of tryptophan.

5.3. Methods

Our experimental approach, except the cryogenically cooled ion pretrap, has been described in detail elsewhere²¹ (see also the Appendix of this chapter and chapter 2). Briefly, the hydrated ions are generated directly from solution using a “gentle” mode of an electrospray ion source.²² Alternatively, the same complexes can be generated by condensing water vapor onto the ions stored in a cryogenic ion pretrap. After the ions of interest are selected with a

quadrupole mass filter, they are transferred to a 10 K ion trap for performing IR photodissociation (IRPD) action spectroscopy.

Structures of the complexes were generated via molecular dynamics annealing and then clustered into groups of similar structures. Geometries and potential energies of the lowest-energy conformers in each group were refined, and then the harmonic spectra and free energies were calculated using density functional theory (see the Appendix of this chapter for details).

5.4. Results and discussion

Figure 5.1 shows IRPD spectra of $\text{TrpH}^+(\text{H}_2\text{O})_n$ ($n = 1-6$) complexes produced by the gentle dehydration of electrosprayed droplets (blue traces). These spectra are almost perfectly identical to the respective spectra measured in the 3 μm spectral region for the complexes generated by the low-temperature condensation of $n = 1-4$ water molecules onto the electrosprayed bare ions (red traces; see also Figure 5.S1). It is essential that the compared spectra have been measured on the same instrument with the same method and under identical conditions. For instance, the recent studies of singly and doubly hydrated protonated glycine, which were produced by the two methods but in two different laboratories, revealed certain ambiguity in the interpretation of the data.^{19,37,38} The ambiguity, potentially, could arise from the method of preparation but also from the difference in the used spectroscopic techniques/experimental conditions. Our modified instrument enables direct assignment of spectral differences, if any, exclusively to the method of microhydration.

The spectral congestion, which increases with the size of the clusters, may hide the fine differences between the IR spectra measured for the same but differently produced complexes. On the other hand, UV spectra of aromatic molecules often exhibit extremely high sensitivity to structural differences of their noncovalent complexes.^{39,40} Regarding this, for the complexes with $n = 4-6$ produced by the two methods, we compared their respective UV spectra (Figure 5.S2).

Again, within the accuracy of the measurements, for each n the pairs of the spectra look identical. This implies that, at least, for each $n = 1-6$, TrpH^+ adopts the same structures regardless of the method of hydration. We rule out any kinetic trapping of gas-phase TrpH^+ , since the geometries of the protonated bare and singly hydrated tryptophan have been solved as the lowest-energy gas-phase conformers. This allows us to suggest that the most stable generated complexes with $n = 1-6$ waters under the conditions of our experiment reside in the global potential energy minima.

In support of our suggestion, Figure 5.1 compares the measured IR spectra to those computed for the low-energy conformers of $\text{TrpH}^+(\text{H}_2\text{O})_n$. Isotopic labeling of the indole ring ($\text{N}^{14} \rightarrow \text{N}^{15}$) allows for direct assignment (Figure 5.S3) of the indole NH-stretch transition. Upon dehydration, its frequency redshifts only a little from 3512 cm^{-1} for $n = 6$ to 3504 cm^{-1} for the bare ion, which allows us to use this transition as a reference for scaling the calculated frequencies. For $n = 1$ they match well to the transitions in the IRPD spectra; the measured spectra, the calculated frequencies, and the two most stable structures appear to be nearly identical to the data earlier reported by Molina et al.³⁶ For $\text{TrpH}^+(\text{H}_2\text{O})_2$, in addition to the IRPD spectrum in Figure 5.1, we explicitly measured conformer-selective IR-UV depletion spectra of this complex (Figure 5.2).

One highly abundant conformer and two low-abundant conformers of the $\text{TrpH}^+(\text{H}_2\text{O})_2$ complex were found while detecting the fragment at $m/z = 188$ Th (loss of two waters and ammonia). The scaled vibrational frequencies calculated for the most stable computed complex, named $2A_1$, match very well to the spectrum of the most abundant conformer, thus validating the calculated geometry (Figure 5.2). The experiment-theory match is equally good between the two conformers of lower abundance (Figure 5.2b, c) and the next two low-energy computed structures (named $2A_2$ and $2A_3$). Similar to the most stable conformer of $\text{TrpH}^+(\text{H}_2\text{O})_1$, the main common structural feature of conformer $2A_{1-3}$ is the insertion of one water molecule between the N-terminus and the indole ring (Figure 5.2). As was discussed above, the insertion interrupts the proton- π coupling that allows fast proton transfer to the indole ring.^{12,36} The structures of the three $\text{TrpH}^+(\text{H}_2\text{O})_2$ conformers validated herein provide a rational explanation of this phenomenon. In these structures the positive charge of the NH_3^+ group is solvated by two H-bonds, leaving one hydrogen atom of the N-terminus free of noncovalent interactions. The unfavorable position of this atom clearly forbids, however, the proton- π coupling.

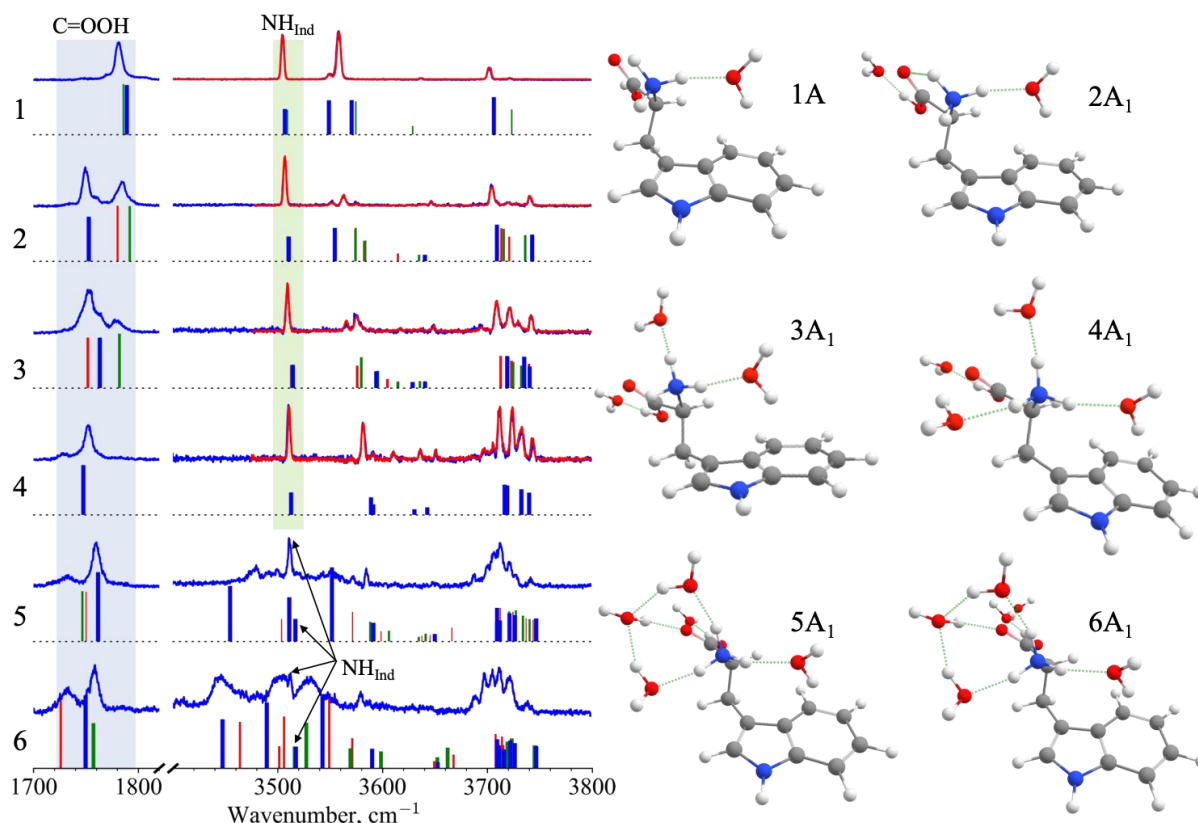


Figure 5.1. IRPD spectra of $\text{TrpH}^+(\text{H}_2\text{O})_n$ complexes generated by retaining (blue) and condensing (red) water molecules. The sticks show the spectra calculated for the low-energy conformers: blue, the most stable structures; green and red, the low-energy structures selected for the best match to the experimental traces (see Table 5.S4). The vertical green bar (for $n = 1-4$) highlights and the arrows (for $n = 5$ and 6) point to the transitions assigned by both experiment and calculations to NH-stretch of the indole ring in the most stable structures; the blue bar highlights the calculated C=OOH stretch transitions. The thickness of the sticks roughly reflects the thermal population of the respective conformers at $T = 300$ K. The computed frequencies are scaled by the factors 0.968 and 0.944 for the 6 and 3 μm spectral regions, respectively. The most stable structures with their labels are shown on the right.

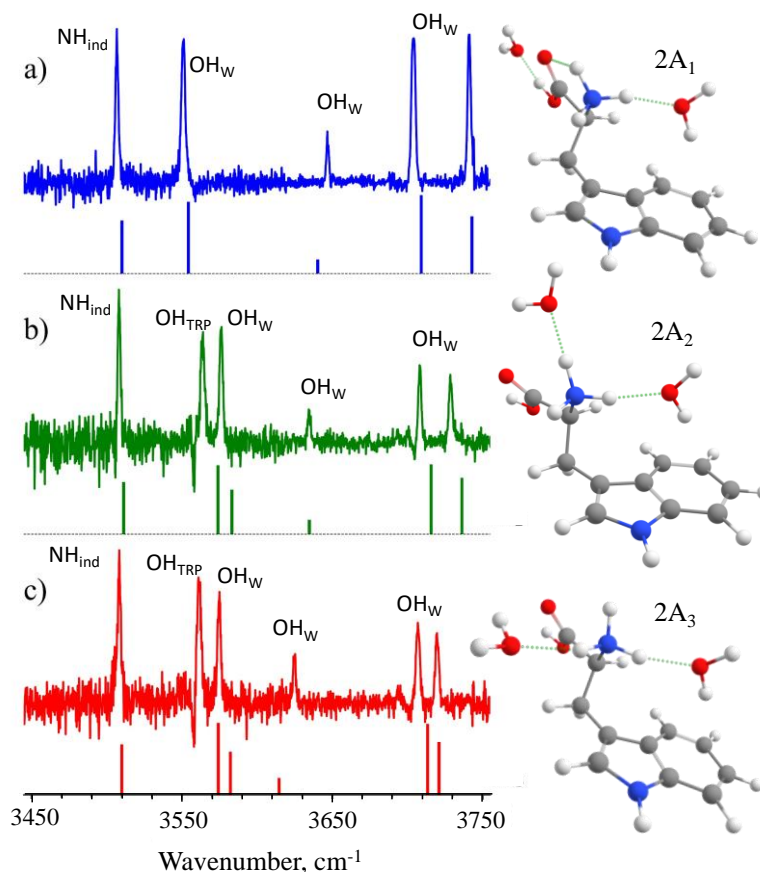


Figure 5.2. Conformer-selective IR-UV depletion spectra of the $\text{TrpH}^+(\text{H}_2\text{O})_2$ complex, measured with UV wavenumber fixed at (a) 35176 cm^{-1} , (b) 35243 cm^{-1} , and (c) 35281 cm^{-1} . The computed spectra of the three most stable conformers $2A_1$, $2A_2$, and $2A_3$ with relative free energy of 0, 0.67, and 0.82 kcal/mol, respectively, are shown by sticks; the respective structures are shown on the right. The complexes were generated from solution by incomplete dehydration.

A close inspection of the UV spectrum (Figure 5.S4) for $n = 2$ reveals a broadband low-intensity absorption beneath the sharp peaks. It must arise from the conformers with a short-lived electronic excited state. Such structures were earlier identified for singly hydrated TrpH^+ .³⁶ Similar conformers were also found among those calculated herein for $n = 1$ and 2 structures with low free energy (named $1B_1$ and $2B_1$; Figure 5.S5), although the very low level of the broadband UV absorption did not allow us to measure their IR spectra. These structures originate from the first excited conformer of bare TrpH^+ , which differ from the most stable one, mainly by the position of carboxyl/amine moieties, relative to the remainder of the molecule.³⁴ Microhydration does not remove this structural difference, enabling two distinct families (nA and nB) of the complexes. IR depletion of the narrow UV peaks assigned to conformers $2A$ makes our experiment have low-sensitivity to conformers $2B$, such that they may contribute only little to the spectra in Figure 5.2.

The very good match between the computed and the measured IR spectra of the complexes with $n = 0-2$ makes us confident in the used level of theory. Regarding this, for the $n = 3-6$ complexes, we limited the conformational search to low-energy structures and our measurements to conformer-nonspecific IRPD spectroscopy only.

The observed similarity of the spectra measured for the dehydrated and rehydrated complexes of the same size implies that upon removal of certain single water molecules from a complex, it may undergo some barrierless (low-barrier) structural rearrangements to the smaller low-energy conformers. Our calculations enable mapping the network of such barrierless transitions from the complexes with $n = 6$ to bare TrpH⁺. Figure 5.3a shows that upon gradual dehydration, the most stable conformer of the largest studied ($n = 6$) complex may relax to the most stable conformer of TrpH⁺ exclusively through the most stable conformers of the intermediate sizes. In support of this suggestion, we directly treated the $2A_1 \rightarrow 1A \rightarrow 0A$ transition, which does not require some large structural changes, by performing DFT optimization of the structures after removing one appropriate water molecule each time. The optimization indeed yields the $1A_1$ and $0A_1$ conformers as the most stable structures of each size.

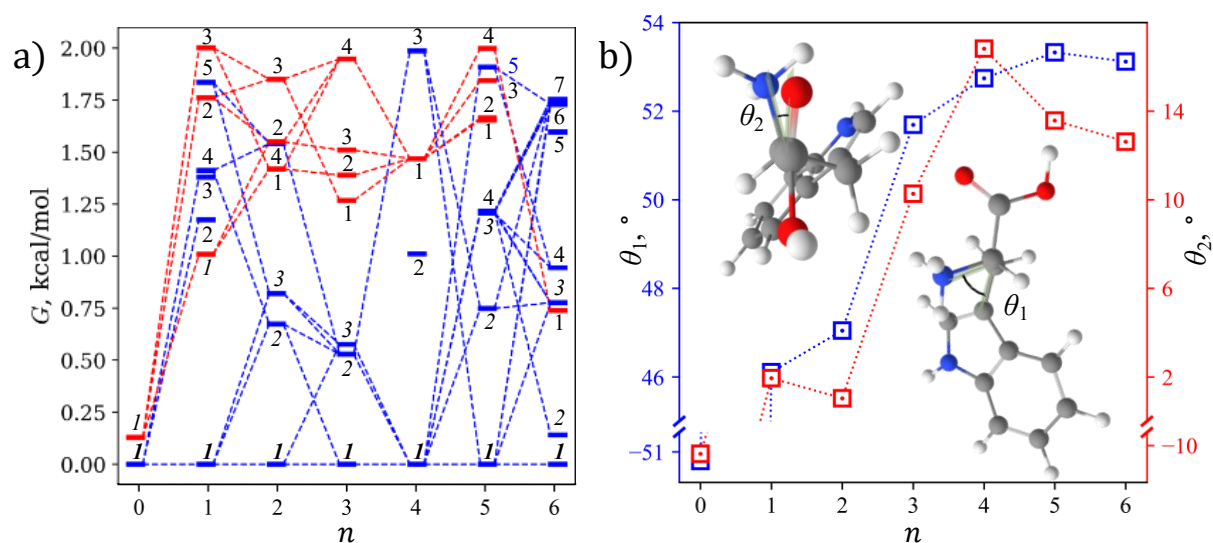


Figure 5.3. (a) Calculated free energies ($G < 2$ kcal/mol) of A (blue bars) and B (red bars) types of TrpH⁺(H₂O)_{*n*} conformers, shown for each *n* relative to the free energies of formation (ΔG_f) of the lowest nA_1 conformer from isolated TrpH⁺ and *n* water molecules; $\Delta G_f = 0, -7.32, -11.92, -15.43, -18.05, -18.9, -19.9$ kcal/mol for $n = 0-6$, respectively. The numbers near the bars indicate subscripts of the conformer labels. Dashed lines connect the conformers, for which the $n \leftrightarrow n + 1$ transitions (except $1A_1 \leftrightarrow 0A_1$) do not require any significant rearrangements in the TrpH⁺ backbone or a migration of water molecules. (b) Evolution of characteristic dihedral angles of the TrpH⁺ structure upon change of *n*.

The calculated geometry of TrpH⁺ in the nA_1 complexes evolves almost gradually upon dehydration with the most prominent changes in the orientation of the indole and COOH groups relative to the NH₃⁺ one. Figure 5.3b plots the dihedral angles between C-NH₃ and C-indole (θ_1) and between C-NH₃ and COOH bonds (θ_2) for $n = 0-6$. Both angles exhibit sharp changes after removing the fourth and the subsequent water molecules. This more than 100° change of θ_2 between the bare TrpH⁺ and the $n = 4$ complex is unlikely in bulk water for this internal rotation of the two large parts of the ion. Reasonably assuming that the geometry of TrpH⁺ is closer to its native structure in the largest studied herein complex of $n = 6$, this change implies that TrpH⁺(H₂O)₄ is the smallest complex, in which tryptophan should still resemble its native structure. The particular role of 4A₁ has a rational explanation. In this complex, four water molecules occupy all four highly hydrophilic hydration sites (NH₃⁺ and OH of the C-terminus), such that the subsequent fifth and sixth waters energetically prefer coupling to these four waters, but not directly to TrpH⁺ (e.g., to NH of imidazole). This limits the impact of the subsequent hydration on the structure of the ion. In addition, the occupation of all hydration sites leads to the lower number of the low-energy conformers for $n = 4$ than for the complexes of the adjacent sizes (3, 5, and 6), which makes the 4A₁ conformer an exclusive bottleneck in the $n = 0 \leftrightarrow 6$ hydration/dehydration pathways.

5.5. Conclusion

In conclusion, cold ion IR/UV spectra of TrpH⁺(H₂O) _{n} ($n = 1-6$) appear to be identical for the complexes of the same size generated by retention and by condensation of water molecules. This observation points to the lack of kinetic trapping of TrpH⁺ in the complexes under our experimental conditions. Consistently, the calculated three lowest free-energy conformers of TrpH⁺(H₂O)₂ have been assigned and validated by IR-UV conformer-selective spectroscopy; their geometry explains the known blocking effect of hydration on the fast proton transfer in isolated tryptophan. The IRPD spectra of the larger complexes are also consistent with the spectra calculated for the respective most stable conformers. Structural changes induced by a gradual dehydration may follow the barrierless pathways from the largest studied complex ($n = 6$) to the fully dehydrated TrpH⁺. The changes remain smooth and gradual down to the $n = 4$ bottleneck structure, which implies that tryptophan hydrated by four waters should yet retain most of the features of its geometry in aqueous solutions. Overall, our study demonstrates that the gas-phase spectroscopy of gradually hydrated/dehydrated small to midsize biomolecules, when combined with quantum chemistry computations, can provide important hints for solving their native-like structures.

Appendix

Materials and methods

L-Tryptophan from Fluka BioChemika ($\geq 99.5\%$) and L-Tryptophan indole- ^{15}N hydrochloride ($\geq 98\%$) from Cambridge Isotope Laboratories were purchased and used without further purification. Methanol of analytical reagent grade is from Fisher Chemical, water of HPLC Plus grade, and acetic acid ($\geq 99\%$) are from Sigma-Aldrich.

Tryptophan was dissolved either in the water/methanol (1/1) mixture (experiments with retained water) or pure water (experiments with condensed water) with 0.2 vol% of acetic acid to the final concentration of 50 μM .

The ions are produced from solution by a nano-electrospray ionization (n-ESI) source and transferred through a metal capillary and three consecutive inline molecular skimmers to a temperature controlled octupole ion trap (pre-trap) for accumulation and thermalization. Microhydrated tryptophan with retained water is produced at the soft conditions of the ion source and accumulated in an octupole ion pre-trap at room temperature. This pre-trap is similar in its design to the 6 K cold trap, but is twice longer and mounted on a cold head that can be cool within 40-310 K only. The details and full characterization of this trap are subject of a forthcoming publication. To produce microhydrated TrpH^+ by condensation of water molecules, the fully dehydrated at the harsh conditions of the ion source ions are trapped in the pre-trap, to which water vapor is continuously introduced through a leak valve. The water vapor flow is adjusted to maintain the total pressure of $2\text{-}4 \cdot 10^{-4}$ mbar and the temperature of the pre-trap is optimized for each complex size of microhydrated tryptophan within 140-180 K.

After accumulation, thermalization and condensation, the protonated complexes are released, mass-selected by a quadrupole mass filter, and guided into a cold octupole ion trap (CIT) which is kept at 6 K. The ions are trapped and cooled by collisions with pulsing He and interrogated by either IR, UV, or IR-UV laser pulses. The resulting parent and fragment ions are released and detected by a second quadrupole mass filter equipped with a channeltron detector. IR pulses of 1 cm^{-1} spectral linewidth and of 4 ± 1 mJ/pulse and 1.8 ± 0.3 mJ energy in the 3 and 6 μm spectral regions, respectively, are produced at 10 Hz repetition rate by an optical parametric oscillator (OPO), which is pumped by 8 ns pulses of a Nd:YAG laser. IR absorption by the complexes produces their photo fragments that correspond to the loss of 1-2 water molecules by the parent ions; the complexes that lost single waters are detected. For UV spectroscopy, the 5-6 ns UV pulses are generated at 10 Hz repetition rate by a frequency-doubled dye laser pumped by 7 ns pulses of a Nd:YAG laser at 355 nm. The pulse energy is

maintained close to 0.5 mJ through the scanning range of the dye laser; the average power of UV light is continuously monitored by a broadband pyroelectric detector and used for normalization of the ion signal. The UV light has 0.15 cm^{-1} spectral linewidth; the wavenumber of the dye laser is continuously measured by a wave meter with $\pm 0.05\text{ cm}^{-1}$ accuracy. The mass spectrometer operates in a 20 Hz cycle and the laser-free cycle is used to measure the signal of the parent ions in the cold trap; this signal then is used to normalize the fragment signal. Each data point is averaged based on 10 measurements and each spectrum is recorded at least three times to ensure its reproducibility.

In order to interpret the experimental data, we perform a stochastic search of possible $\text{TrpH}^+(\text{H}_2\text{O})_n$ ($n = 1-6$) conformers using molecular dynamics (MD) annealing followed by density functional theory (DFT) structures and energy refinement, as well as calculation of harmonic vibrations for the lowest energy conformers.

MD simulations were carried out in NAMD2 software (NAMD was developed by the Theoretical and Computational Biophysics Group in the Beckman Institute for Advanced Science and Technology at the University of Illinois at Urbana-Champaign.)⁴¹ with CHARMM36 force-field for tryptophan,⁴²⁻⁴⁵ and TIP3P water model.⁴⁶ For each simulation, we set the initial temperature to 5000 K with a decrease rate of 100 K/ps until reaching 400 K; the final temperature was held for 46 ps (time step – 1 fs). For various $\text{TrpH}^+(\text{H}_2\text{O})_n$ ($n = 1-6$) complexes, we performed a series of annealing simulations until the number of new conformers ceased to increase sharply. Thus, we ran 250, 250, 500, 1500, 1500, and 2000 annealing simulations for $n=1, 2, 3, 4, 5,$ and $6,$ respectively. After the MD annealing procedure, we performed a classification of structures based on the independent comparison of differences in tensors of inertia of TrpH^+ and $(\text{H}_2\text{O})_n$ with the thresholds adjusted to maximum values which allow us to distinguish $\text{TrpH}^+(\text{H}_2\text{O})_6$ clusters. We obtain the total number of clusters: 62, 54, 92, 485, 650, and 812 for $n=1, 2, 3, 4, 5,$ and $6,$ respectively, and the size of each cluster is in the range 1-58, depending on the conformer energy and n . The size of the lowest energy clusters is 15, 18, 58, 19, 9, and 7 for $n=1, 2, 3, 4, 5,$ and $6,$ respectively. The median size of the clusters taken for further DFT refinement is 2.

Conformers with MD energy lower than 10 kcal/mol above the lowest energy structures were selected for further DFT geometry and energy refinement (17, 18, 53, 64, 103 and 121 conformers for $n=1, 2, 3, 4, 5$ and $6,$ respectively). DFT simulations were carried out in Gaussian 16 package⁴⁷ with Minnesota M05-2X exchange-correlation functional⁴⁸ and augmented correlation-consistent polarized basis set aug-cc-pVDZ.^{49,50} After DFT refinement, harmonic frequencies were calculated for the lowest energy conformers ($E < 5\text{ kcal/mol}$; 10,

14, 24, 33, 41, and 75 conformers for $n=1, 2, 3, 4, 5,$ and $6,$ respectively). In this paper, we present and compare the free energy of the conformers.

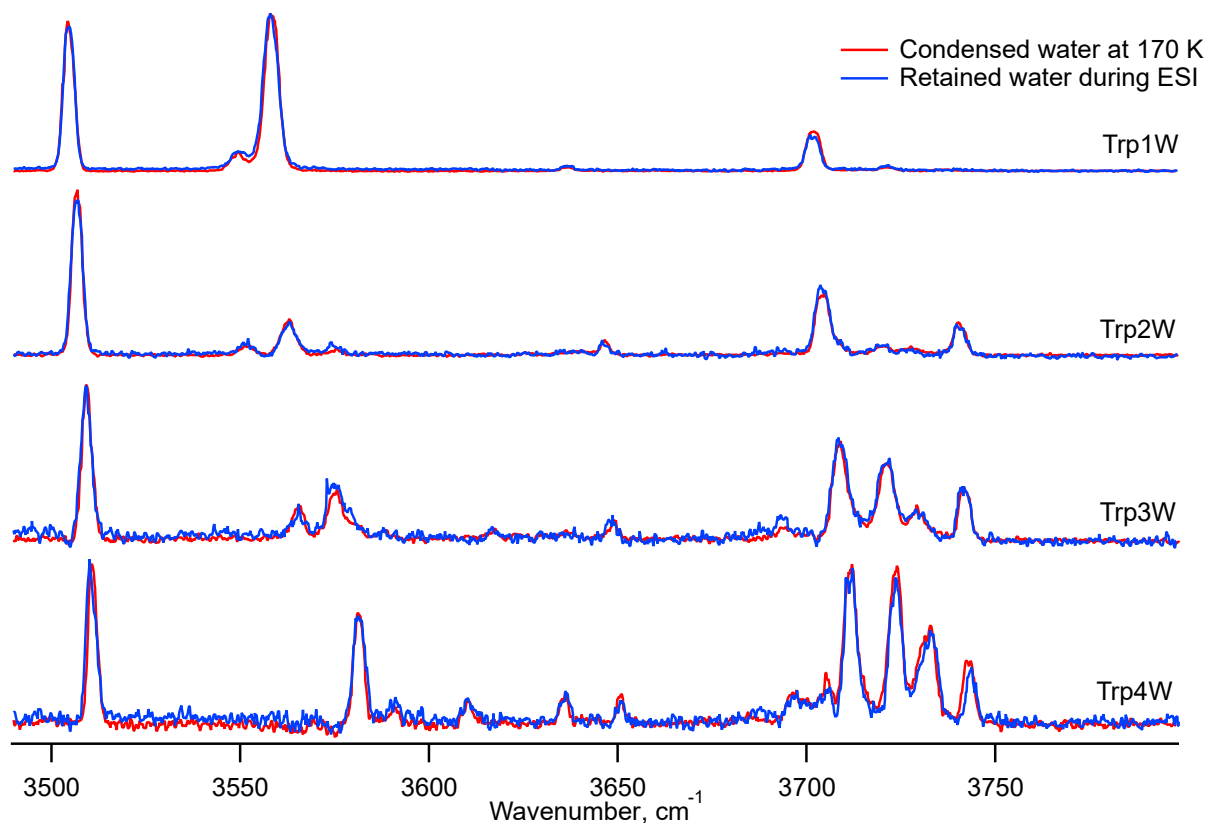


Figure 5.S1. IR photofragment spectra of TrpH⁺(H₂O)_n ($n = 1-4$) complexes with retained (blue traces) and condensed (red traces) water molecules.

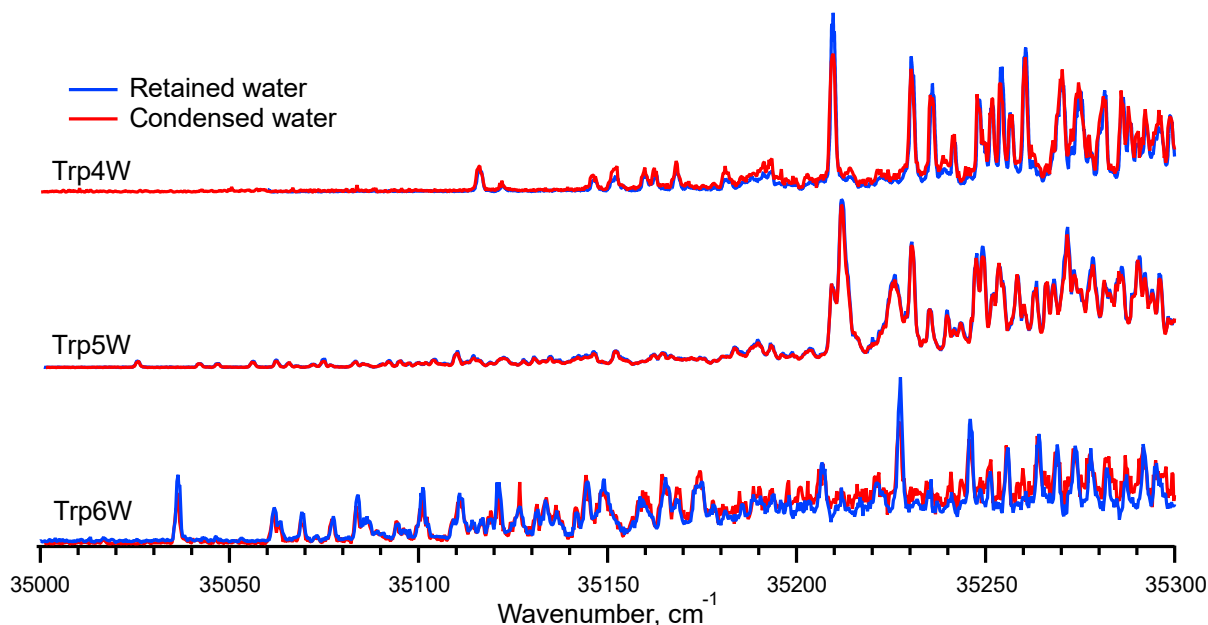


Figure 5.S2. UV photofragment spectra of TrpH⁺(H₂O)_n ($n = 4-6$) complexes with retained (blue traces) and condensed (red traces) water molecules. The latter complexes were prepared at the temperature of the cryogenic pre-trap of 170 K, 150 K, and 140 K for $n= 4, 5,$ and $6,$ respectively.

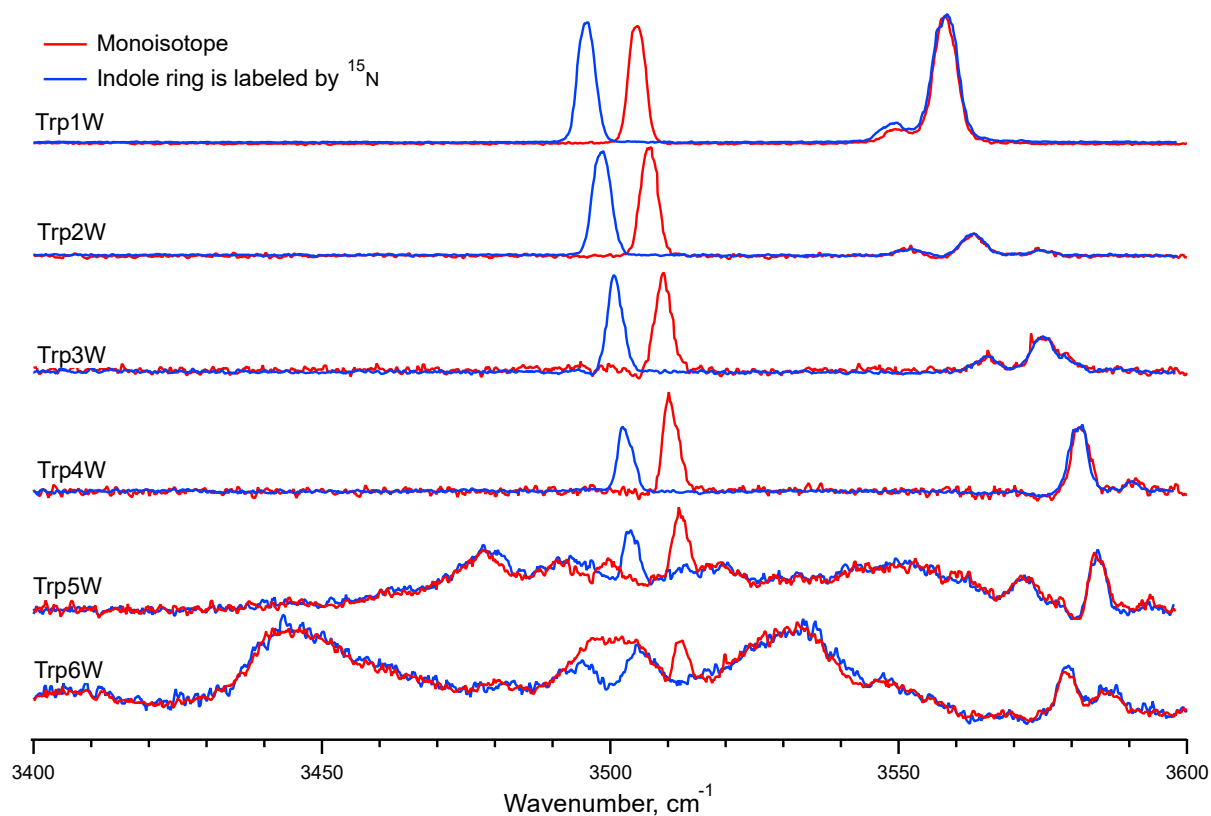


Figure 5.S3. IR photofragment spectra of $\text{TrpH}^+(\text{H}_2\text{O})_n$ ($n = 1-6$) complexes with monoisotopic (red traces) and isotopically-labeled (blue traces) indole nitrogen (^{15}N) of tryptophan.

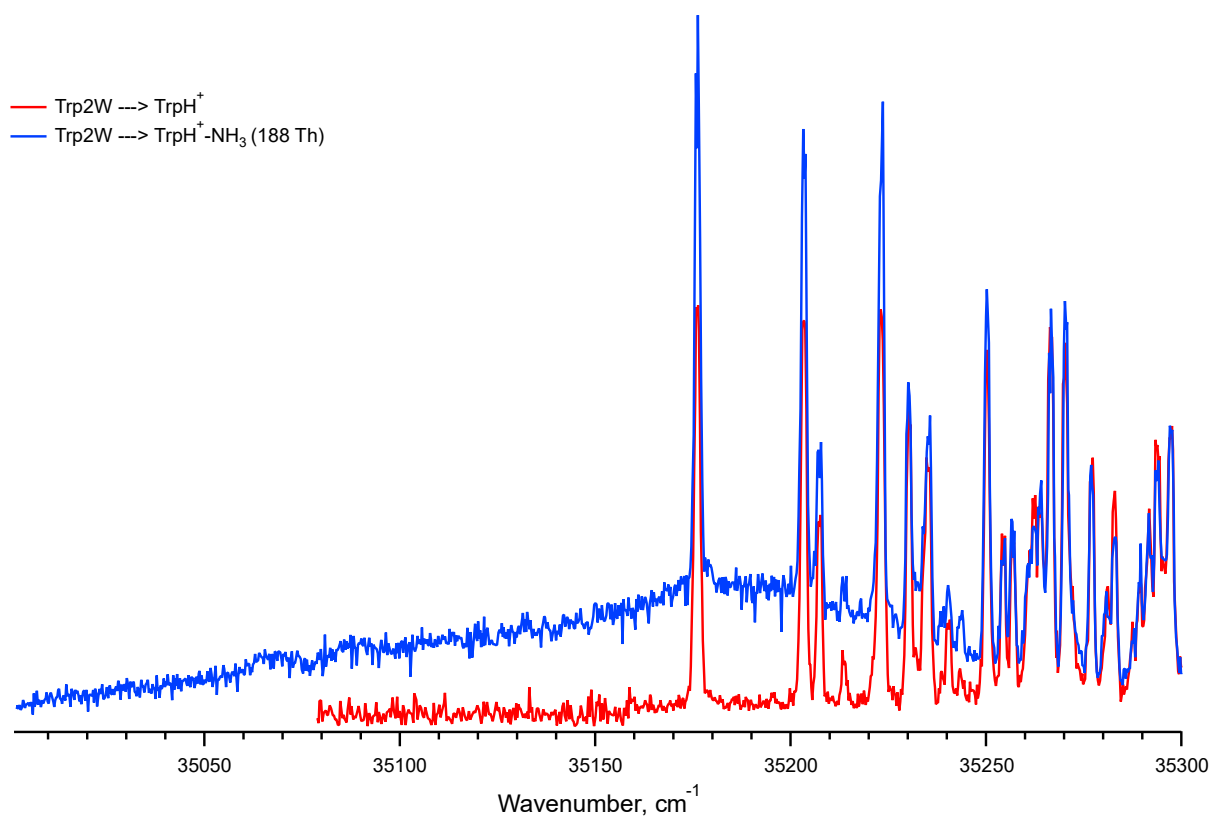


Figure 5.S4. UV photofragment spectra of $\text{TrpH}^+(\text{H}_2\text{O})_2$ recorded through TrpH^+ (red trace) and $\text{TrpH}^+-\text{NH}_3$ (blue trace) fragmentation channels.

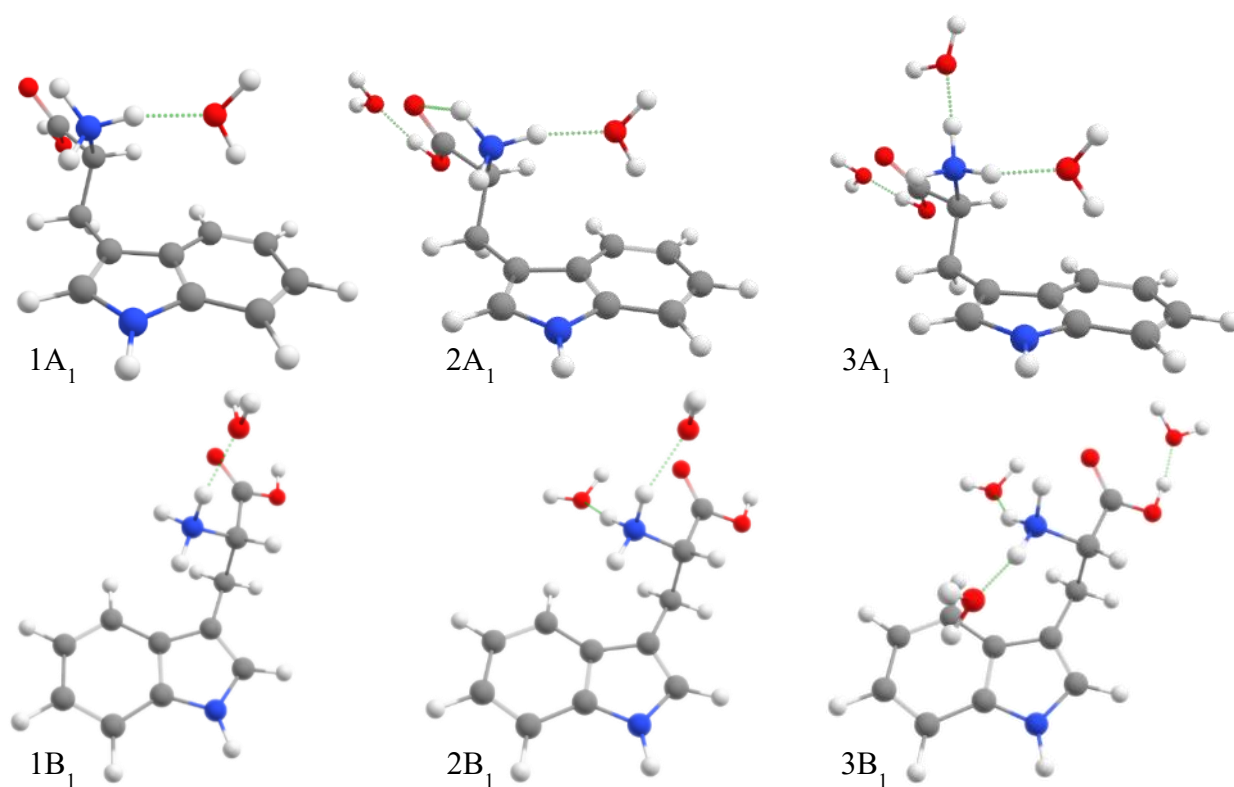


Figure 5.S5. Structures of the lowest energy A- and B-type conformers of $\text{TrpH}^+(\text{H}_2\text{O})_n$ ($n = 1-3$). Note that in the 3B_1 structure a water molecule resides between the indole ring and the N-terminus, which implies that the proton transfer from the latter to the former should be blocked in this conformer.

Table 5.S1. Relative free-energies of $\text{TrpH}^+(\text{H}_2\text{O})_n$ complexes (in kcal/mol), whose calculated IR spectra exhibit the best match to the measured spectra and are shown in Figure 5.1.

n	1	2	3	4	5	6
	$1\text{A}_1 : 0.00$	$2\text{A}_1 : 0.00$	$3\text{A}_1 : 0.00$	$4\text{A}_1 : 0.00$	$5\text{A}_1 : 0.00$	$6\text{A}_1 : 0.00$
	$1\text{B}_1 : 1.01$	$2\text{A}_2 : 0.67$	$3\text{A}_2 : 0.53$	–	$5\text{A}_2 : 0.75$	$6\text{A}_2 : 0.14$
	–	$2\text{A}_3 : 0.82$	$3\text{A}_3 : 0.58$	–	$5\text{A}_3 : 1.21$	$6\text{A}_3 : 0.78$

References

1. Boyarkin, O. V., Mercier, S. R., Kamariotis, A. & Rizzo, T. R. Electronic Spectroscopy of Cold, Protonated Tryptophan and Tyrosine. *J. Am. Chem. Soc.* **128**, 2816–2817 (2006).
2. Rizzo, T. R., Stearns, J. A. & Boyarkin, O. V. Spectroscopic studies of cold, gas-phase biomolecular ions. *Int. Rev. Phys. Chem.* **28**, 481–515 (2009).
3. Wolk, A. B., Leavitt, C. M., Garand, E. & Johnson, M. A. Cryogenic Ion Chemistry and Spectroscopy. *Acc. Chem. Res.* **47**, 202–210 (2014).
4. Boyarkin, O. V. Cold ion spectroscopy for structural identifications of biomolecules. *Int. Rev. Phys. Chem.* **37**, 559–606 (2018).
5. Kirschbaum, C. & Pagel, K. Lipid Analysis by Mass Spectrometry coupled with Laser Light. *Anal. Sens.* e202200103 (2022).
6. Stearns, J. A. *et al.* Conformation-Specific Spectroscopy and Photodissociation of Cold, Protonated Tyrosine and Phenylalanine. *J. Am. Chem. Soc.* **129**, 11814–11820 (2007).
7. Nagornova, N. S. *et al.* Cold-Ion Spectroscopy Reveals the Intrinsic Structure of a Decapeptide. *Angew. Chem. Int. Ed.* **50**, 5383–5386 (2011).
8. Burke, N. L., Redwine, J. G., Dean, J. C., McLuckey, S. A. & Zwier, T. S. UV and IR spectroscopy of cold protonated leucine enkephalin. *Int. J. Mass Spectrom.* **378**, 196–205 (2015).
9. Sekiguchi, T. *et al.* Molecular Recognition by a Short Partial Peptide of the Adrenergic Receptor: A Bottom-Up Approach. *Angew. Chem. Int. Ed.* **57**, 5626–5629 (2018).
10. Zhang, H. *et al.* Cryogenic “Iodide-Tagging” Photoelectron Spectroscopy: A Sensitive Probe for Specific Binding Sites of Amino Acids. *J. Phys. Chem. Lett.* **11**, 4346–4352 (2020).
11. Kirschbaum, C. *et al.* Unravelling the structural complexity of glycolipids with cryogenic infrared spectroscopy. *Nat. Commun.* **12**, 1201 (2021).
12. Mercier, S. R. *et al.* Microsolvation Effects on the Excited-State Dynamics of Protonated Tryptophan. *J. Am. Chem. Soc.* **128**, 16938–16943 (2006).
13. Bush, M. F., Prell, J. S., Saykally, R. J. & Williams, E. R. One Water Molecule Stabilizes the Cationized Arginine Zwitterion. *J. Am. Chem. Soc.* **129**, 13544–13553 (2007).
14. Gao, B., Wyttenbach, T. & Bowers, M. T. Protonated Arginine and Protonated Lysine: Hydration and Its Effect on the Stability of Salt-Bridge Structures. *J. Phys. Chem. B* **113**, 9995–10000 (2009).

15. Nagornova, N. S., Rizzo, T. R. & Boyarkin, O. V. Interplay of Intra- and Intermolecular H-Bonding in a Progressively Solvated Macrocyclic Peptide. *Science*. **336**, 320–323 (2012).
16. Silveira, J. A. *et al.* From Solution to the Gas Phase: Stepwise Dehydration and Kinetic Trapping of Substance P Reveals the Origin of Peptide Conformations. *J. Am. Chem. Soc.* **135**, 19147–19153 (2013).
17. Chang, T. M., Chakrabarty, S. & Williams, E. R. Hydration of Gaseous *m*-Aminobenzoic Acid: Ionic vs Neutral Hydrogen Bonding and Water Bridges. *J. Am. Chem. Soc.* **136**, 10440–10449 (2014).
18. Roy, T. K., Nagornova, N. S., Boyarkin, O. V. & Gerber, R. B. A Decapeptide Hydrated by Two Waters: Conformers Determined by Theory and Validated by Cold Ion Spectroscopy. *J. Phys. Chem. A* **121**, 9401–9408 (2017).
19. Fischer, K. C., Sherman, S. L., Voss, J. M., Zhou, J. & Garand, E. Microsolvation Structures of Protonated Glycine and L-Alanine. *J. Phys. Chem. A* **123**, 3355–3366 (2019).
20. Hirata, K., Haddad, F., Dopfer, O., Ishiuchi, S. & Fujii, M. Collision-assisted stripping for determination of microsolvation-dependent protonation sites in hydrated clusters by cryogenic ion trap infrared spectroscopy: the case of benzocaineH⁺ (H₂O)_n. *Phys. Chem. Chem. Phys.* **24**, 5774–5779 (2022).
21. Zviagin, A., Kopysov, V., Nagornova, N. S. & Boyarkin, O. V. Tracking local and global structural changes in a protein by cold ion spectroscopy. *Phys. Chem. Chem. Phys.* **24**, 8158–8165 (2022).
22. Zviagin, A., Kopysov, V. & Boyarkin, O. V. Gentle nano-electrospray ion source for reliable and efficient generation of microsolvated ions. *Rev. Sci. Instrum.* **93**, (2022).
23. Patrick, A. L., Cismesia, A. P., Tesler, L. F. & Polfer, N. C. Effects of ESI conditions on kinetic trapping of the solution-phase protonation isomer of *p*-aminobenzoic acid in the gas phase. *Int. J. Mass Spectrom.* **418**, 148–155 (2017).
24. Wako, H. *et al.* A conformational study of protonated noradrenaline by UV–UV and IR dip double resonance laser spectroscopy combined with an electrospray and a cold ion trap method. *Phys. Chem. Chem. Phys.* **19**, 10777–10785 (2017).
25. Marsh, B. M., Voss, J. M. & Garand, E. A dual cryogenic ion trap spectrometer for the formation and characterization of solvated ionic clusters. *J. Chem. Phys.* **143**, 204201 (2015).
26. Voss, J. M., Fischer, K. C. & Garand, E. Accessing the Vibrational Signatures of Amino

- Acid Ions Embedded in Water Clusters. *J. Phys. Chem. Lett.* **9**, 2246–2250 (2018).
27. Gabelica, V. & Pauw, E. De. Internal energy and fragmentation of ions produced in electrospray sources. *Mass Spectrom. Rev.* **24**, 566–587 (2005).
 28. Chen, R. F. Fluorescence Quantum Yields of Tryptophan and Tyrosine. *Anal. Lett.* **1**, 35–42 (1967).
 29. Robbins, R. J. *et al.* Photophysics of aqueous tryptophan: pH and temperature effects. *J. Am. Chem. Soc.* **102**, 6271–6279 (1980).
 30. Sobolewski, A. L., Domcke, W., Dedonder-Lardeux, C. & Jouvet, C. Excited-state hydrogen detachment and hydrogen transfer driven by repulsive $1\pi\sigma^*$ states: A new paradigm for nonradiative decay in aromatic biomolecules. *Phys. Chem. Chem. Phys.* **4**, 1093–1100 (2002).
 31. Nolting, D., Marian, C. & Weinkauff, R. Protonation effect on the electronic spectrum of tryptophan in the gas phase. *Phys. Chem. Chem. Phys.* **6**, 2633 (2004).
 32. Kang, H. *et al.* Ultrafast deactivation mechanisms of protonated aromatic amino acids following UV excitation. *Phys. Chem. Chem. Phys.* **7**, 394–398 (2005).
 33. Lepère, V. *et al.* Comprehensive characterization of the photodissociation pathways of protonated tryptophan. *J. Chem. Phys.* **127**, 134313 (2007).
 34. Pereverzev, A. Y. *et al.* Vibrational Signatures of Conformer-Specific Intramolecular Interactions in Protonated Tryptophan. *J. Phys. Chem. A* **120**, 5598–5608 (2016).
 35. Spieler, S. *et al.* Vibrational Predissociation Spectroscopy of Cold Protonated Tryptophan with Different Messenger Tags. *J. Phys. Chem. A* **122**, 8037–8046.
 36. Molina, F. *et al.* Conformer-selective Photodynamics of $\text{TrpH}^+ - \text{H}_2\text{O}$. *ChemPhysChem* **24**, (2023).
 37. Sapparbaev, E., Aladinskaia, V., Zviagin, A. & Boyarkin, O. V. Microhydration of Biomolecules: Revealing the Native Structures by Cold Ion IR Spectroscopy. *J. Phys. Chem. Lett.* **12**, 907–911 (2021).
 38. Sherman, S. L., Nickson, K. A. & Garand, E. Comment on “Microhydration of Biomolecules: Revealing the Native Structures by Cold Ion IR Spectroscopy”. *J. Phys. Chem. Lett.* **13**, 2046–2050 (2022).
 39. Cocinero, E. J., Carcabal, P., Vaden, T. D., Simons, J. P. & Davis, B. G. Sensing the anomeric effect in a solvent-free environment. *Nature* **469**, 76–79 (2011).
 40. Sapparbaev, E., Kopysov, V., Yamaletdinov, R., Pereverzev, A. Y. & Boyarkin, O. V. Interplay of H-Bonds with Aromatics in Isolated Complexes Identifies Isomeric Carbohydrates. *Angew. Chem. Int. Ed.* **131**, 7424–7428 (2019).

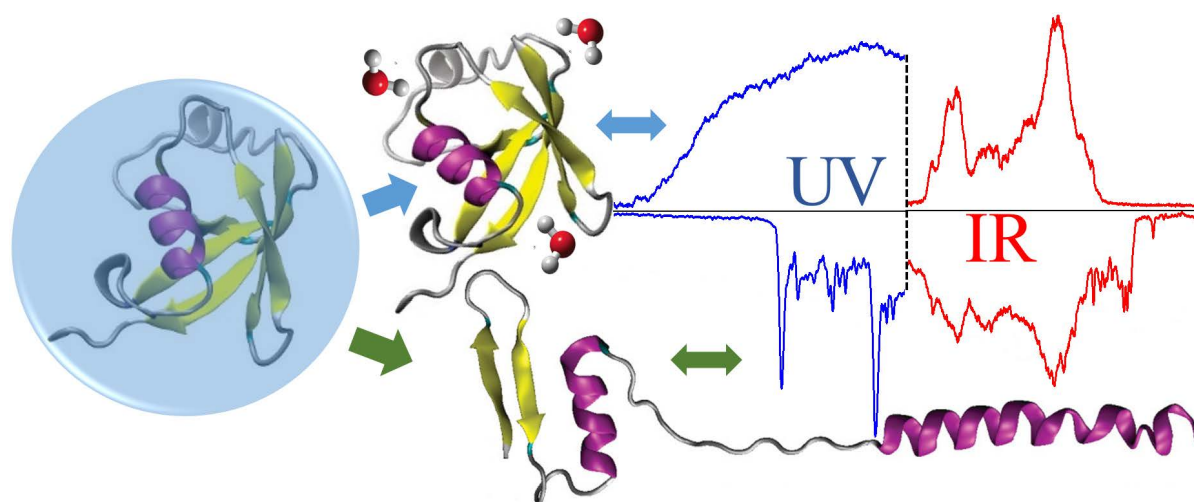
41. Phillips, J. C. *et al.* Scalable molecular dynamics on CPU and GPU architectures with NAMD. *J. Chem. Phys.* **153**, 044130 (2020).
42. MacKerell, A. D. *et al.* All-Atom Empirical Potential for Molecular Modeling and Dynamics Studies of Proteins. *J. Phys. Chem. B* **102**, 3586–3616 (1998).
43. MacKerell, A. D., Feig, M. & Brooks, C. L. Improved Treatment of the Protein Backbone in Empirical Force Fields. *J. Am. Chem. Soc.* **126**, 698–699 (2004).
44. Best, R. B. *et al.* Optimization of the Additive CHARMM All-Atom Protein Force Field Targeting Improved Sampling of the Backbone ϕ , ψ and Side-Chain χ 1 and χ 2 Dihedral Angles. *J. Chem. Theory Comput.* **8**, 3257–3273 (2012).
45. Huang, J. *et al.* CHARMM36m: an improved force field for folded and intrinsically disordered proteins. *Nat. Methods* **14**, 71–73 (2017).
46. Jorgensen, W. L., Chandrasekhar, J., Madura, J. D., Impey, R. W. & Klein, M. L. Comparison of simple potential functions for simulating liquid water. *J. Chem. Phys.* **79**, 926–935 (1983).
47. Frisch, M. J. *et al.* Gaussian 16, Revision C.01. Gaussian, Inc.: Wallingford, CT (2016).
48. Zhao, Y., Schultz, N. E. & Truhlar, D. G. Design of Density Functionals by Combining the Method of Constraint Satisfaction with Parametrization for Thermochemistry, Thermochemical Kinetics, and Noncovalent Interactions. *J. Chem. Theory Comput.* **2**, 364–382 (2006).
49. Dunning, T. H. Gaussian basis sets for use in correlated molecular calculations. I. The atoms boron through neon and hydrogen. *J. Chem. Phys.* **90**, 1007–1023 (1989).
50. Kendall, R. A., Dunning, T. H. & Harrison, R. J. Electron affinities of the first-row atoms revisited. Systematic basis sets and wave functions. *J. Chem. Phys.* **96**, 6796–6806 (1992).

Chapter 6. Tracking local and global structural changes in a protein by cold ion spectroscopy

Disclaimer: This chapter is adapted from a published article with permission of the publisher and all co-authors.

Zviagin, A., Kopysov, V., Nagornova, N. S., & Boyarkin, O. V. (2022). Tracking local and global structural changes in a protein by cold ion spectroscopy. *Physical Chemistry Chemical Physics*, 24(14), 8158-8165, DOI: <https://doi.org/10.1039/D2CP00217E>.

Personal contribution: Conceptualization, methodology, formal analysis, visualization, original draft preparation.



6.1. Abstract

Characterization of native structures of proteins in the gas phase remains challenging due to the unpredictable conformational changes the molecules undergo during desolvation and ionization. We spectroscopically studied cryogenically cooled protonated protein ubiquitin and its microhydrated complexes prepared in the gas phase in a range of charge states under different ionization conditions. The UV spectra appear vibrationally resolved for the unfolded protein, but become redshifted and smooth for the native-like structures of ubiquitin. This spectroscopic change results from the H-bonding of the hydroxyl of Tyr to the amide group of Glu-51 in the compact structures; the minimum length of this bond was estimated to be ~ 1.7 Å. IR spectroscopy reflects the global structural change by observing redshifts of free NH/OH-stretch vibrational transitions. Evaporative cooling of microhydrated complexes of ubiquitin keeps the protein chilly during ionization, enabling native-like conformers with up to eight protons to survive in the gas phase.

6.2. Introduction

Characterization of 3D native structures of proteins remains the focus of life science. Nuclear magnetic resonance, X-ray crystallography and cryogenic electron microscopy within their known limitations are capable of solving the 3D structures of proteins in the condensed phase. Mass spectrometry (MS)-based methods can characterize molecules in the gas phase with unprecedented sensitivity and selectivity and on short timescales, which allows for high throughput screening of biological samples in a variety of -omics applications. Although MS, when combined with different methods of molecular fragmentation (*e.g.*, collisional, electron transfer or photo), is the key approach for sequencing of proteins, the ability of MS itself to reveal 3D structures of these large biomolecules remains fairly limited. Moreover, the stress that proteins experience in MS measurements during the transfer from solution to the gas phase may crucially alter their native geometry. Along with other MS-based approaches, the ion mobility (IM) technique allows monitoring of these changes and the selection of specific conformers prior to MS investigations. However, IM determines the collisional cross-section of ions, which characterizes their geometry globally only, without revealing any local structural changes. Cold ion photofragmentation spectroscopy (CIS) is a recent addition to the toolbox of gas phase structural studies.^{1,2} Cooling suppresses thermal broadening in the UV/IR spectra,^{3,4} making them vibrationally resolved, while MS detection of charged fragments adds many benefits to this technique. The resolved spectra allow for the indirect but stringent structural characterization of biomolecules. Accurate gas-phase geometries of biomolecules as large as decapeptides and of their non-covalent complexes have been determined by validating quantum chemistry computations with CIS data.^{5,6} However, the extension of spectroscopy to proteins is questionable due to their large number of vibrations. UV and IR spectra of a small protein cytochrome *c*, for instance, exhibit no vibrationally resolved structure even under cryogenic cooling.⁷ Here, we report the gas-phase UV and IR spectra of a small protein, ubiquitin (Ubi), as well as of its microhydrated complexes, produced in a range of protonated charge states, from different solutions and under different conditions of electrospray ionization. Referring to the known global geometries of Ubi, evaluated in IM studies, the spectra have been related to some local and global structural changes in the protein.

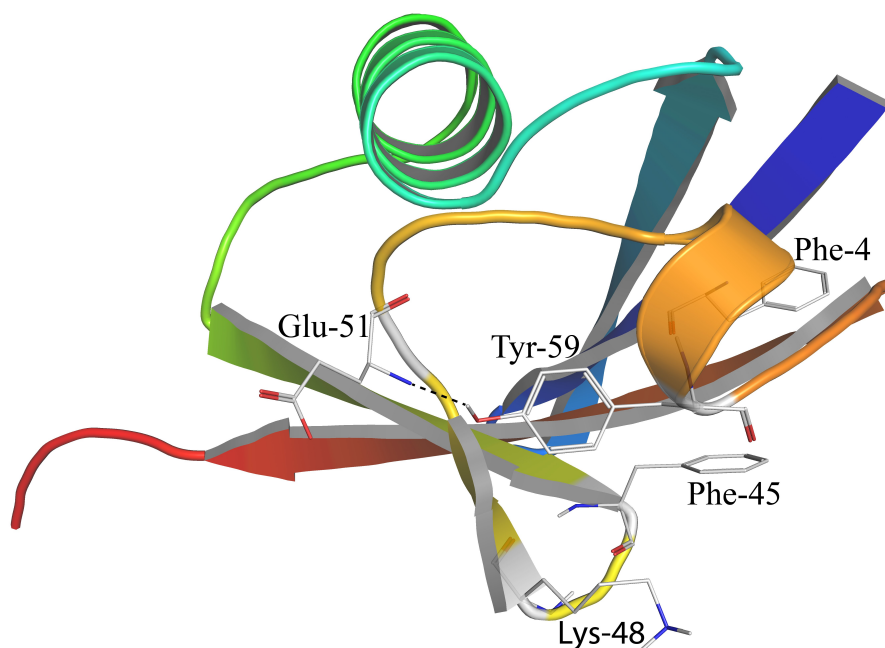


Figure 6.1. 3D backbone structure of ubiquitin measured by X-ray diffraction (1UBQ).⁸ Lys-48, Glu-51 and aromatic residues are shown explicitly. The dashed line indicates the hydrogen bond between the hydroxyl of Tyr-59 and the amide group of Glu-51.

Ubiquitin is a highly conserved eukaryotic protein, which is involved in the processes of intracellular protein degradation. It contains 76 residues, including one tyrosine and two phenylalanine aromatic residues (Fig. 6.1). It is known to be highly stable in a wide range of pH and temperatures due to a rich network of hydrogen bonds and a large hydrophobic core. The secondary structure of Ubi includes one large and one short α -helices, a mixed β -sheet and a disordered C-terminus domain.⁹ The tertiary gas-phase structure of this benchmark protein in different charge states and under different conditions of desolvation-ionization was extensively studied by H/D exchange,^{10–13} proton transfer reactions^{14–16} and, particularly, by IM-MS methods, which are occasionally accompanied by structural calculations.^{16–22} Overall, most of these studies led to a few main consistent conclusions. The global gas-phase tertiary structure of ubiquitin differs in different charge states and it is strongly influenced by the composition of the solution and by the conditions of electrospray ionization. The typically “harsh” conditions of ESI that maximize the concentration of ions in the gas phase imply their significant collisional heating. Under such conditions, only the proteins in low charge states conserve their folded, solution-like, structures. Upon increasing the number of protons, these compact geometries progressively, partially and then fully unfold to the extended conformers. This trend is explained by the interplay of intramolecular non-covalent bonds and the repulsive electrostatic force, which increases with the number of protons. Ubiquitin in the charge states

with $n \leq 6$ protons is compact in the gas phase and closely resembles the folded native structure of the protein in the solution.²⁰ The ions with $n \geq 12$ can only be observed as the extended conformers, while Ubi with $n = 7-11$ exhibits broad transient distributions with compact, partially and fully unfolded conformers. The “gentle” ESI conditions minimize collisional heating of the ions and hinder unfolding. Under such conditions, the ions with $n = 7$ retain their native compact structures, although, already for $n = 8$, the proteins become partially unfolded and only a fraction of them remains compact.²⁰ In opposite, the “harsh” ESI conditions and denaturing solutions (*e.g.*, methanol/water) assist in partial unfolding: the charge distribution shifts toward high states due to a facile access to internal protonation sites, such that, for the same charge state, the conformational distribution shifts toward (partially) unfolded structures.^{16,23} This rich suite of global structural information will be used herein for calibrating the spectroscopic data obtained below for Ubi under similar conditions.

6.3. Experimental section

Our apparatus and procedure of cold ion spectroscopy was described in detail elsewhere.^{2,24,25} Briefly, multiple protonated ubiquitin ions are brought to the gas phase directly from solution and transferred into the low-pressure region of the spectrometer by an orthogonal, double ion-funnel (DIF) nano-electrospray ionization (ESI) source or by an inline triple skimmer “super gentle” nano-ESI for the experiments with the microhydrated protein. The latter source allows the adjustment of ESI conditions (*e.g.*, by increasing the inter skimmer potentials) from the “super gentle” to gentle and harsh, but produces a lower ion current than the former source. The settings of the triple skimmer source for the gentle and harsh conditions were determined by obtaining UV spectra that are nearly identical to the ones recorded with a DIF ESI source under the same category of the conditions (gentle or harsh).

The electrosprayed ions of interest in a certain charge state are pre-selected using a quadrupole mass filter and guided into a $T = 6$ K octupole ion trap,²⁶ where they get trapped and cooled in collisions with He buffer gas. Once cooled, the ions are fragmented using a UV laser pulse of ns duration for electronic spectroscopy or by IR and UV laser pulses for vibrational spectroscopy. The ions are then released from the trap and analyzed using a quadrupole mass spectrometer. The loading of the cold ion trap is performed at a 20 Hz repetition rate, while the laser sources work at 10 Hz. The appearance of unresolved mass peaks of UV photofragments corresponds to a mass loss of 45-100 Da by the bare protein (Fig. 6.S1b). The maximum fragmentation yield of 0.3% is achieved at an optimal time delay of 20 ms between the trap load and UV laser pulse as a compromise between vibrational cooling of the

UV excited ions by the residual He and the remaining 25 ms time allowed for statistical dissociation. The low UVPD yield (compared, for instance, with a yield of 7% for pentapeptides enkephalins that exhibit similar spectra) also suggests a statistical rather than a prompt mechanism of fragmentation.

An electronic photofragmentation spectrum is recorded by measuring the dissociation yield of all these fragment ions as a function of UV wavelength in the loading cycles with the laser pulses, while the number of parent ions is measured in the alternative, “laser-free” cycles. The vibrational “gain” spectra of the bare protein are recorded by fixing the UV laser wavelength at the red from the electronic band origin, while monitoring the appearance of photofragments as a function of the wavelength of the preceding IR laser pulse. The photodissociation vibrational spectra of the microhydrated proteins are recorded by detecting the complexes that lose 3-5 water molecules upon absorption of IR photons. Each data point in a spectrum is averaged over 10 measurements and normalized on the average signal of parent ions and the average UV energy of the respective 10 laser shots. We typically measure each spectrum three times and, finally, average them.

Ubiquitin from bovine erythrocytes ($\geq 98\%$ purity) was purchased and used without further purification. A stock solution of ubiquitin was prepared by dissolving it in pure water. For electrospray ionization, an aqueous stock solution was further diluted to yield a 50 μM solution either in water or in a water/methanol (50/50) mixture with the addition of 1% of acetic acid. Water, methanol, and acetic acid are of LC-MS grade.

The use of nano-electrospray capillaries with a small diameter of opening (the typical flow rate as small as 80-120 nL/min) was crucial for preventing the formation of Ubi dimers at a used concentration of $< 50 \mu\text{M}$.²⁷ The lack of dimers was confirmed by a lack in mass spectra of any noticeable peaks that correspond to the ions with a non-integer m/z ; these dimers could arise from clustering of highly abundant ions in n and $(n + 1)$ charge states (Fig. 6.S1a).

6.4. Results and discussion

6.4.1. UV spectroscopy of bare Ubi

Fig. 6.2 shows the panoramic UV photofragmentation spectra of the +6 to +12 charge states of cold ubiquitin in the spectral range that overlaps the electronic band origins of both Tyr and Phe aromatic residues.⁴ Except for the +6 and +7 states, the ions were electrosprayed from a denaturing solution (methanol/water/acetic acid, 50/50/1). Ubi in all the charge states experienced “harsh” conditions of ESI, which were tuned to maximize the number of ions. The spectra are dominated by Tyr absorption, which is 5-6 times stronger than that of Phe.²⁸ For

the number of protons $n = 6$, the absorption extends to the red from the band origin of Tyr by as much as $\sim 1200 \text{ cm}^{-1}$ and, apart from a few “bumps” and one broad peak, appears vibrationally unresolved. The lack of prominent sharp peaks is in line with the general expectation that no/little vibrationally resolved structure can be observed for a large molecule like Ubi. IM studies firmly assign Ubi⁶⁺ in the gas phase to compact, native-like, structures.^{20,29}

We, thus, can tentatively correlate a broadband spectrum with folded conformers of Ubi⁶⁺. In contrast to the spectrum of the protein with $n = 6$, a striking feature in all other spectra in Fig. 6.2 is the clearly resolved vibrational bands, which are the most prominent for the $n = 7-9$ states. The largest well-resolved peaks in these spectra are of $\sim 40 \text{ cm}^{-1}$ wide. They exhibit a Franck–Condon progression with the characteristic for the Tyr aromatic ring frequency of the “breathing” mode ($\sim 810 \text{ cm}^{-1}$).⁴ The maximum of the first absorption band (35469.4 cm^{-1}) in the spectra of the +7 to +9 states of Ubi appears to be very close to that of the band origin of neutral Tyr.^{30,31} The position of the electronic band origin in Tyr is known to be very sensitive to the local environment of its side chain. Non-covalent interactions with hydroxyl of the residue as well as the proton– π and the weaker H– π couplings with the aromatic ring can induce large spectral shifts of the UV absorption onset.^{32–34} The lack of a spectral shift ($n = 7-9$) implies the lack of substantial non-covalent interactions of the Tyr side chain with its environment. This local isolation of the side chain is consistent with the IM observations of, mainly, the partially unfolded structures for the +7 to +9 charge states of Ubi in the gas phase.^{20,29}

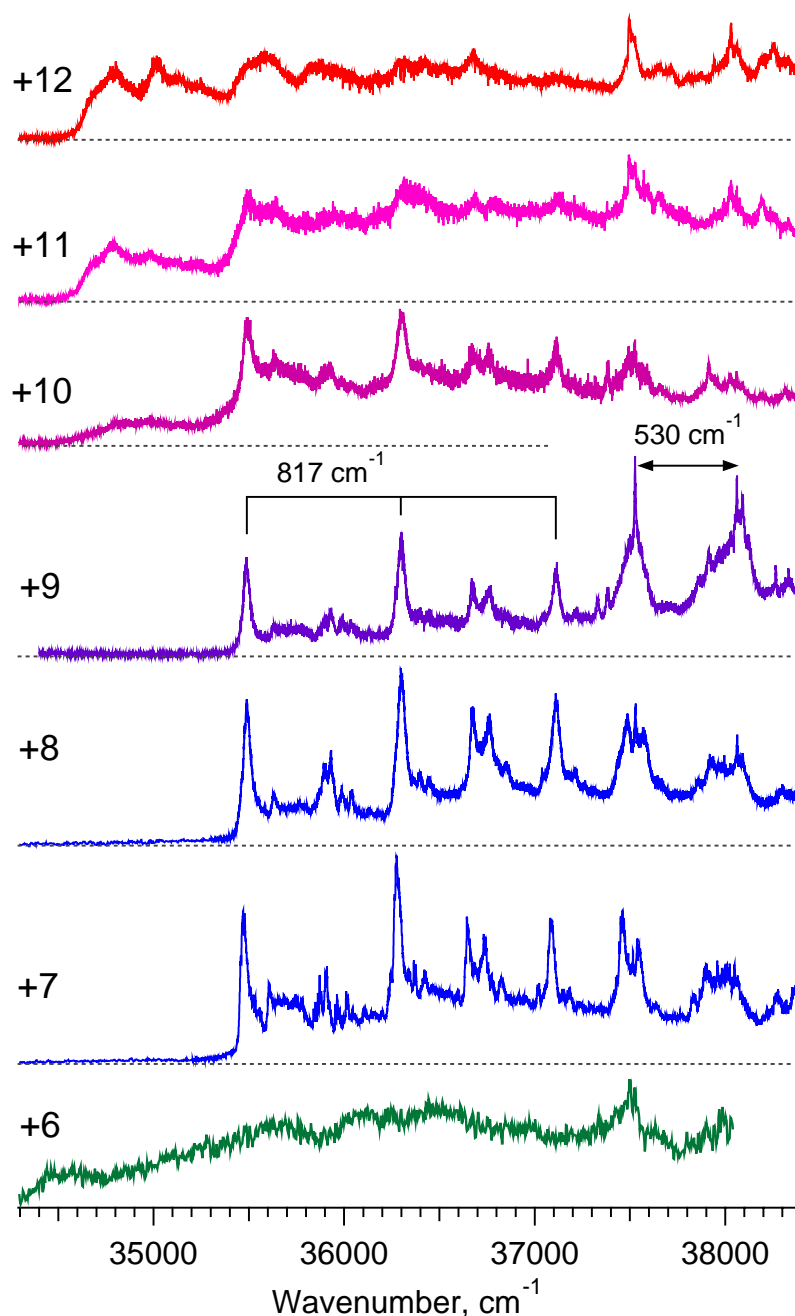


Figure. 6.2. UV photofragmentation spectra of the protonated $[\text{Ubi} + n \cdot \text{H}]^{n+}$, $n = 6-12$, recorded for the ions produced under harsh settings of the ESI source from methanol/water solution for $n = 8-12$ and from water for $n = 6-7$. The numbers on the left indicate the charge states of Ubi; the numbers above the spectrum of the +9 state indicate the spacing in vibrational progressions that are specific to Tyr and Phe.

The spectral resolution progressively degrades and the onset of the absorption redshifts for the +10 to +12 charge states. Different from the smooth spectrum of the +6 state, the arising redshifted bands remain, however, structured. For $n = 10-12$, Ubi in the gas phase was found to adopt, mostly, the unfolded structures. We tentatively attribute the redshifted bands to these

conformers, in which the additional charges occupy the protonation sites that are close to the side chain of Tyr. This may lead to a long-range proton- π interaction, which is known to shift the UV band origin of Tyr to the red.^{35,36} The conformers that differ by protonation in the vicinity of Tyr side chain should exhibit distinct onsets of UV absorption. The overlap of these similar but shifted absorptions of different intensities may generate the stepwise spectra observed for $n = 10-12$.

In addition to the large peaks of Tyr, a few well-reproducible spikes appear on top of the Tyr absorption bands above $\sim 37500\text{ cm}^{-1}$ (Fig. 6.2 and Fig. 6.S2, 6.S3). Regarding the size of the studied molecule, the widths of some of these spikes are amazingly small, below 2 cm^{-1} . The most intense of them appears in the spectrum for $n = 9$ at 37527 cm^{-1} . This is very close to the electronic band origin of the Phe residue in, for instance, helical peptides, where the aromatic side chain of Phe is free of any non-covalent interactions.³⁷ The sharp peaks are spaced by $\sim 530\text{ cm}^{-1}$, which is a highly conservative frequency of the in-plane bending of the Phe ring.³⁸ Based on these observations, we firmly assign these peaks to the absorption by the Phe residues of the protein. The Phe peaks of different intensities remain sharp and can be tracked in the spectra of all the charged states. However, we cannot distinguish whether these electronic transitions originate from the two different Phe residues of ubiquitin or from the same Phe but residing in different conformers of the protein. The lack of a shift for $n = 6$ and 7 (*e.g.*, Fig. 6.S2, red traces) implies no interactions of the Phe aromatic rings with the environment in these charge states. A small shift with no broadening of the peaks for $n = 8$ and 9 (Fig. 6.S3) suggests some weak interactions of the rings and therefore a (slightly) different environment of the chromophores in these states compared with the $n = 6$ and 7 states. The detected small spectral redshifts, splitting and broadening of the sharp peaks for $n = 10-12$ (Fig. 6.S3), indicate certain changes in the local environment of the Phe residues in Ubi in these charge states too.

The observation of the vibronic structure in the spectra of ubiquitin is interesting on its own. One might expect that any structure in a UV spectrum of such a large molecule as a protein will be completely washed out due to inhomogeneous spectral broadening, which arises from a large number of low-frequency vibrations. UV-active vibrations are to be, however, associated with the changes in the protein geometry occurring upon electronic excitation. Because of the local character of electronic excitation, the major UV-induced structural changes occur around the Tyr chromophore, such that the Franck-Condon active modes are also localized in the proximity of the chromophore or are coupled to it by H-bonds. The limited number of such modes does not yet grant the observed vibrational resolution. Thermal

congestion, conformational heterogeneity and lifetime broadening of the excited state may also wash out the vibrational structure. Cooling ions to cryogenic temperatures suppresses the thermal spectral broadening.³⁹ The observation of the sharp peaks with $< 2 \text{ cm}^{-1}$ (Fig. 6.2, 6.3 and Fig. 6.S2, 6.S3) indicates that Ubi is, indeed, cold in our experiments, although we cannot quantify its vibrational temperature. Consistently, with the concept of UV-active modes, the spectra of the cold protein that contains as many as 76 residues overall look for $n = 7-9$ somewhat similar to the spectra of, for instance, cold gas-phase enkephalins,^{36,40} which contain only five residues.

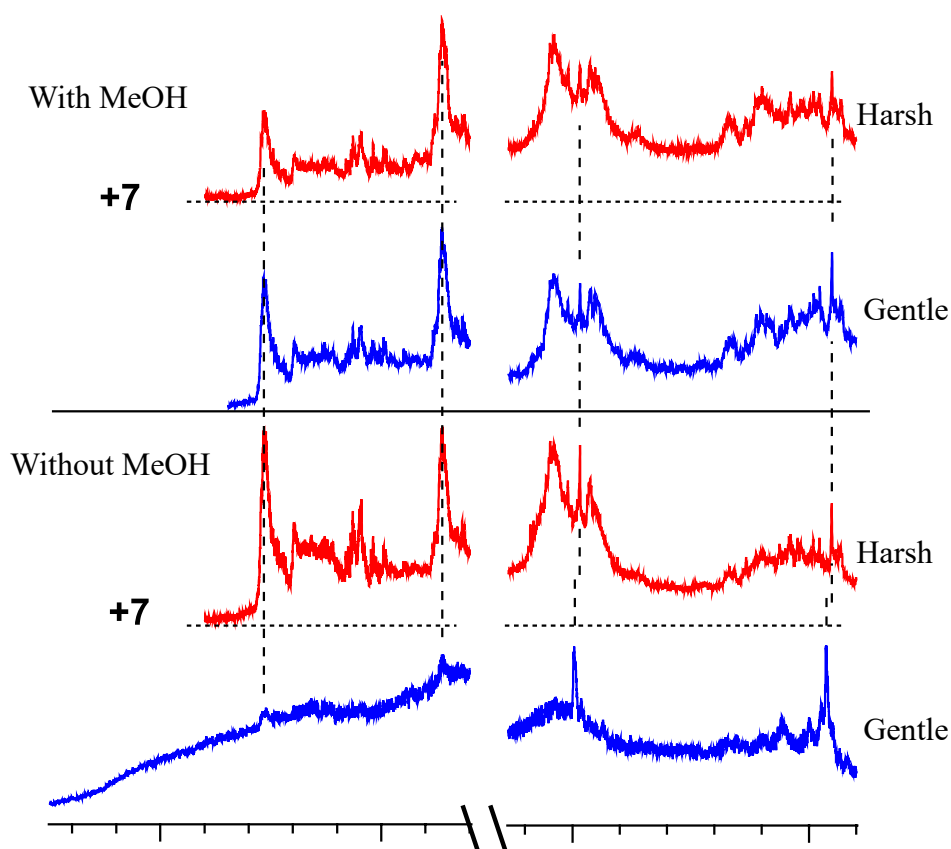


Figure 6.3. Parts of UV photofragmentation spectra of $[\text{Ub} + 7\text{H}]^{7+}$ recorded for the protein electrosprayed (upper panel) from water/methanol/acetic acid (50/50/1) solution and (lower panel) from water/acetic acid (100/1) solution. Blue and red spectra correspond to the gentle and harsh ESI conditions, respectively. Vertical dashed lines show the alignments/shifts of the characteristic transitions.

Two more observations further support the revealed above spectroscopy–structure correlation. Fig. 6.3 shows four UV spectra of the +7-charge state, which were recorded under four different experimental conditions. The solution for ESI was either water or 50/50

water/methanol mixture with 1% acetic acid, and the ion source conditions were either gentle (minimum RF amplitudes of the ion funnels) or harsh (maximum RF amplitudes of the ion funnels). The spectra of $[\text{Ubi} + 7\text{H}]^{7+}$ appear almost identical, when ubiquitin is electrosprayed from the water/methanol solution or else from water but under harsh ion source conditions. Minimization of collisional activation in the ion source (gentle conditions) results, however, in a dramatic change of the UV spectrum of ubiquitin, which is dissolved in water. The spectrum extends to the red by more than a thousand cm^{-1} and drastically broadens. It resembles the structureless spectrum of the $n = 6$ state in Fig. 6.2, although still exhibits a few partially resolved Tyr absorption peaks. In contrast, Phe transitions broaden only twice, with a width of 5-6 cm^{-1} (Fig. 6.S2) and a red shift by 13 cm^{-1} only. Such changes are, again, fully consistent with IM studies, which detect compact forms of the protein in the $n = 7$ state only for “gentle” ESI from aqueous solutions.²⁰ The changes in absorption by Tyr clearly manifest the crucial changes in its local environment; the shift and broadening of the Phe peaks suggest certain changes in their environment too.

Fig. 6.4 compares the UV spectra measured under the harsh (red traces) and gentle (blue traces) ESI conditions for the +6 to +8 charge states of Ubi dissolved in water. The two UV spectra for $n = 6$ look quite similar and resemble the broad spectrum of Ubi^{7+} produced by gentle ESI, which implies a compact structure of Ubi^{6+} under both conditions. Regardless of the conditions, the UV spectra of the +8 state exhibit the same vibrationally resolved structure, although, in the “gentle” spectrum, the peaks sit on a broad substrate that extends to the red by $\sim 1100 \text{ cm}^{-1}$. Regarding IM studies,²⁰ such a superposition of the resolved and broadband spectral components in the “gentle” spectrum indicates the presence of both compact and extended structures of the protein. In contrast to Tyr, the sharp peaks of Phe do not exhibit a dramatic change (Fig. 6.S2). The gentle production of Ubi nearly doubles the width of these peaks and redshifts them by $\sim 12 \text{ cm}^{-1}$ for the +7 and +6 states, but does not influence the peaks for the +8 state. This implies a change of the local environment for the +6 and +7 states upon collisional activation, such that the Phe side chain becomes free of any non-covalent interactions, while, for Ubi^{8+} , the interactions (and the environment) remain the same.

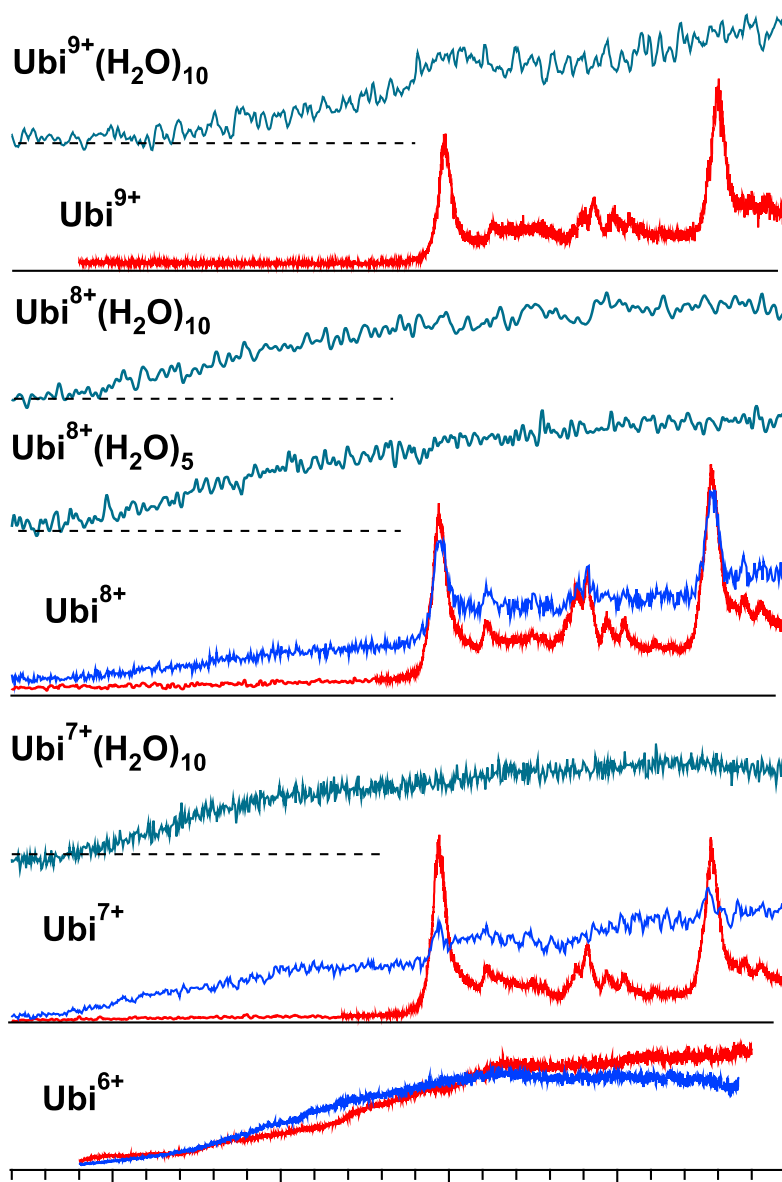


Figure 6.4. UV photofragmentation spectra recorded around the UV band origin of Tyr for $[\text{Ubi} + n\text{H}]^{n+}$ ($n = 6-9$ from the bottom to the top) and of the protein ($n = 7-9$), microhydrated by 5 and 10 water molecules as labeled. For all the charge states the bare proteins were produced from water/acetic acid (100/1) solution under the gentle (blue traces) and harsh (red traces) conditions of ESI. The microhydrated ubiquitin was produced from the same solution by “super gentle” ESI in the triple skimmer ion source.

6.4.2. UV spectroscopy of hydrated Ubi

Tuning the triple skimmer ESI source to further minimize collisional heating enables retaining water molecules on ubiquitin in the gas phase. The $\text{Ubi}^{7+}(\text{H}_2\text{O})_{10}$ complex produced under such “super gentle” ionization conditions exhibits a broad spectrum (Fig. 6.4) in the region of Tyr absorption. The spectrum looks similar to the one recorded for the +6 state of the

gently electrosprayed bare protein but becomes smoother, with no features at all. This similarity prompts us to suggest that the microhydrated Ubi^{7+} appears in the gas phase in its folded, native-like, structure, at least, around the Tyr chromophore. Retaining 10 or even only 5 water molecules on Ubi^{8+} also completely removes the resolved transitions, making the UV spectra of the Tyr residue smooth and eventually identical to the spectrum of the $\text{Ubi}^{7+}(\text{H}_2\text{O})_{10}$ complex. No sharp peaks have been detected at the achieved level of the S/N ratio in the Phe spectral region for all the studied complexes. A broadband structure centered on the band origin of Tyr re-appears, however, for the microhydrated Ubi^{9+} . The spectrum also spans to the red less than that for the $n = 6-8$ states. These differences indicate certain structural changes around the chromophore, compared to the lower charge states. Microhydration is not capable anymore of retaining the intact folded structure of the proteins around the chromophore, such that a fraction of them resides in the partially unfolded $n = 9$ states.

We rule out a direct influence of water molecules on the UV absorption by Tyr in the complexes with only 5 and 10 water molecules, since no water molecules close to the Tyr residue were detected in NMR⁴¹ and X-ray⁸ studies for a partially hydrated (folded) Ubi. NMR studies explicitly observed the H-binding of the Tyr side chain to the nearby Glu-51 residue even in the presence of a hydration shell of the protein.⁴¹ These facts and our observations suggest that, even for $n = 8$ and, largely, for $n = 9$, the protein in the gas phase can retain its compact, solution-like, structures, provided that the protein was “super gently” electrosprayed from an aqueous solution. It is unlikely that the folded structures of the large protein can be preserved just by five remaining water molecules. We suggest that the retained water molecules allow adiabatic evaporative cooling of ubiquitin during ESI, thus protecting the protein from excessive vibrational heating required for its unfolding in the gas phase.^{42,43} The computations estimate that the evaporation may reduce the internal temperature of ubiquitin by as much as 60-70 K.⁴⁴ The remaining water molecules are to be those that have the highest binding energy to the protein, further contributing to its structural stabilization. Only the fully compact structures of Ubi in the $n = 8$ and 9 states have never been observed in ion mobility studies, which revealed mixed distributions of the compact and partially unfolded geometries of the protein.²⁹ This difference implies that the “super gentle” ESI conditions created in our experiments are the key to protect the native structure of Ubi with $n = 8$ and, partially, of $n = 9$ in the gas phase.

The broadening of Tyr absorption in the compact structures of the cold protein can be rationally explained by the (i) short lifetime of the excited electronic state of Tyr, (ii) high conformational heterogeneity of the native-like structures of ubiquitin. The lifetime of the

S_1 state of Tyr, potentially, could be substantially shortened due to hydrogen or charge transfer through the H-bond to Glu-51. To result in $\sim 1000\text{ cm}^{-1}$ homogeneous broadening, the lifetime is to be on the scale of ~ 5 fs. This would be much faster than the ~ 370 fs timescale of the electron transfer through the H-bond in the phenol-(NH_3)₅ noncovalent complex, which is the fastest process ever observed for the S_1 state of Tyr or phenol.⁴⁵ We thus consider it highly unlikely that a lifetime broadening alone can explain the observed spectral broadening in the spectra of the compact Ubi. NMR studies suggest tens of conformers of Ubi in the condensed phase.^{46,47} The position of the UV band origin of Tyr is highly sensitive to the strength of non-covalent bonds.^{32,33} Variation of this strength among numerous conformers would lead to different shifts of the UV band origin in the ensemble of the folded structures. We propose that it is the combination of the lifetime broadening and the conformational heterogeneity that results in the observed smooth broadening in the spectra of the compact structures for $n = 6-8$. Two types of non-covalent interactions can lead to large UV spectral shifts: H-bonding of the Tyr hydroxyl to the amide group of Glu-51 and proton- π interaction of the aromatic ring of Tyr. The shift of the electronic band origin to the red in the spectra points to the binding of the hydrogen but not oxygen of the Tyr hydroxyl group to the amide group of Glu-51.³² The available data for redshifts of the UV band origin in function of the length of H-bond between hydroxyl oxygen in phenylalanine and the amide group of different species (Fig. 6.S4) suggest that the minimum length of the OH(Tyr) \cdots NH(Glu-51) bond should be as short as ~ 1.7 Å. This, however, contradicts the available NMR structures of the protein, in most of which the oxygen of OH is closer to the hydrogen of the Glu-51 amide (PDB structures 1D3Z (10 models),⁴⁸ 2MSG⁴⁷). It is worth noting that these structures are not charge-specific and all differ in the position of the atoms involved in the binding. NMR and X-ray structures do not favor the proton- π interaction too. For $n = 6-8$, the nearest proton resides on the side chain of the lysine-48 residue⁴⁹ at a distance of 6-7 Å;^{8,48} the occupancy of this site is unknown for $n = 9$. Such a ring-to-charge spacing seems to be too large to account for $\sim 1000\text{ cm}^{-1}$ redshifts. Moreover, the large redshift and broadening remains in the UV spectrum of the $n = 5$ state, in which the lysine-48 side chain was found not to be protonated in the gas phase (Fig. 6.S5). We thus rule out this interaction and suggest that the observed spectral broadening is due to OH(Tyr) \cdots NH(Glu-51) binding. Certainly, full/partial desolvation of the protein reshapes its structure and may lead to some modifications of the network of H-bonds, including the binding of Tyr hydroxyl. Vibrational spectroscopy data below provide a direct support for this suggestion.

6.4.3. IR spectroscopy

Vibrational spectroscopy, which reflects the global structure of a protein, provides direct evidence of the transition from unfolded to folded structures and allows the unambiguous assignment of the Tyr-Glu hydrogen bond. Fig. 5 compares the IR spectrum of Ubi^{7+} electro sprayed from water solution under the harsh conditions with the spectrum of the $\text{Ubi}^{7+}(\text{H}_2\text{O})_5$ complex. The IR spectrum of the bare protein contains a number of sharp resolved peaks in the region of $3430\text{-}3590\text{ cm}^{-1}$ and a distinct peak at 3647 cm^{-1} . The sharpness of these peaks implies that they originate from non- or weakly-disturbed vibrations. Bearing this in mind and based on the known characteristic frequencies of molecular transitions in peptides,² the observed sharp peaks in the regions of $3430\text{-}3500\text{ cm}^{-1}$ and $3500\text{-}3590\text{ cm}^{-1}$ can be assigned to free NH and carboxylic OH stretches, respectively. The sharp peak at 3647 cm^{-1} perfectly matches to the free phenolic OH stretch of Tyr,^{4,35} while carboxylic OH stretches lie below 3600 cm^{-1} (Table 2 in ref. 2) and the free aliphatic OH stretches of serine and threonine are somewhat higher in frequency ($3665\text{-}3690\text{ cm}^{-1}$).^{50,51} We therefore assigned the transition at 3647 cm^{-1} to the free hydroxyl of the Tyr residue. In the native folded conformers of Ubi, the hydroxyl is not free, but coupled to Glu-51.⁴⁹ The appearance of this characteristic transition is a direct evidence of the protein unfolding in the region of Tyr. The disappearance of this characteristic transition may imply that it redshifts and becomes buried in the manifold of transitions of H-bound OH/NH groups. This is consistent with the proposed above explanation of UV spectral broadening and shifts observed for the compact states of the protein. We cannot completely rule out, however, that single isolated peaks, including the transition in question, can be suppressed due to the IRMPD nature of this spectrum.⁵²

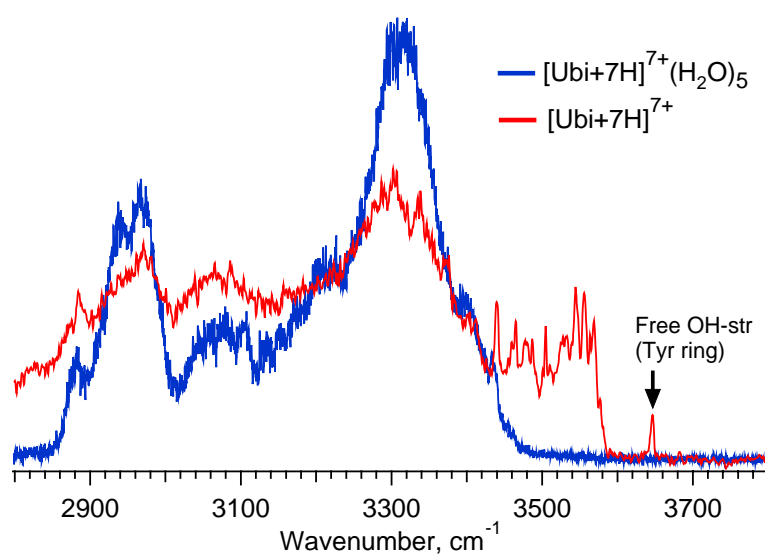


Figure 6.5. IRPD spectra of $[\text{Ubi} + 7\text{H}]^{7+}$ electro sprayed from water under the harsh ion source conditions (red) and of the same protein microhydrated by five water molecules (blue).

The observation of a large number of free NH/OH stretch vibrations in the IR spectrum of the $n = 7$ state of the “harshly” electrosprayed Ubi manifests a break of many intramolecular H-bonds present in native conformers of the protein.⁵³ Consistent with UV spectroscopy and IM studies, this observation implies an unfolded global structure of Ubi⁷⁺ ions, brought to the gas phase under the “harsh” ESI conditions. The IR spectrum changes drastically, when Ubi⁷⁺ is produced under the “super gentle” conditions that allow retaining of five waters on it. All the sharp transitions shift to the red and become unresolved. This change unambiguously indicates an involvement of the previously free NH/OH groups to H-bonds. Regarding the large number of these free groups, it is highly unlikely that five waters only can take up all these vacancies. We thus conclude that the observed spectral change reflects the retaining of the network of intramolecular H-bonds in the gas-phase protein, which implies its globally compact structure. Unfortunately, computations of vibrational (and electronic) spectra with an “experimental” accuracy is yet unrealistic for a molecule of such a big size as ubiquitin. This hinders the use of the measured IR spectra for the stringent validation of computed structures.

6.5. Conclusion

To sum up, this study demonstrates that, even for biomolecules as large as proteins, cold ion spectroscopy can provide valuable structural information. Complementary to other methods, CIS allows the tracking of not only the global (in IR) but also the local (in UV) structural changes in the gas phase. We recorded the UV and IR gas-phase spectra of the cryogenically cooled protonated protein ubiquitin and its microsolvated complexes, electrosprayed from aqueous and denaturing solutions under different conditions of collisional heating in the ion source and in different charged states from +5 to +12. Some of the UV spectra exhibit a vibrational resolution in the spectral regions of absorption by Tyr and Phe residues. Being calibrated by earlier IM studies, these resolved spectroscopic fingerprints were assigned to partially/fully unfolded conformers of Ubi. These conformers dominate for Ubi not only in the +9 to +12 charged states, but also in the +7 and +8 states, provided that the ions are produced from denaturing solutions or undergo substantial (*e.g.*, “standard”) heating (harsh conditions) during the ESI process. The unresolved spectra correspond to the protein in the native-like, folded, states, in which the hydroxyl of the Tyr residue forms H-bonds with the amide group of the Glu-51 residue. Regardless of the ESI conditions, the vast majority of conformers exhibit the spectroscopic signature of the compact, native-like, structure for ubiquitin with $n = 6$. Ubi⁷⁺ retains its native-like structure in the gas phase only if produced from an aqueous solution under “gentle” ESI conditions that prevent substantial heating of the

protein. Consistently, IR spectroscopy reveals the breaking of many intramolecular H-bonds, including the one with Tyr hydroxyl, under the “harsh” conditions of ESI, and the disappearance of the free NH/OH transitions in the “chilly” microhydrated protein. The increasing electrostatic repulsion partially unfolds Ubi⁸⁺ even by mild heating under the “gentle” ESI conditions. Retaining a few water molecules on Ubi⁸⁺ and Ubi⁹⁺ protects these ions from heating by evaporative cooling of waters, which allows the folded structures of the protein to survive in the gas phase for a longer time. Our observation of OH⋯NH but not HO⋯HN hydrogen binding between the Tyr-59 and Glu-51 residues provides example evidence that the compact gas-phase structures are not really “native”, but rather the native-like ones only.

The observed crucial role of water molecules in retaining the compact structure of ubiquitin in the gas phase is practically relevant to the field of “native mass spectrometry”.⁵⁴ Retaining a native-like structure of large biomolecules (*e.g.*, proteins and complexes of proteins) in the gas phase requires softening of the ESI conditions. However, this need for gentle ionization contradicts the desire for a high mass resolution, which favors complete desolvation of ions. Our study demonstrates that the appearance of microhydrated ions in the gas phase ensures their low internal energy: evaporative cooling keeps the ions “chilly” for the best protection of the solution-phase structures of biomolecules. Native MS should take this fact into account; the ionization and desolvation procedures, perhaps, can be separated.

Appendix

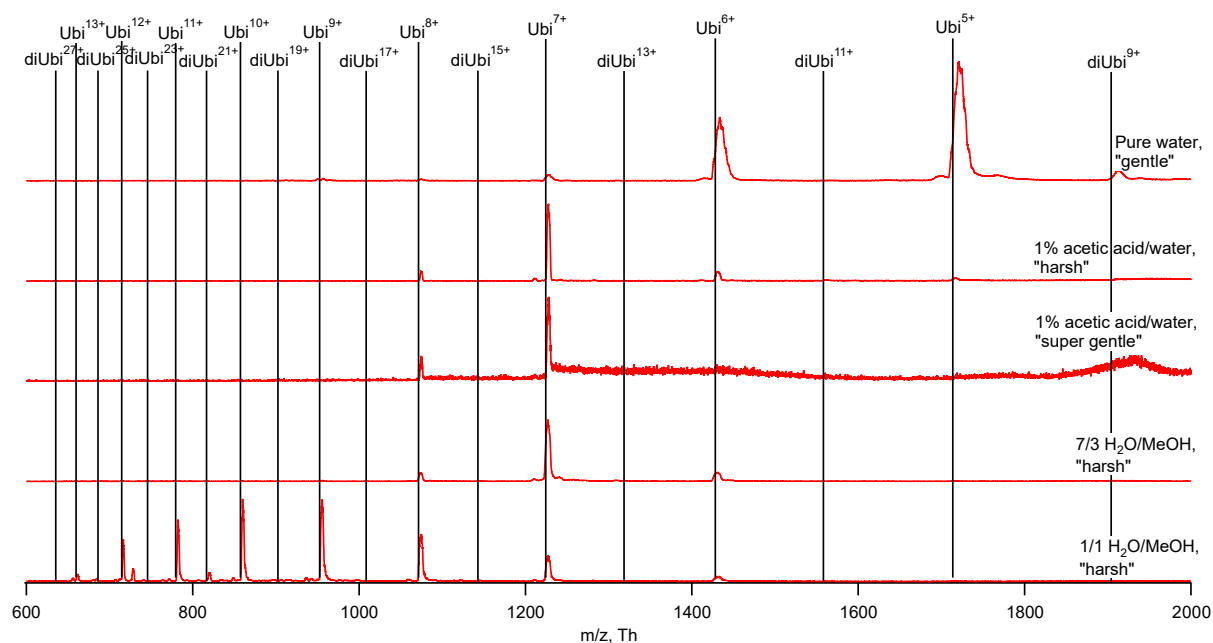


Figure 6.S1a. Mass spectra showing charge-distribution of protonated ubiquitin electrosprayed from different solutions and under different (“super gentle”, “gentle” and “harsh”) conditions of ESI.

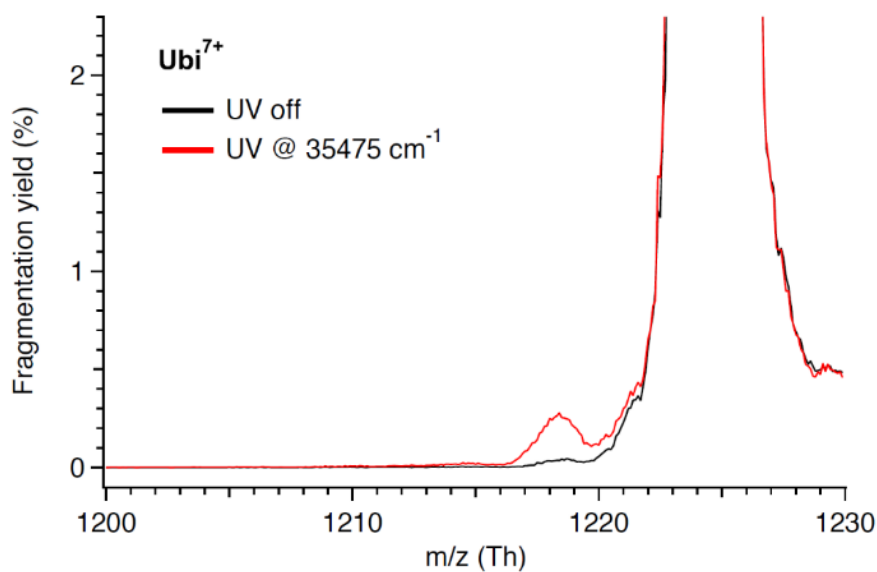


Figure 6.S1b. UV fragment MS of Ubi⁷⁺ (red trace) and of this protein with UV light blocked (black trace). The ion peak intensity is normalized on the intensity of the parent ion peak (100%).

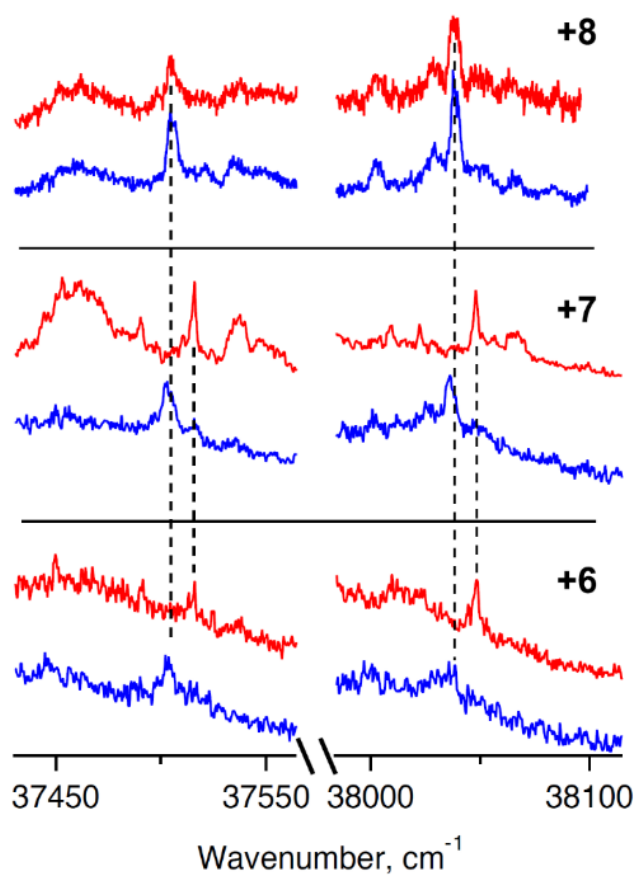


Figure 6.S2. Photofragmentation UV spectra of Ubi⁷⁺ and Ubi⁸⁺ in the region of absorption by Phe residue. The protein was electrosprayed from water solution with 1% of acetic acid under the “gentle” (blue traces) and “harsh” (red traces) conditions of ESI.

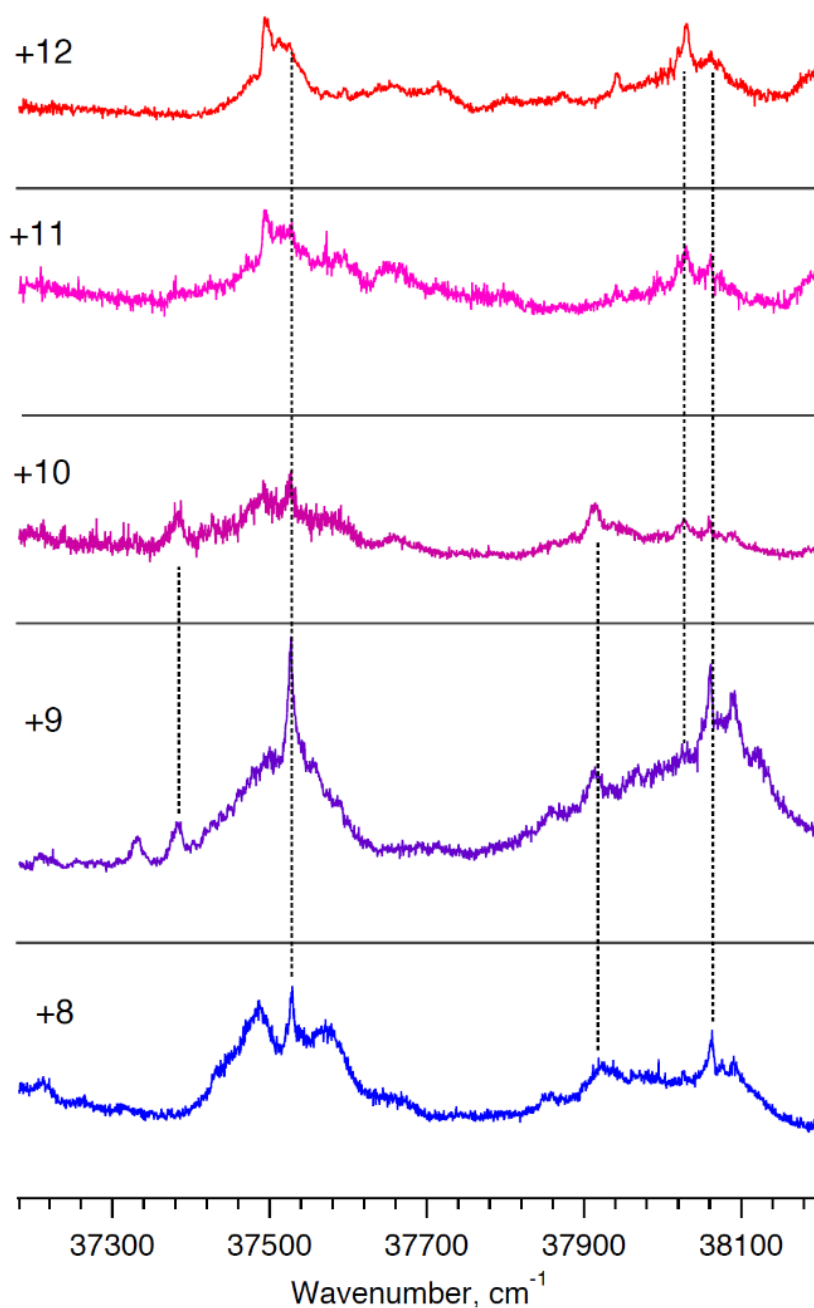


Figure 6.S3. Photo fragmentation UV spectra of Ubiⁿ⁺ for $n = 8-12$ in the region of absorption by Phe residue. The protein was electrosprayed from water/methanol/acetic acid (50/50/1) solution under the “harsh” conditions of ESI. Vertical dashed line show alignment of sharp peaks in different spectra.

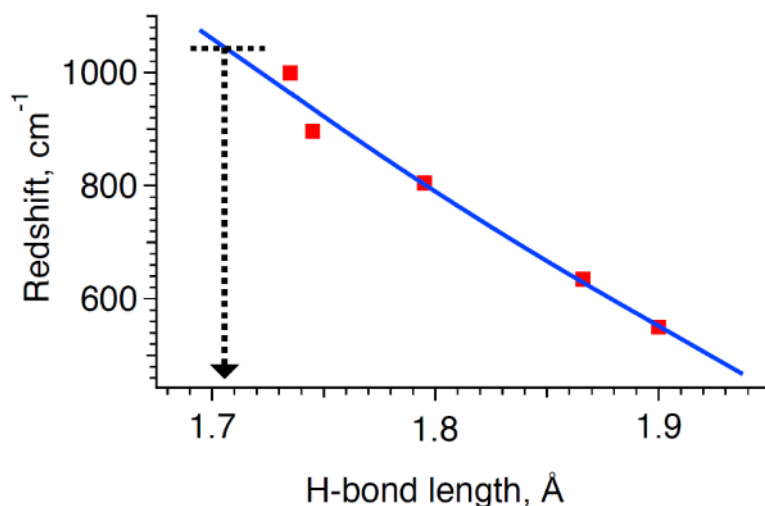


Figure 6.S4. The available data (red squares) for the red shifts of the UV band origin of neutral phenol as a function of the H-bond length between the hydrogen of the phenol hydroxyl and the nitrogen of the acceptor molecules in the studied non-covalent complexes.^{55–58} The data points were fitted by a power function $y(x) = 7300 - 1850 \cdot x^{-1.7}$ that exhibits a nearly linear dependence. The vertical dotted line shows the largest red shift detected for the UV band origin of Tyr residue in this work for protonated ubiquitin ($n = 6-8$) and its complexes with 5 and 10 water molecules; the dotted arrow line points to the corresponding most likely minimal length of the H-bond (~ 1.7 Å). The evaluation does not consider the variations of the bond angle.

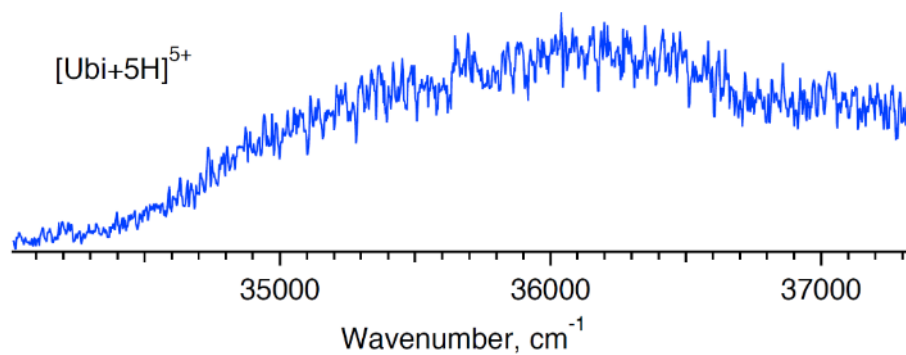


Figure 6.S5. Photofragment UV spectrum of $[\text{Ubi} + 5\text{H}]^{5+}$, produced from pure water solution under “harsh” ESI conditions.

References

1. Rizzo, T. R., Stearns, J. A. & Boyarkin, O. V. Spectroscopic studies of cold, gas-phase biomolecular ions. *Int. Rev. Phys. Chem.* **28**, 481–515 (2009).
2. Boyarkin, O. V. Cold ion spectroscopy for structural identifications of biomolecules. *Int. Rev. Phys. Chem.* **37**, 559–606 (2018).
3. Mercier, S. R. *et al.* Microsolvation Effects on the Excited-State Dynamics of Protonated Tryptophan. *J. Am. Chem. Soc.* **128**, 16938–16943 (2006).
4. Stearns, J. A. *et al.* Conformation-Specific Spectroscopy and Photodissociation of Cold, Protonated Tyrosine and Phenylalanine. *J. Am. Chem. Soc.* **129**, 11814–11820 (2007).
5. Nagornova, N. S. *et al.* Cold-Ion Spectroscopy Reveals the Intrinsic Structure of a Decapeptide. *Angew. Chemie Int. Ed.* **50**, 5383–5386 (2011).
6. Roy, T. K., Nagornova, N. S., Boyarkin, O. V. & Gerber, R. B. A Decapeptide Hydrated by Two Waters: Conformers Determined by Theory and Validated by Cold Ion Spectroscopy. *J. Phys. Chem. A* **121**, 9401–9408 (2017).
7. Nagornova, N. S., Rizzo, T. R. & Boyarkin, O. V. Exploring the Mechanism of IR-UV Double-Resonance for Quantitative Spectroscopy of Protonated Polypeptides and Proteins. *Angew. Chemie* **125**, 6118–6121 (2013).
8. Vijay-kumar, S., Bugg, C. E. & Cook, W. J. Structure of ubiquitin refined at 1.8 Å resolution. *J. Mol. Biol.* **194**, 531–544 (1987).
9. Vijay-Kumar, S., Bugg, C. E., Wilkinson, K. D. & Cook, W. J. Three-dimensional structure of ubiquitin at 2.8 Å resolution. *Proc. Natl. Acad. Sci.* **82**, 3582–3585 (1985).
10. Suckau, D. *et al.* Coexisting stable conformations of gaseous protein ions. *Proc. Natl. Acad. Sci.* **90**, 790–793 (1993).
11. Evans, S. E., Lueck, N. & Marzluff, E. M. Gas phase hydrogen/deuterium exchange of proteins in an ion trap mass spectrometer. *Int. J. Mass Spectrom.* **222**, 175–187 (2003).
12. Geller, O. & Lifshitz, C. A Fast Flow Tube Study of Gas Phase H/D Exchange of Multiply Protonated Ubiquitin. *J. Phys. Chem. A* **109**, 2217–2222 (2005).
13. Freitas, M. A., Hendrickson, C. L., Emmett, M. R. & Marshall, A. G. Gas-phase bovine ubiquitin cation conformations resolved by gas-phase hydrogen/deuterium exchange rate and extent. *Int. J. Mass Spectrom.* **185–187**, 565–575 (1999).
14. Schnier, P. D., Gross, D. S. & Williams, E. R. On the maximum charge state and proton transfer reactivity of peptide and protein ions formed by electrospray ionization. *J. Am. Soc. Mass Spectrom.* **6**, 1086–1097 (1995).

15. Zhang, X. & Cassady, C. J. Apparent gas-phase acidities of multiply protonated peptide ions: Ubiquitin, insulin B, and renin substrate. *J. Am. Soc. Mass Spectrom.* **7**, 1211–1218 (1996).
16. Valentine, S. J., Counterman, A. E. & Clemmer, D. E. Conformer-dependent proton-transfer reactions of ubiquitin ions. *J. Am. Soc. Mass Spectrom.* **8**, 954–961 (1997).
17. Laszlo, K. J., Munger, E. B. & Bush, M. F. Folding of Protein Ions in the Gas Phase after Cation-to-Anion Proton-Transfer Reactions. *J. Am. Chem. Soc.* **138**, 9581–9588 (2016).
18. Myung, S., Badman, E. R., Lee, Y. J. & Clemmer, D. E. Structural Transitions of Electrosprayed Ubiquitin Ions Stored in an Ion Trap over ~10 ms to 30 s. *J. Phys. Chem. A* **106**, 9976–9982 (2002).
19. El-Baba, T. J. *et al.* Melting Proteins: Evidence for Multiple Stable Structures upon Thermal Denaturation of Native Ubiquitin from Ion Mobility Spectrometry–Mass Spectrometry Measurements. *J. Am. Chem. Soc.* **139**, 6306–6309 (2017).
20. Wyttenbach, T. & Bowers, M. T. Structural Stability from Solution to the Gas Phase: Native Solution Structure of Ubiquitin Survives Analysis in a Solvent-Free Ion Mobility–Mass Spectrometry Environment. *J. Phys. Chem. B* **115**, 12266–12275 (2011).
21. Bohrer, B. C., Atlasevich, N. & Clemmer, D. E. Transitions between Elongated Conformations of Ubiquitin [M+11H]¹¹⁺ Enhance Hydrogen/Deuterium Exchange. *J. Phys. Chem. B* **115**, 4509–4515 (2011).
22. Shi, H. & Clemmer, D. E. Evidence for Two New Solution States of Ubiquitin by IMS–MS Analysis. *J. Phys. Chem. B* **118**, 3498–3506 (2014).
23. Li, J., Taraszka, J. A., Counterman, A. E. & Clemmer, D. E. Influence of solvent composition and capillary temperature on the conformations of electrosprayed ions: unfolding of compact ubiquitin conformers from pseudonative and denatured solutions. *Int. J. Mass Spectrom.* **185–187**, 37–47 (1999).
24. Pereverzev, A. Y., Szabó, I., Kopysov, V. N., Rosta, E. & Boyarkin, O. V. Gas-phase structures reflect the pain-relief potency of enkephalin peptides. *Phys. Chem. Chem. Phys.* **21**, 22700–22703 (2019).
25. Saparbaev, E., Aladinskaia, V., Zviagin, A. & Boyarkin, O. V. Microhydration of Biomolecules: Revealing the Native Structures by Cold Ion IR Spectroscopy. *J. Phys. Chem. Lett.* **12**, 907–911 (2021).
26. Boyarkin, O. V. & Kopysov, V. Cryogenically cooled octupole ion trap for spectroscopy of biomolecular ions. *Rev. Sci. Instrum.* **85**, 033105 (2014).

27. Xia, Z. & Williams, E. R. Effect of droplet lifetime on where ions are formed in electrospray ionization. *Analyst* **144**, 237–248 (2019).
28. Pereverzev, A. Y., Kopysov, V. & Boyarkin, O. V. High Susceptibility of Histidine to Charge Solvation Revealed by Cold Ion Spectroscopy. *Angew. Chemie Int. Ed.* **56**, 15639–15643 (2017).
29. Koeniger, S. L. & Clemmer, D. E. Resolution and structural transitions of elongated states of ubiquitin. *J. Am. Soc. Mass Spectrom.* **18**, 322–331 (2007).
30. Martinez, S. J., Alfano, J. C. & Levy, D. H. The electronic spectroscopy of the amino acids tyrosine and phenylalanine in a supersonic jet. *J. Mol. Spectrosc.* **156**, 421–430 (1992).
31. Cohen, R., Brauer, B., Nir, E., Grace, L. & de Vries, M. S. Resonance-Enhanced Multiphoton Ionization Spectroscopy of Dipeptides. *J. Phys. Chem. A* **104**, 6351–6355 (2000).
32. Saparbaev, E., Kopysov, V., Yamaletdinov, R., Pereverzev, A. Y. & Boyarkin, O. V. Interplay of H-Bonds with Aromatics in Isolated Complexes Identifies Isomeric Carbohydrates. *Angew. Chemie* **131**, 7424–7428 (2019).
33. Saparbaev, E., Aladinskaia, V., Yamaletdinov, R., Pereverzev, A. Y. & Boyarkin, O. V. Revealing Single-Bond Anomeric Selectivity in Carbohydrate–Protein Interactions. *J. Phys. Chem. Lett.* **11**, 3327–3331 (2020).
34. Saparbaev, E., Yamaletdinov, R. & Boyarkin, O. V. Identification of Isomeric Lipids by UV Spectroscopy of Noncovalent Complexes with Aromatic Molecules. *Anal. Chem.* **93**, 12822–12826 (2021).
35. Stearns, J. A., Guidi, M., Boyarkin, O. V. & Rizzo, T. R. Conformation-specific infrared and ultraviolet spectroscopy of tyrosine-based protonated dipeptides. *J. Chem. Phys.* **127**, 154322 (2007).
36. Kopysov, V. & Boyarkin, O. V. Resonance Energy Transfer Relates the Gas-Phase Structure and Pharmacological Activity of Opioid Peptides. *Angew. Chemie* **128**, 699–702 (2016).
37. Stearns, J. A., Boyarkin, O. V. & Rizzo, T. R. Spectroscopic Signatures of Gas-Phase Helices: Ac-Phe-(Ala) 5 -Lys-H + and Ac-Phe-(Ala) 10 -Lys-H +. *J. Am. Chem. Soc.* **129**, 13820–13821 (2007).
38. Féraud, G. *et al.* Excited State Dynamics of Protonated Phenylalanine and Tyrosine: Photo-Induced Reactions Following Electronic Excitation. *J. Phys. Chem. A* **119**, 5914–5924 (2015).

39. Boyarkin, O. V., Mercier, S. R., Kamariotis, A. & Rizzo, T. R. Electronic Spectroscopy of Cold, Protonated Tryptophan and Tyrosine. *J. Am. Chem. Soc.* **128**, 2816–2817 (2006).
40. Burke, N. L., Redwine, J. G., Dean, J. C., McLuckey, S. A. & Zwier, T. S. UV and IR spectroscopy of cold protonated leucine enkephalin. *Int. J. Mass Spectrom.* **378**, 196–205 (2015).
41. Nucci, N. V, Pometun, M. S. & Wand, A. J. Site-resolved measurement of water-protein interactions by solution NMR. *Nat. Struct. Mol. Biol.* **18**, 245–249 (2011).
42. Signorell, R. & Bertram, A. Physical chemistry of aerosols. *Phys. Chem. Chem. Phys.* **11**, 7759 (2009).
43. Thirumuruganandham, S. P. & Urbassek, H. M. Water Evaporation and Conformational Changes from Partially Solvated Ubiquitin. *Biochem. Res. Int.* **2010**, 1–6 (2010).
44. Patriksson, A., Marklund, E. & van der Spoel, D. Protein Structures under Electrospray Conditions. *Biochemistry* **46**, 933–945 (2007).
45. Miyazaki, M., Washio, N. & Fujii, M. Electron-proton transfer mechanism of excited-state hydrogen transfer in phenol–(NH₃) (n = 5) studied by delayed ionization detected femtosecond time-resolved NIR spectroscopy. *Chem. Phys.* **515**, 580–585 (2018).
46. Lange, O. F. *et al.* Recognition Dynamics Up to Microseconds Revealed from an RDC-Derived Ubiquitin Ensemble in Solution. *Science.* **320**, 1471–1475 (2008).
47. Fasshuber, H. K. *et al.* Structural heterogeneity in microcrystalline ubiquitin studied by solid-state NMR. *Protein Sci.* **24**, 592–598 (2015).
48. Cornilescu, G., Marquardt, J. L., Ottiger, M. & Bax, A. Validation of Protein Structure from Anisotropic Carbonyl Chemical Shifts in a Dilute Liquid Crystalline Phase. *J. Am. Chem. Soc.* **120**, 6836–6837 (1998).
49. Morrison, L. J. & Brodbelt, J. S. Charge site assignment in native proteins by ultraviolet photodissociation (UVPD) mass spectrometry. *Analyst* **141**, 166–176 (2016).
50. Linder, R., Seefeld, K., Vavra, A. & Kleinermanns, K. Gas phase infrared spectra of nonaromatic amino acids. *Chem. Phys. Lett.* **453**, 1–6 (2008).
51. Scutelnic, V. *et al.* The Structure of the Protonated Serine Octamer. *J. Am. Chem. Soc.* **140**, 7554–7560 (2018).
52. Yacovitch, T. I. *et al.* Vibrational Spectroscopy of Bisulfate/Sulfuric Acid/Water Clusters: Structure, Stability, and Infrared Multiple-Photon Dissociation Intensities. *J. Phys. Chem. A* **117**, 7081–7090 (2013).
53. Cordier, F. & Grzesiek, S. Quantitative Comparison of the Hydrogen Bond Network of

- A-State and Native Ubiquitin by Hydrogen Bond Scalar Couplings. *Biochemistry* **43**, 11295–11301 (2004).
54. Tamara, S., den Boer, M. A. & Heck, A. J. R. High-Resolution Native Mass Spectrometry. *Chem. Rev.* **122**, 7269–7326 (2022).
 55. Solgadi, D., Jouvet, C. & Tramer, A. Resonance-enhanced multiphoton ionization spectra and ionization thresholds of phenol-(ammonia)_n clusters. *J. Phys. Chem.* **92**, 3313–3315 (1988).
 56. Jacoby, C., Hering, P., Schmitt, M., Roth, W. & Kleinerhanns, K. Investigations of OH–N- and NH–O-type hydrogen-bonded clusters by UV laser spectroscopy. *Chem. Phys.* **239**, 23–32 (1998).
 57. Pietraperzia, G. *et al.* Noncovalent Interactions in the Gas Phase: The Anisole–Phenol Complex. *J. Phys. Chem. A* **115**, 9603–9611 (2011).
 58. Tachikawa, H. & Iyama, T. Proton Transfer Reaction Rates in Phenol–Ammonia Cluster Cation. *J. Phys. Chem. A* **124**, 7893–7900 (2020).

Chapter 7. Revealing the folded and unfolded structure of differently formed microhydrated complexes of the ubiquitin protein

This chapter contains a description and discussion of our latest, yet unpublished results on microhydrated ubiquitin, produced by retention as well as by condensation of water molecules, and can be considered as a continuation of the previous chapter. The previous study examined the bare and microhydrated ubiquitin with retained water molecules only. It showed, in particular, that retained water molecules preserve the folded structure of ubiquitin due to evaporative cooling. However, the question of whether the unfolded structure of ubiquitin can be folded back by condensation of water molecules remained unanswered. In this follow-up study, we performed additional experiments and provide direct evidence that answer this question. Since the motivation and experimental setup have already been described in previous chapters, this chapter begins with the results and discussion section.

7.1. Results and discussion

Figure 7.1 shows UV photofragmentation spectra of the +7 charge state of cold ubiquitin and its microhydrated complexes with 5 and 10 water molecules in the spectral range of the electronic band origin of Tyr aromatic residue. The protein was electrosprayed from a water/acetic acid (100/1) solution. The ions were accumulated in the pre-trap at room temperature and conditions were optimized to maximize the signal of the Ubi^{7+} microhydrated by 5 and 10 water molecules. The spectra of these complexes (Fig. 7.1, blue traces) are smooth and do not contain any vibrationally resolved transitions. As it has been discussed in the previous chapter, this smoothness indicates that the protein is in the folded, native-like state with the hydrogen bond between the hydroxyl of Tyr-59 and the amide group of Glu-51. The slight variations of the length of this bond among different conformers result in broadened and featureless spectra. Another reason of this broadening, not mentioned in the previous chapter, may be caused by the interaction of charged Arg-72 or Arg-74 residues with the aromatic ring of Tyr-59. The results of radical-directed fragmentation indicate the presence of this interaction for the +6 and +7 charge state of Ubi.¹ To record the spectrum of bare Ubi^{7+} , the ion source was tuned to maximize the signal of the bare ions, leading to the evaporation of all water molecules from the protein (Fig. 7.2). The spectrum of Ubi^{7+} (Fig. 7.1, black trace) exhibits

vibrationally resolved features, with the first absorption band observed at 35470 cm^{-1} . The position of this band is closely aligned with the position of the band origin in neutral Tyr.^{2,3} This observation implies that the side chain of Tyr-59 in the protein is not involved in any non-covalent interactions with other residues and the protein is in its unfolded or partially unfolded state. To condense water molecules onto the bare protein, the pre-trap was cooled to 200 K, and a controlled amount of water vapor was continuously introduced into the pre-trap. After condensation, microhydrated complexes with 5 and 10 water molecules were mass-selected and spectroscopically interrogated (Fig. 7.1, red traces). The spectra of the complexes with both 5 and 10 water molecules closely resemble the spectrum of the bare Ubi⁷⁺. The only noticeable difference is some broadening of the otherwise still well-resolved vibrational bands in the spectra of ubiquitin with condensed water molecules. These changes should originate from different sites of rehydration, which may lead to the observed inhomogeneous broadening of vibrational bands. It is clear, however, that these spectra of the complexes produced by the condensation of water (red traces in figure 7.1) crucially differ from the spectra of the same complexes formed by retaining water molecules (blue traces in the same figure). We thus conclude that condensation of a few water molecules cannot induce refolding of the protein, at least on the 50-ms timescale of our experiment.

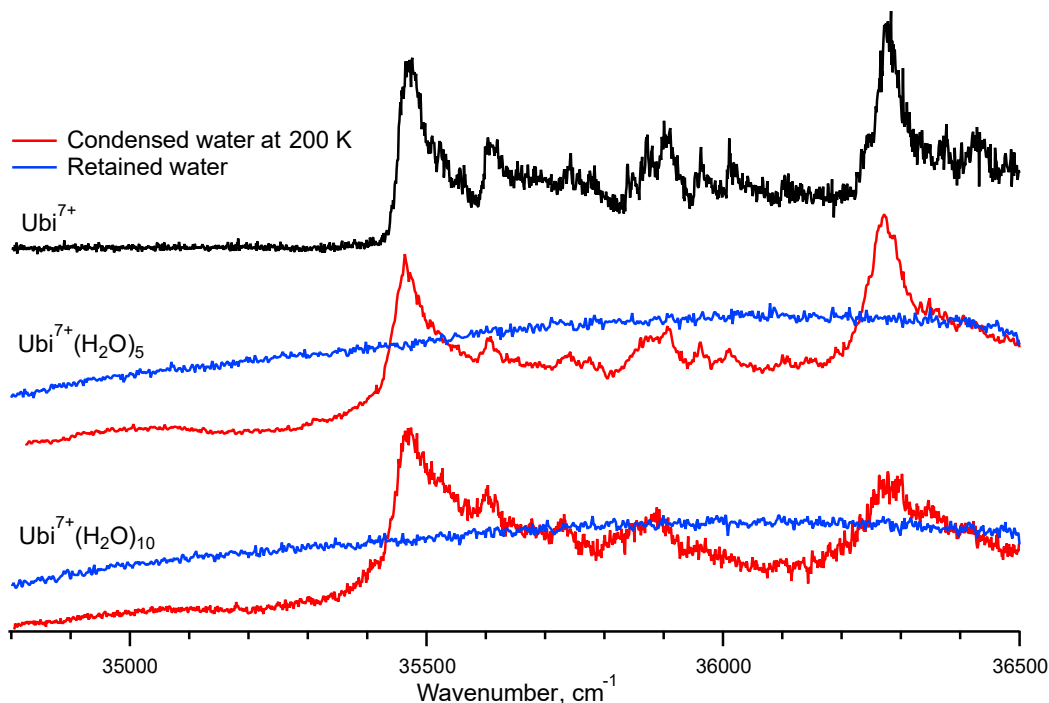


Figure 7.1. UV photofragmentation spectra of bare $[\text{Ubi} + 7\text{H}]^{7+}$ (black trace) and microhydrated by 5 and 10 water molecules by retaining water during ESI (blue traces) or condensing in the pre-trap at 200 K (red traces). In the case of retained water molecules, the complexes were thermalized and accumulated in pre-trap at room temperature.

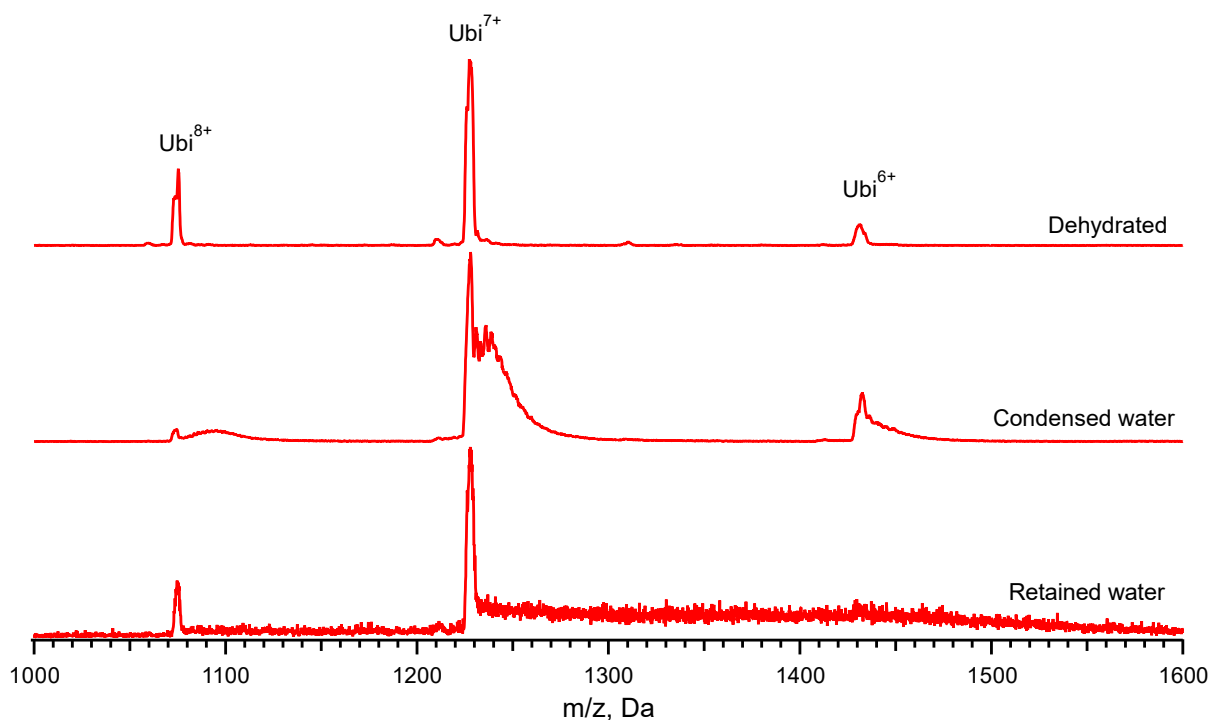


Figure 7.2. Typical mass spectra for dehydrated ubiquitin and its complexes with condensed and retained water molecules.

Figure 7.3 shows the UV photofragmentation spectra of microhydrated protein formed by water condensation at different temperatures. The upper temperature limit of 200 K is determined by the beginning of effective condensation, while 60 K is the lowest temperature achievable in our pre-trap. The spectra in the region below 35400 cm^{-1} look different and small features above 35400 cm^{-1} are more pronounced for the complexes formed at 60 K. Overall, the spectrum of complexes formed at 60 K looks more like the spectrum of the bare, unfolded Ubi^{7+} . It is important to note that the temperature of the pre-trap solely influences the spectra of microhydrated complexes formed through condensation. Conversely, the obtained spectra for complexes with retained water and the bare protein are nearly identical regardless of the pre-trap temperature (Fig. 7.4).

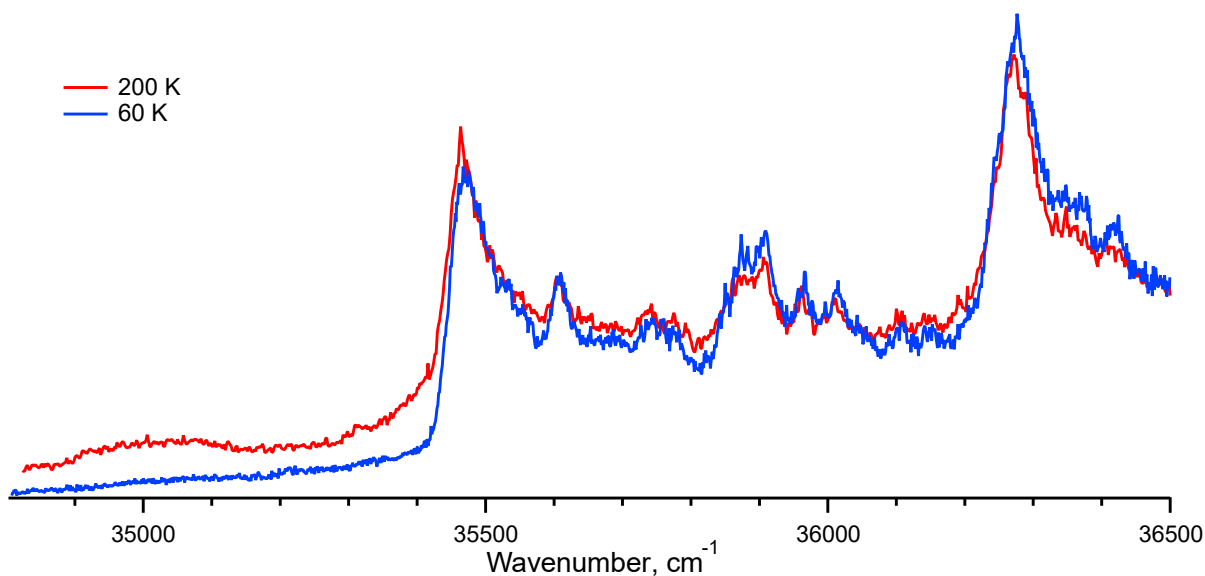


Figure 7.3. UV photofragmentation spectra of $[\text{Ubi} + 7\text{H} + (\text{H}_2\text{O})_5]^{7+}$. Microhydrated complexes were formed by condensation in pre-trap at 200 K and 60 K.

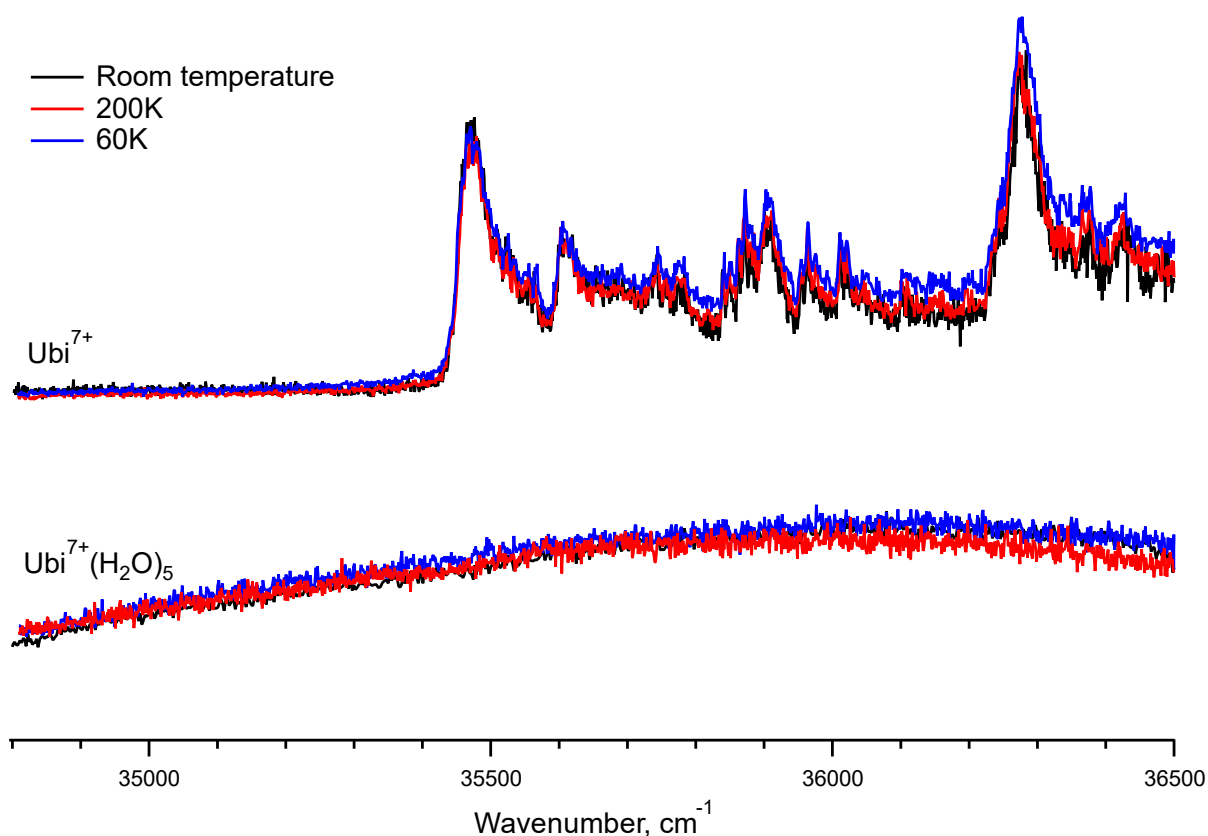


Figure 7.4. UV photofragmentation spectra of $[\text{Ubi} + 7\text{H}]^{7+}$ and its complexes with 5 water molecules after thermalization in pre-trap at room temperature (296 K), 200 K, and 60 K. Microhydrated complexes were retained after ESI.

While UV spectra are sensitive only to the structure of the protein near the chromophore, IR spectra can shed light on the structure of the whole protein. Figure 7.5 shows the IRMPD

spectra of differently formed complexes of Ubi^{7+} with 5 water molecules. The key distinction between complexes formed through water retention and condensation lies within the 3420-3580 cm^{-1} region. The spectra of complexes formed by water condensation contain several sharp, resolved peaks in this region. These peaks can be unambiguously assigned to free NH and carboxylic OH stretches.⁴ On the other hand, the spectrum of complexes with retained water molecules lacks any peaks above 3470 cm^{-1} . Considering that these spectra were acquired under identical conditions, insufficient photon fluence or other affecting parameters cannot account for the absence of peaks above 3470 cm^{-1} in complexes with retained water. Thus, the observed spectral differences can only be attributed to structural differences among the differently formed complexes. The absence of free NH and carboxylic OH stretches in complexes with retained water molecules suggests a folded, native-like structure of the protein, where all/most of these groups are involved in forming hydrogen bonds. In opposite, the presence of numerous free OH/NH vibrations in the spectra of complexes with condensed water molecules indicates the disruption of intramolecular hydrogen bonds, which are present in folded ubiquitin.⁵ Comparable spectral changes were previously observed for Ubi^{7+} electrosprayed under "gentle" and "harsh" conditions. IR spectra of complexes formed through water condensation at 200 K and 60 K display similarities, with only minor variations in the intensity of specific peaks and bumps. This similarity suggests that the structures of complexes formed at different temperatures are also likely to be similar.

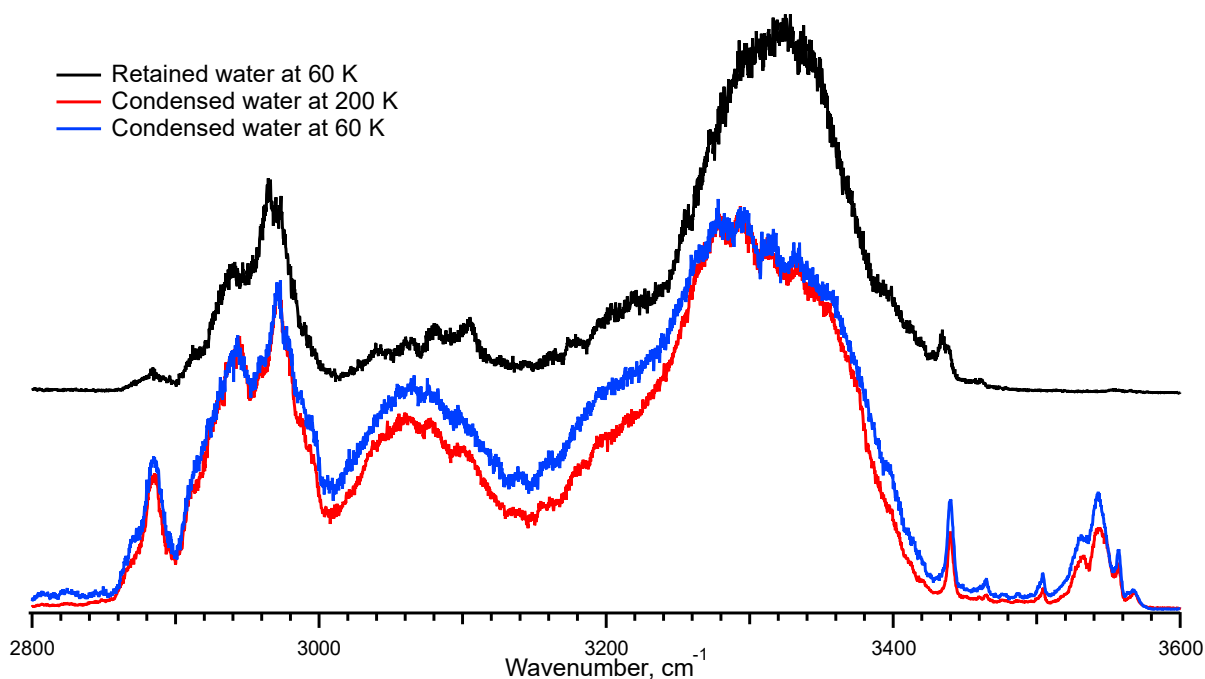


Figure 7.5. IRMPD spectra of $[\text{Ubi} + 7\text{H} + (\text{H}_2\text{O})_5]^{7+}$ complexes with retained and condensed water molecules.

7.2 Conclusion

In conclusion, this study provides the first firm experimental evidence that differently formed microhydrated complexes exhibit distinct 3D structures. Although the protein considered in this study is a relatively large system, it is possible that a similar trend can extend to smaller systems, such as peptides or even individual amino acids, as discussed in Chapter 4 regarding microhydrated arginine. The structures of these systems can be theoretically calculated using a high level of theory and compared with experiment. In order to successfully assign a theoretically calculated structure to the experimental one, it is crucial to have knowledge of the specific structure obtained in the experiment. If the structures of the microhydrated complexes formed through solvent retention and solvent condensation are identical, it implies that the complexes adopt gas-phase structures. In this case, the conformational search can be performed exclusively among a few the most stable structures, as demonstrated in Chapter 5. However, if the experimental spectra differ, the structure of the complex with retained solvent represents a kinetically-trapped native-like structure. In such cases, to match the experiment, the calculations should take into account the origin of the complexes, which are formed after evaporation of the solvent molecules from the larger complexes. The experimental approach of bidirectional hydration proposed in this study can be readily implemented in any suitable laboratory setup; such experiments will help theory in distinguishing between kinetically-trapped solution structures and the gas-phase structures of microhydrated complexes.

References

1. Ly, T., & Julian, R. R. Elucidating the tertiary structure of protein ions in vacuo with site specific photoinitiated radical reactions. *J. Am. Chem. Soc.* **132**, 8602–8609 (2010).
2. Cohen, R., Brauer, B., Nir, E., Grace, L. & de Vries, M. S. Resonance-Enhanced Multiphoton Ionization Spectroscopy of Dipeptides. *J. Phys. Chem. A* **104**, 6351–6355 (2000).
3. Martinez, S. J., Alfano, J. C. & Levy, D. H. The electronic spectroscopy of the amino acids tyrosine and phenylalanine in a supersonic jet. *J. Mol. Spectrosc.* **156**, 421–430 (1992).
4. Boyarkin, O. V. Cold ion spectroscopy for structural identifications of biomolecules. *Int. Rev. Phys. Chem.* **37**, 559–606 (2018).
5. Cordier, F. & Grzesiek, S. Quantitative Comparison of the Hydrogen Bond Network of A-State and Native Ubiquitin by Hydrogen Bond Scalar Couplings. *Biochemistry* **43**, 11295–11301 (2004).

Chapter 8. Summary and Outlook

In this thesis, we took a step towards a challenging objective of studying native biomolecular structures in the gas phase. We focused our studies on microhydration of biomolecules, as it is the most promising approach for solving their native structures in the gas phase. In order to facilitate the workflow of searching the 3D structures, the approach that compares IR/UV spectra of hydrated biomolecules with retained and condensed water molecules was proposed and demonstrated. It allows quick verification of the presence of kinetically trapped structures in the gas phase. This knowledge opens up the possibility of optimizing the search for 3D structures *in silico*. Additionally, we have successfully applied cold ion spectroscopy to a large system, a microhydrated protein ubiquitin, showcasing its versatility and potential.

Firstly, we designed a nano-ESI source that is capable to produce microsolvated complexes with either retained or condensed water molecules. The ion source is based on a triple molecular skimmer configuration and can be easily tuned for generation of ions with a large amount of retained water molecules. When the ion source is in a “harsh” mode, water molecules evaporate and the bare ions are formed, which then can be trapped in a temperature-controlled pre-trap. The molecules of water vapor that is injected into the trap then can condense onto the ions. When the ion source is optimized to produce the bare ions, its efficiency and short-term stability is comparable to a double ion funnel nano-ESI source.

Next, we spectroscopically studied different microhydrated biomolecular ions in the gas phase. Microhydrated arginine and tryptophan studied in this thesis represent the examples of the molecules with and without kinetic trapping. Tryptophan undergoes adiabatic structural changes upon dehydration/hydration. The evidence of this is the observed identity of IR and UV spectra of $\text{TrpH}^+(\text{H}_2\text{O})_n$ ($n = 1-6$) prepared by retaining and condensing water molecules. In support of this conclusion, the computed lowest energy conformers have been successfully validated by the measured vibrational spectra for every $n = 1-4$. On the other hand, microhydrated arginine is a striking example of kinetically trapped system that, upon dehydration, retains its most characteristic native-like feature upon dehydration with as few as 3-4 water molecules. This result differs significantly from the theory, which predicts that at least 8 water molecules are required to stabilize the salt bridge structure of ArgH^+ in the gas phase. The key factor that assists in such kinetic trapping is the evaporative cooling of microhydrated complexes. It reduces the temperature of the complexes to $\lesssim 200$ K and hinders

the transition from the native-like to the gas-phase structures. Because the conventional approaches of conformational search target the lowest energy structures only, we proposed an approach that mimics the experimental conditions. It is based on the sequential water removal from the large complexes followed by the structural optimization of such reduced ones. By using this approach, we found locally stable salt bridge conformers in the complexes of microhydrated arginine with as low as 2 water molecules.

Finally, we demonstrated that cold ion spectroscopy can provide a valuable structural information even for biomolecules as large as proteins. We showed the ability of CIS to track such global structural changes as unfolding of the protein ubiquitin using IR spectroscopy. Moreover, UV spectroscopy enabled tracking the local structural changes near the chromophores. It was found that evaporative cooling again plays a key role in retaining the folded, native-like structures of the protein. Even a few water molecules retained on the protein ensure its low internal energy all the time from the generation by ESI to the moment of the spectroscopic interrogation. This hinders unfolding of the protein. Condensing water on the bare unfolded protein does not refold its structure back.

Thus, a high final level of hydration of biomolecules may not be a must to preserve the main features of their native structures. Evaporative cooling is a crucial effect that enables probing the kinetically trapped native-like structures of biomolecules in the gas phase. This effect has been shown to be important not only for large molecules such as proteins, but also for small molecules such as amino acids.

In this thesis we showed only some applications of the developed ion source, and its potential is not fully exploited yet. It is also possible to produce heterogeneous complexes with, for instance, retained water molecules and condensed deuterated water, another solvent or any volatile molecules of interest. Once such complexes are produced, one can study, for instance, the diffusion of this foreign molecules within the complex.

Although microhydration provides an opportunity for studying native-like structures in the gas phase, the application of this approach in its current form remains rather limited. The main reason of this is a quick increase of spectral congestion upon hydration. This congestion arises due to several factors. Firstly, as the size of the complex increases, the number of vibrational transitions, many of which occur in the same spectral range, increases. Non-covalent interactions result in broadening of these closely spaced transition, finally leading to their overlap and loss of vibrational resolution. In addition, the number of conformers often increases with the size of the complex. All these factors quickly make the spectra of the complexes barely usable for structural elucidation.

To overcome the issue of congested spectra resulting from hydration, an approach involving a rapid removal of water molecules followed by an immediate cooling to prevent any significant rearrangements of biomolecular 3D structure could be used. A recently demonstrated, so-called, collision-assisted stripping spectroscopy allows reducing the issue of the spectral congestion significantly.¹ In this approach, microhydrated complexes are dehydrated in high-energy collisions with cold He and immediately cooled. This enables freezing biomolecular ions in their native-like structures, but also suppress the spectral congestion that could be due to the removed water molecules. This method implies, however, that the entire complex is collisionally heated. If the energy barriers between the native-like and gas-phase structures are low, certain structural rearrangements to the gas-phase structure still remain possible, however. This narrows application of the method to the specific ions that exhibit high barriers of structural rearrangement. Perhaps, a broader and more accurate approach to strip-off water from a biomolecule could be a use of mode-selective coherent excitation of water molecules in the complexes by a short IR laser pulse followed by water detachment. Such short photoexcitation should allow for a temporal location of the imported vibrational energy, mainly, within the water envelope. Vibrational relaxation of this excitation to the parent ion will pass through the weak H-bonds, which should therefore break them prior a complete IVR. This could not only reduce the probability of structural rearrangements to the gas-phase structures but also allow for tracking time-resolved structural changes of biomolecules after such prompt dehydration.

Another promising approach could be to extend cold ion action spectroscopy to the far-IR and terahertz spectral regions. Unlike the range above 1000 cm^{-1} , the range below 1000 cm^{-1} is less prone to spectral congestion and contains many delocalized vibrations that are highly sensitive to secondary structural motifs.² The use of appropriate narrow bandwidth THz laser sources should enable the resolution of individual vibrational transitions, even for biomolecules of moderate size. Furthermore, DFT-MD theoretical methods account for the strong anharmonicity associated with this domain and can provide a good match with experimental spectra.^{2,3}

Finally, the remarkable advances in AI are expected to have a significant impact on the field of computational chemistry. AI can be useful in a variety of applications, enhancing the accuracy of different quantum-mechanical methods, reducing computational cost, enabling high-throughput, and potentially automating the assignment of experimental spectra to 3D structures.

Despite the considerable progress made in the gas-phase spectroscopy for elucidating 3D structures over the years, there is still ample room for improvement, and this method remains perspective for a wide range of applications in the field of life sciences, particularly when coupled with other gas-phase methods.

¹Hirata, K., Haddad, F., Dopfer, O., Ishiuchi, S. & Fujii, M. *Phys. Chem. Chem. Phys.* **24**, 5774–5779 (2022).

²Bakels, S., Gaigeot, M. P., & Rijs, A. M. *Chem. Rev.* **120**, 3233–3260 (2020).

³Gaigeot, M. P. *Spectrochim. Acta A.* **260**, 119864 (2021).

Acknowledgments

I express my sincere gratitude to all my past and present teachers, supervisors, and colleagues. The emergence of this thesis and obtaining the title of PhD would not have been possible if I had not met you at different milestones of my life's journey.

First of all, I am deeply grateful to my PhD advisor, Prof. **Oleg V. Boyarkine**, who gave me the possibility to join his research group, provided a place and resources to develop myself in the state-of-the-art scientific field, and supported me all these years.

Many thanks to Dr. **Aleksandr Pereverzev** and Dr. **Erik Saparbayev** for their substantial help and equally substantial patience in teaching me how to work with a complex scientific instrument as is in our lab. They are the first students whom I met at EPFL, and they helped me immerse myself in the life of a PhD student. I am also very thankful to our postdocs. Dr. **Ruslan Yamaletdinov** introduced me to the technical side of computational chemistry and stimulated my interest in doing some calculations by myself. Dr. **Vladimir Kopysov** inspired me to explore different simulation software and we all had a lot of fruitful discussions and work together.

Technical modifications of our instrument and subsequent scientific results would not have been possible without the support of our mechanical and electronic workshops. **André Fattet**, **Roger Mottier**, and other members of the mechanical workshop were always ready to help with various requests, ranging from small and simple but urgent matters to the manufacture of a large number of complex parts. Similarly, **Benjamin Charles Le Geyt** and **Harald Holze** on behalf of the electronic workshop provided their quick and quality support whenever needed. Thank you very much for your help.

Special thanks to our secretary, **Angeles Alarcon**, who provides invaluable assistance with administrative duties, especially during the first days at EPFL.

My gratitude also goes to Prof. **Marie-Pierre Gageot** and Dr. **Álvaro Cimas**, our collaborators from the University of Évry Val d'Essonne who greatly enhanced our study on arginine by performing highly valuable calculations.

And finally, I would like to thank all the other wonderful people I have met at EPFL and beyond, with whom we shared ups and downs and who made my PhD studies an amazing and unforgettable period of my life.

Andrei Zviagin

Date of birth: 06.02.1996;

Place of birth: Bishkek, Kyrgyzstan

Phone number: +41 78 720 4940;

E-mail: andrei.zviagin@epfl.ch

Address: Chemin de Jouxens 13, 1020 Renens VD, Switzerland.



Education

Since August 2019: PhD student in Chemistry and Chemical Engineering, École polytechnique fédérale de Lausanne (EPFL), Lausanne, Switzerland.

August 2013 – July 2019: BSc (GPA: 4.91/5) and MSc (GPA: 5/5) in Applied Physics. Major: Beam and Plasma Technologies. National Research Tomsk Polytechnic University (TPU), Tomsk, Russia.

Research and Work Experience

Since August 2019: Doctoral Assistant at Laboratory of Molecular Physical Chemistry, EPFL, Switzerland.

- Mass spectrometry (including Orbitrap-based MS and LC-MS), cold ion spectroscopy (IR, UV, double resonance) and structural determination of solvated biomolecules.
- Proposed, designed and implemented a unique ion source capable to produce microsolvated ions with both retained and condensed solvent molecules.
- Extensive service and troubleshooting experience on home-build and commercial analytical equipment.

March 2018 – July 2019: Engineer at Research Center of Physical Materials Science and Composite Materials, TPU, Russia.

- Production, modification, and characterization of biodegradable polymer electrospun scaffolds with piezoelectric properties.
- Experience with SEM, EDS, TEM, XRD, AFM, XPS, FTIR, wettability, and piezoelectric response measurement techniques.

February 2019 – March 2019: Internship at VNIITF, Snezhinsk, Russia.

- Developed a method for manufacturing of a dielectric mirror with the required reflection coefficient in the radial direction using electron beam evaporation process.
- Experience working in a cleanroom environment.

July 2018 – August 2018: Internship at JINR, Dubna, Russia.

- Performed simulations in Geant4 software package and designed a detector for estimating electron energies in the linear accelerator LINAC-800.

November 2017 – December 2017, August 2018 – September 2018 and April 2019: Internships at the University of Cologne, Germany.

- Proposed and developed a method for hydrothermal deposition of ZnO coating onto electrospun polymer scaffolds.

August 2017: Internship at the University of Duisburg-Essen, Germany.

- Modified electrospun polymer scaffolds to increase their wettability and bioactivity.

July 2016: Internship at the Institute of Theoretical and Experimental Biophysics, Russia.

- Performed *in vitro* analysis of polymer electrospun scaffolds with different structure, morphology, and composition.

Teaching Experience

Since February 2020: Teaching assistant for undergraduate courses at EPFL, Switzerland.

- Chief teaching assistant for General Physics: Electromagnetism courses.
 - Coordinate a group of 7 teaching assistants, ensure their preparation for the classes.
 - Coordinate livestream of lectures via Zoom for over 150 students, answering questions in the online chat, ensuring image and audio quality and assisting in demonstration experiments.
 - Grade written exams.
- Support third year bachelor students during preparation of 30 min presentation for Methods in Spectroscopy and Dynamics course.
- Support third year bachelor students throughout exercise session for Structural Analysis course.

Languages

English: Fluent

German: A2

Russian: Native

Scholarships, Grants and Awards

- IBBI 2022 conference, Austria: Best poster award.
- Leonhard-Euler-Program – DAAD scholarship. Three G-RISC DAAD scholarships. “The best student” of TPU award and scholarship. Increased academic scholarships for achievements in scientific activities. Won UMNIG Grant to carry out research activity in the field of electrospun polymer scaffolds for biomedical application.
- June 2016: Participation in the workshop “Territory Identity of Russia and America through the Eyes of Young Generations” in the frame of U.S.-Russia Peer-to-Peer-Dialogue program, Colorado State University, Fort Collins, USA.

Publications

- **Zviagin, A.**, Yamaletdinov, R., Nagornova, N., Dömer, M., & Boyarkin, O. V. *J. Phys. Chem. Lett.* 14, 6037-6042 (2023).
- **Zviagin, A.**, Cimas, A., Gageot, M. P., & Boyarkin, O. V. *J. Phys. Chem. A.* 127, 4832-4837 (2023).
- **Zviagin, A.**, Kopysov, V., Nagornova, N. S. & Boyarkin, O. V. *Phys. Chem. Chem. Phys.* 24, 8158–8165 (2022).
- **Zviagin, A.**, Kopysov, V. & Boyarkin, O. V. *Rev. Sci. Instrum.* 93, 114104 (2022).
- Saparbaev, E., **Zviagin, A.** & Boyarkin, O. V. *Anal. Chem.* 94, 9514–9518 (2022).
- Saparbaev, E., Aladinskaia, V., **Zviagin, A.** & Boyarkin, O. V. *J. Phys. Chem. Lett.* 12, 907–911 (2021).
- **Zviagin, A.** *et al. Eur. Polym. J.* 117, 272–279 (2019).
- **Zviagin, A.**, *et al. IOP Conf. Ser.: Mater. Sci. Eng.* 597, 012061 (2019).